JOURNAL OF PETROLOGY | VOLUME 55 | NUMBER 3 | PAGES 459–498 | 2014 | doi:10.1093/petrology/egt068

Petrology and Trace Element Budgets of High-pressure Peridotites Indicate Subduction Dehydration of Serpentinized Mantle (Cima di Gagnone, Central Alps, Switzerland)

MARCO SCAMBELLURI[1]*, THOMAS PETTKE[2], ELISABETTA RAMPONE[1], MARGUERITE GODARD[3] AND ERIC REUSSER[4]

[1]DIPARTIMENTO DI SCIENZE DELLA TERRA, AMBIENTE E VITA, UNIVERSITY OF GENOVA, CORSO EUROPA 26, 16132 GENOVA, ITALY

[2]INSTITUTE OF GEOLOGICAL SCIENCES, UNIVERSITY OF BERN, BALTZERSTRASSE 1, CH-3012, BERN, SWITZERLAND

[3]GEOSCIENCES MONTPELLIER, UNIVERSITE MONTPELLIER 2, PLACE EUGENE BATAILLON 34095, MONTPELLIER, FRANCE

[4]ETH ZÜRICH, INSTITUT FÜR GEOCHEMIE UND PETROLOGIE, CLAUSIUSSTRASSE 25, 8092 ZÜRICH, SWITZERLAND

RECEIVED JANUARY 19, 2013; ACCEPTED OCTOBER 24, 2013
ADVANCE ACCESS PUBLICATION JANUARY 7, 2014

At Cima di Gagnone, garnet peridotite and chlorite harzburgite lenses within pelitic schists and gneisses correspond to eclogite-facies breakdown products of hydrated peridotites and are suitable for studying dehydration of serpentinized mantle. Thermobarometry and pseudosection modelling yield peak temperatures of 750–850°C and pressures <3 GPa. The minimum temperature recorded by the garnet peridotite corresponds to the maximum conditions experienced by the chlorite harzburgite, suggesting that these rocks recrystallized cofacially at ~800°C. Alternatively, they might have decoupled during subduction, as achieved in tectonically active plate interface boundaries. The major and rare earth element (REE) variability of the peridotites was mostly acquired during pre-subduction mantle evolution as a result of partial melting and reactive melt flow. The ultramafic suite is also characterized by fluid-mobile element enrichments (B, Pb, As, Sb, Cs, Li, U, Be), which confirm derivation from variably serpentinized protoliths. Similarity in the U, Pb, B, Li and Sr contents of the Gagnone peridotites to present-day oceanic serpentinites suggests that these elements were partly taken up during initial serpentinization by seawater-derived fluids. Positive Be, As and Sb anomalies suggest involvement of fluids equilibrated with crustal (metasedimentary) reservoirs during subsequent subduction metamorphism and peridotite entrainment in (meta)sediments. Fluid-mobile element enrichment characterizes all peak eclogitic minerals, implying that multiple hydration events and element influx pre-dated the eclogite-facies dehydration. Peak anhydrous minerals retain B, Li, As and Sb concentrations exceeding primitive mantle values and may introduce geochemical anomalies into the Earth's mantle. The relatively low contents of large ion lithophile elements and light REE in the Gagnone peridotites with respect to much higher enrichments shown by metasomatized garnet peridotite pods hosted in migmatites (Ulten Zone, Eastern Alps) suggest that the crustal rocks at Gagnone did not experience partial melting. The Gagnone garnet peridotite, despite showing evidence for chlorite dehydration, retains significant amounts of fluid-mobile elements documenting that no partial melting occurred upon chlorite breakdown. We propose that the Gagnone ultramafic rocks represent a prime example of multi-stage peridotite hydration and subsequent dehydration in a plate interface setting.

KEY WORDS: *garnet peridotite; chlorite harzburgite; subduction; serpentinized mantle; trace elements; subduction fluid; subduction mélange*

*Corresponding author. E-mail: marco.scambelluri@dipteris.unige.it

INTRODUCTION

In recent years there has been an explosion of interest in serpentinites. This is due to their role as (1) volatile and fluid-mobile element repositories in the ocean basins and in subduction zones, (2) triggers of arc magmatism and of seismic activity, (3) the main constituents of low-viscosity channels located at plate interfaces, which affect both subduction and exhumation dynamics, (4) producers of hydrogen and methane with implications for the potential origin of life in Earth, (5) reservoirs for CO_2 sequestration (Ulmer & Trommsdorff, 1995; Scambelluri *et al.*, 1997, 2004a,b; Schmidt & Poli, 1998; Hermann *et al.*, 2000; Guillot *et al.*, 2001; Schwartz *et al.*, 2001; Dobson *et al.*, 2002; Gerya *et al.*, 2002; Straub & Layne, 2003; Jung *et al.*, 2004; Sharp & Barnes, 2004; Federico *et al.*, 2007; Hilairet *et al.*, 2007; Kelemen & Matter, 2008; Barnes & Straub, 2010; Deschamps *et al.*, 2010; Evans, 2010). Interest in serpentinites has progressively increased since the second half of the 1990s, when ocean drilling programs documented their wide exposure in the Atlantic seafloor and combined experimental and field studies demonstrated antigorite stability to eclogite-facies conditions and to sub-arc depths (Cannat *et al.*, 1995; Scambelluri *et al.*, 1995; Ulmer & Trommsdorff, 1995). These rocks have also been identified along mega-fractures in bending subducting plates (Ranero *et al.*, 2003; Alt & Shanks, 2006) and in mantle-wedge domains flushed by ascending slab fluids (Peacock, 1993; Bostock *et al*; 2002; Savov *et al.*, 2005). Since these discoveries, the contribution of hydrated (serpentinized) mantle to volatile and light element recycling in arc magmas, and its involvement in subduction and exhumation tectonics, has been investigated and modelled (Gerya *et al.*, 2002; Scambelluri *et al.*, 2004*b*; Marschall *et al.*, 2006; Bonifacie *et al.*, 2008; Faccenda *et al.*, 2008; Healy *et al.*, 2009; Barnes & Straub, 2010; John *et al.*, 2011; Kendrick *et al.*, 2011; Scambelluri & Tonarini, 2012). Understanding the role of serpentinites in subduction zones is thus highly relevant and timely for constraining geochemical recycling and tectonics at convergent plate margins.

A major event in the subduction cycle of hydrated mantle concerns the relevant fluid loss (5–13 wt % water) related to final breakdown of antigorite serpentine to olivine plus orthopyroxene at sub-arc depths (Ulmer & Trommsdorff, 1995; Schmidt & Poli, 1998; Scambelluri *et al.*, 2001; Alt *et al.*, 2012). De-serpentinized peridotites are made of anhydrous minerals with subordinate modal amounts of chlorite and Ti-clinohumite (Trommsdorff *et al.*, 1998; Ulmer & Trommsdorff, 1999; Fumagalli & Poli, 2005), which control the water budgets and partial melting of ultramafic rocks beyond antigorite stability. Several experimental studies have recently discussed the relevance of chlorite breakdown to garnet-bearing assemblages for fluid release at sub-arc depths (Fumagalli & Poli, 2005; Grove *et al.*, 2006). Besides providing additional water loss from subducting ultramafic systems, the chlorite dehydration curve may intersect the H_2O-saturated peridotite solidus from 2 to 3·6 GPa, potentially triggering peridotite dehydration-melting and arc magmatism (Grove *et al.*, 2006; Till *et al.*, 2012). These highly debated topics are little documented in nature; consequently, field-based studies of high- and ultrahigh-pressure orogenic peridotites may allow us to clarify the processes associated with serpentine and chlorite dehydration during subduction metamorphism. However, although many orogens display the association of olivine-bearing antigorite schists with eclogite-facies rocks (e.g. Scambelluri *et al.*, 1995; Hermann *et al.*, 2000; Li *et al.*, 2004; Fontana *et al.*, 2008; Rebay *et al.*, 2012), discoveries of high-pressure ultramafic rocks recording subduction breakdown of antigorite are rare (Trommsdorff *et al.*, 1998). This scarcity must be related to the strong density increase caused by antigorite breakdown that inhibits exhumation and represents a no-return transformation for large domains of slabs and mantle wedges. A major process associated with antigorite breakdown is the conspicuous fluid delivery to the mantle: determining the compositions of this fluid and of dehydrated rock residues would permit us to define fractionation and recycling of fluid-mobile elements during dehydration of both slab and supra-subduction zone mantle. Studies so far have emphasized the efficiency of serpentinites in releasing halogens, B, As and Pb for arc magmatism, and of residual harzburgites in retaining unexpectedly high amounts of B, Li, halogens and noble gases and in returning them to the deep mantle (Scambelluri *et al.*, 1997, 2004a; Hattori & Guillot, 2003; Garrido *et al.*, 2005; John *et al.*, 2011; Kendrick *et al.*, 2011).

As mentioned above, direct knowledge of such features is hampered by the scarcity of de-serpentinized ultramafic rocks in high- and ultrahigh-pressure terrains, the best occurrence being Cerro del Almirez, in the Betic Cordillera (Spain). In this locality spinifex-textured chlorite harzburgite, derived from antigorite schists (Trommsdorff *et al.*, 1998; Puga *et al.*, 1999; Lòpez Sànchez-Vizcaìno *et al.*, 2005; Padròn-Navarta *et al.*, 2010a,b , widely retains major dehydration features, such as fluid remnants and fluid-escape channels (Scambelluri *et al.*, 2001, 2004*a*, 2004*b*; Garrido *et al.*, 2005; Padròn-Navarta *et al.*, 2010c and has inherited from its serpentinite precursor light element, halogen, noble gas and sulphur contents higher than normal mantle reservoirs (Scambelluri *et al.*, 2004*a*; John *et al.*, 2011; Kendrick *et al.*, 2011; Alt *et al.*, 2012). To date, petrological and geochemical studies of other comparable field occurrences extensively recording structural and petrological features of serpentine breakdown are still lacking.

Considering this, the earliest recognition of dehydrated subduction-zone serpentinized ultramafic rocks was by

Evans & Trommsdorff (1978), who interpreted the garnet peridotite of Cima di Gagnone (Central Alps, Ticino, Switzerland) as the breakdown product of hydrated oceanic mantle. Major evidence for this was provided by the presence in the peridotite of rodingitized mid-ocean ridge basalt (MORB) dikes recrystallized at eclogite-facies conditions (Evans *et al.*, 1979), and by the survival of relict F-rich Ti-clinohumite, derived from previous serpentinite assemblages (Evans & Trommsdorff, 1983). For about two decades this was the only recognition of dehydrated subduction-zone serpentinite, well before explosion of the 'serpentinite seduction' (Kerrick, 2002). Thus far, the Gagnone garnet peridotite has been studied for its petrology and phase relations, but its trace element geochemistry has remained essentially unexplored. This study aims at filling this gap by providing new field and microstructural observations and an extensive trace element dataset for rocks and minerals. Our goal is to test on geochemical grounds whether the Gagnone peridotite is actually derived from serpentinized mantle rocks and to discuss the major petrological and geochemical implications of serpentinite breakdown in deep subduction environments.

GEOLOGICAL SETTING

Several ultramafic rock bodies form kilometre- to metre-sized lenses in the crustal Adula–Cima Lunga Unit, Central Swiss Alps. These correspond to the famous masses of Alpe Arami, Cima di Gagnone and Monte Duria, which are exposed along a continuous narrow horizon (Möckel, 1969; Fumasoli, 1974; Evans & Trommsdorff, 1978; Pfiffner & Tromsdorff, 1998). Among these ultramafic rocks, garnet peridotite and enstatite–olivine–chlorite rocks (chlorite harzburgite) from Cima di Gagnone (Fig. 1) are of particular interest. During Alpine subduction these rocks crystallized at higher grades than most of the serpentinized peridotites widely exposed in the Central and Western Alpine ophiolites (e.g. Voltri Massif, Monviso, Zermatt–Saas, Malenco; Evans & Trommsdorff, 1978; Trommsdorff *et al.*, 2000).

The Adula–Cima Lunga Unit consists of a crystalline basement made of pelitic, mafic and granitoid rocks, partly overlain by Mesozoic quartzite and dolomite. It has been considered part of the European continental margin involved in the Alpine subduction–collision cycle (Schmid *et al.*, 1990). The Adula–Cima Lunga Unit is regionally affected by subduction-related high-pressure metamorphism (Heinrich, 1982, 1986) that is absent in the other Central Alpine nappes and that pre-dates the collision-related Lepontine amphibolite-facies metamorphism, which is widespread in the Central Alps (Trommsdorff, 1966; Jäger *et al.*, 1967). Within this unit, the high-pressure metamorphic conditions increase from about 1 GPa and 500°C in the northern domain to more than 2·5 GPa and 800°C, and possibly to ultrahigh-pressure conditions (e.g. Dobrzhinetskaya *et al.*, 1996) in the south, where the Arami, Gagnone and Duria peridotite bodies occur (Heinrich, 1982, 1986; Meyre *et al.*, 1997, 1999; Pfiffner, 1999).

At Cima di Gagnone the ultramafic rocks form elongated lens-shaped bodies tens to hundreds of metres in size enclosed within semi-pelitic and quartzo-feldspathic gneiss (Fig. 1). These bodies predominantly consist of chlorite harzburgite and dunite, minor carbonated ultramafic rocks (ophicarbonates) and garnet peridotite, associated with rodingite and layers of amphibolitic eclogite. Garnet peridotite is mostly confined to outcrop Mgl60 (Fig. 1). The Gagnone garnet peridotite has been the subject of several studies concerning its petrography, petrology, thermobarometry and fabric (Trommsdorff & Evans, 1974; Evans & Trommsdorff, 1983; Pfiffner & Trommsdorff, 1998; Nimis & Trommsdorff, 2001; Freese *et al.*, 2003; Skemer *et al.*, 2006). These studies all point to the occurrence of polyphase metamorphism in these rocks, with early olivine, orthopyroxene, clinopyroxene and amphibole foliations overgrown by peak poikiloblastic garnet stable with olivine, orthopyroxene and clinopyroxene (Evans & Trommsdorff, 1978; Morten & Trommsdorff, 2003). The peak garnet-bearing assemblage probably contained stable Mg-hornblende, which was then replaced by a retrograde amphibolite-facies assemblage made of chlorite, Ca-amphibole, cummingtonite and spinel. Thermobarometry of the peak garnet-facies assemblage at Gagnone has provided estimates of 750–800°C and 2·5–3 GPa for the eclogitic event (Evans & Trommsdorff, 1978; Pfiffner, 1999; Nimis & Trommsdorff, 2001). Much less known are the phase relations and metamorphic crystallization conditions of the chlorite harzburgite. Trommsdorff (1990) proposed the formation of two types of chlorite peridotite in the Adula–Cima Lunga unit: chlorite-peridotite 1, stable at eclogite-facies conditions, and chlorite-peridotite 2, formed by retrogression of the garnet-peridotite. The simultaneous high-pressure (co-facial) crystallization of garnet- and chlorite-peridotite 1 was proposed by Trommsdorff (1990) and attributed to variable bulk-rock compositions and water contents (see also Morten & Trommsdorff, 2003).

The association of the above ultramafic rocks with eclogite and rodingite has been widely reported (Evans *et al.*, 1979, 1981); these rocks clearly indicate co-facial development of high-pressure metamorphism in the Gagnone mafic–ultramafic rock association. Eclogites and rodingites mainly occur within the chlorite harzburgite (Figs 1 and 2); they display a MORB-type geochemical affinity and are inferred to be derived from basaltic and/or gabbroic intrusions in the mantle rocks (Evans *et al.*, 1979, 1981). Great importance has been given to the Gagnone rodingites, as evidence of an early stage of peridotite serpentinization (Evans *et al.*, 1979, 1981). Moreover, the presence in the garnet peridotite of olivine + ilmenite

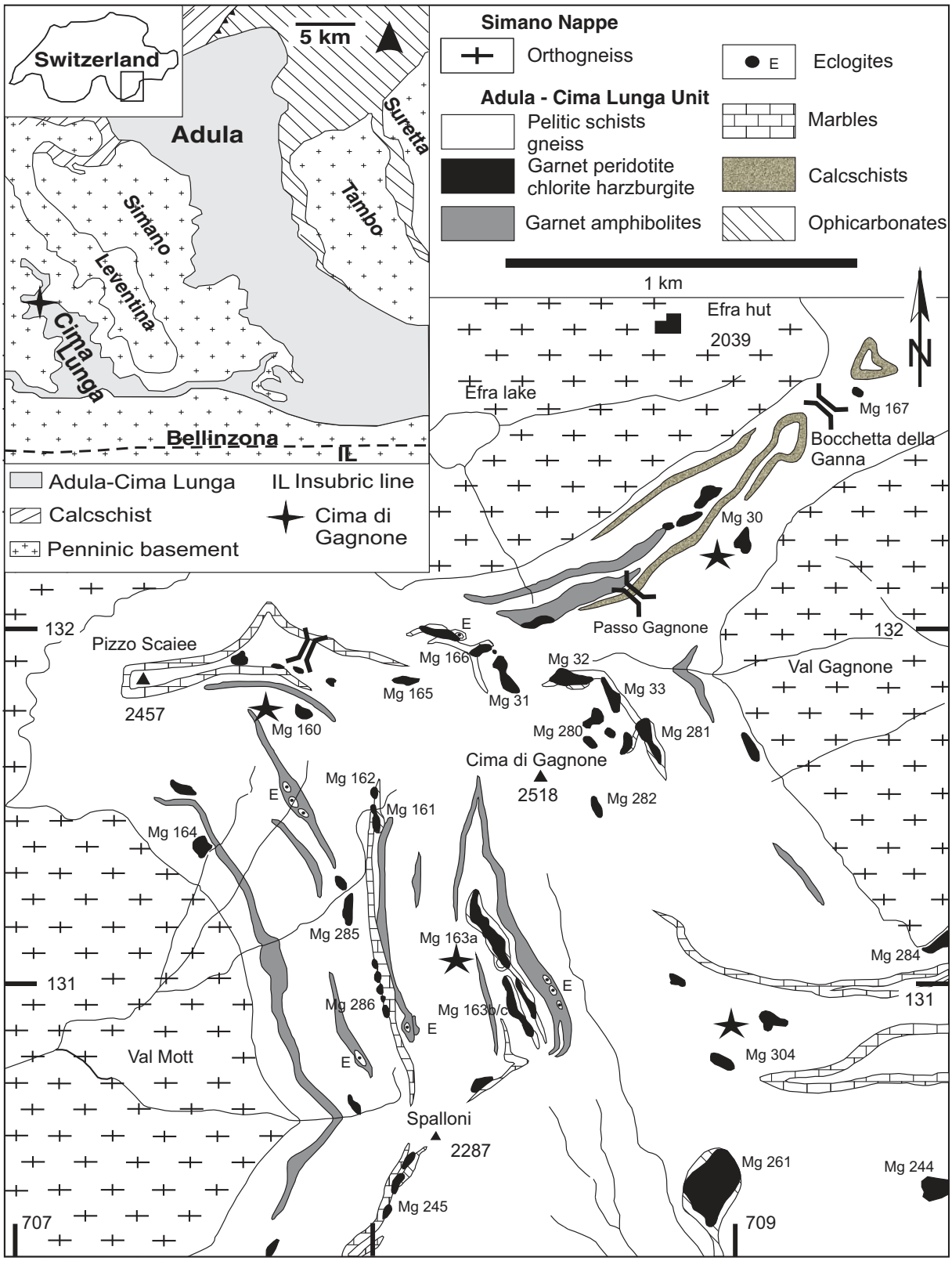

Fig. 1. Geological map of the Cima di Gagnone area, indicating the main outcrops of chlorite harzburgite and garnet peridotite sampled and investigated in this study. Redrawn after Pfiffner & Trommsdorff (1998) and Pfiffner (1999).

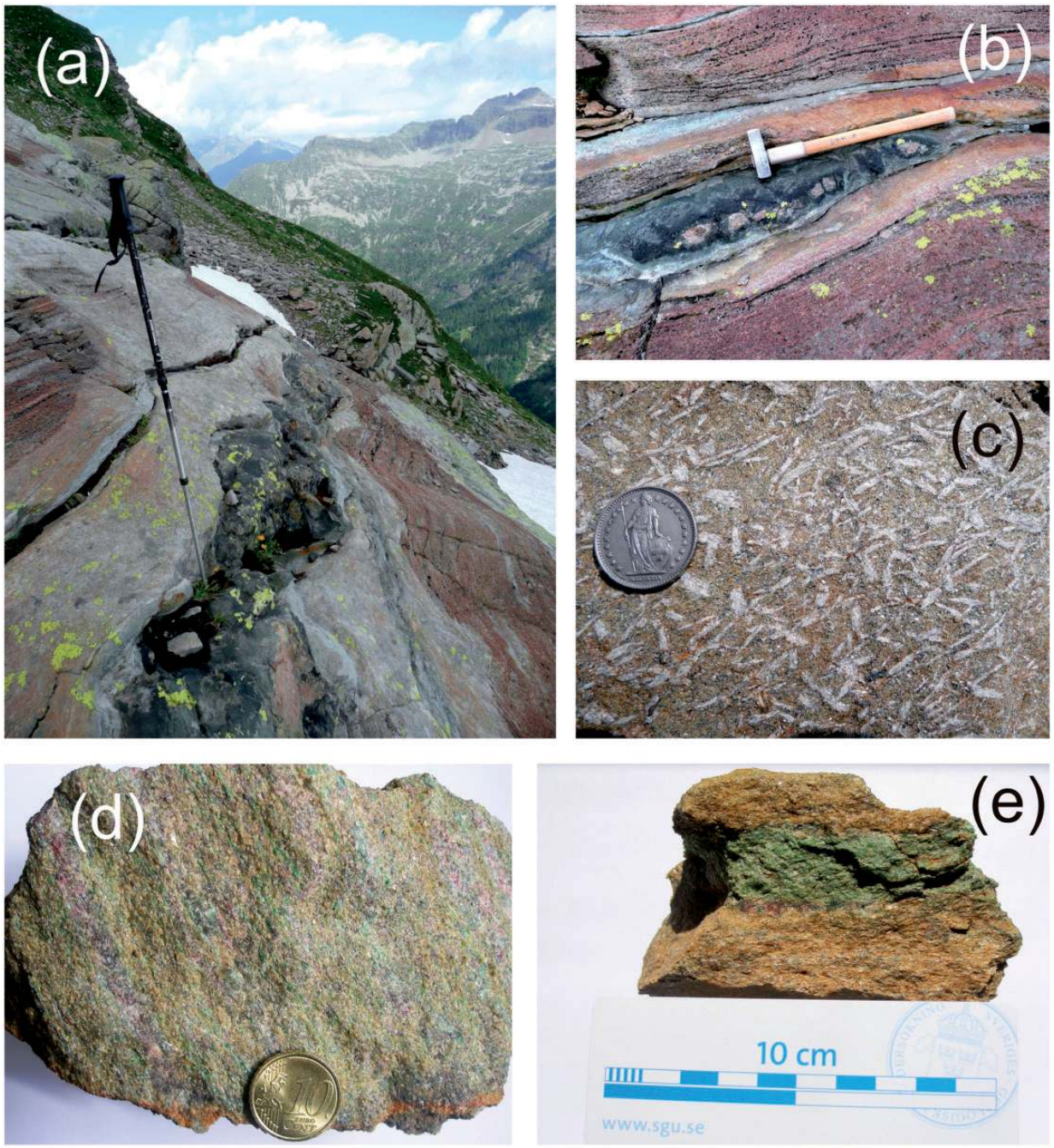

Fig. 2. Field photographs and rock samples form the Gagnone area. (a) Outcrop Mg3l, made of chlorite harzburgite hosting boudinaged rodingitized mafic dykes. The olivine, orthopyroxene, chlorite foliation in the harzburgite flows around the boudins. (b) Rodingite, showing a garnet-rich core overgrown by retrograde amphibole blackwalls (outcrop Mg3l). (c) Undeformed chlorite harzburgite showing coarse, randomly oriented orthopyroxene in a chlorite and olivine matrix. (d) Garnet-rich peridotite showing millimetre-thick layers of poikiloblastic garnet (from outcrop Mg-l60; sample Mgl60 09-l0G). (e) Pyroxenite layer in garnet peridotite. Loose block from outcrop Mgl60.

pseudomorphs after former Ti-clinohumite, and the stability of fluorine-rich varieties of this mineral in some chlorite harzburgite, further indicates serpentinite precursors (Evans & Trommsdorff, 1978, 1983), as Ti clinohumite is a typical rock- and vein-forming mineral in high-pressure Alpine serpentinites (Cimmino *et al.*, 1979; Scambelluri *et al.*, 1991; Li *et al.*, 2004; Fontana *et al.*, 2008; Rebay *et al.*, 2012). Finally, the presence of carbonated peridotites and ophicarbonate in the chlorite harzburgite bodies from Gagnone further suggest the presence of former (shallow)

ophicalcite formed during exposure of ultramafic rocks on the seafloor (Trommsdorff *et al.*, 2000).

Isotopic investigations of minerals from Alpe Arami and the Cima di Gagnone garnet lherzolite have yielded consistent Eocene ages of ~40 Ma, based on garnet–clinopyroxene whole-rock Sm–Nd and Lu–Hf isochrons (Becker, 1993; Brouwer *et al.*, 2005), and of 43–35 Ma for zircon, based on the U–Pb method and sensitive high-resolution ion microprobe (SHRIMP) analysis (Gebauer *et al.*, 1992; Gebauer, 1996). These ages are consistent with the dating of late-Eocene high-pressure metamorphism in the Western Alps (Froitzheim *et al.*, 1996; Gebauer *et al.*, 1997; Rubatto *et al.*, 1998) and date the peak of Alpine subduction zone metamorphism in these rock suites.

The chemical compositions of garnet lherzolites from the Central Alps (O'Hara & Mercy, 1966; Fumasoli, 1974; Rost *et al.*, 1974; Ernst, 1977; Evans & Trommsdorff, 1978; Pfiffner, 1999) are similar to those of fertile mantle and of subcontinental mantle exhumed and exposed near the ocean floor during formation of the Alpine and Ligurian Mesozoic Tethys (Menzies & Dupuy, 1991; Rampone & Piccardo, 2000; Rampone *et al.*, 2005). The ultramafic–mafic–carbonate suite at Cima di Gagnone has thus been interpreted as derived from an ocean basin near a thinned continental margin (Pfiffner & Trommsdorff, 1998), with the ultramafic rocks representing former subcontinental mantle exhumed during oceanic rifting and exposed close to the seafloor (Trommsdorf, 1990; Trommsdorff *et al.*, 2000). The observed garnet-bearing assemblages and the chlorite harzburgite at Gagnone formed as a result of prograde subduction-zone metamorphism of variably serpentinized peridotite. According to Trommsdorff (1990), tectonic mixing of crustal (the gneiss and metasedimentary portion of the Adula unit) and mantle slices since the beginning of Alpine subduction led to formation of a lithospheric mélange now represented by the Adula–Cima Lunga Unit, similar to what is presently envisaged for subduction channels (Trommsdorff *et al.*, 2000; Engi *et al.*, 2001; Angiboust *et al.*, 2011). On the other hand, the recent finding of superimposed Variscan and Alpine high-pressure ages in the same Adula eclogite sample, led Herwartz *et al.* (2011) to conclude that tectonic mixing of Adula gneiss with eclogite-facies rocks is Variscan and that the mélange behaved as a coherent unit during Alpine subduction. The mechanisms, timing and P–T conditions of high-pressure rock emplacement in the Adula gneiss and mélange formation are thus a matter of debate. Similarly, the timing of Gagnone peridotite emplacement within the host felsic rocks, whether before or after the subduction peak, still needs to be resolved.

FIELD OCCURRENCE

All peridotite bodies from Cima di Gagnone are reported in Fig. 1, redrawn after Pfiffner & Trommsdorff (1998). The starred outcrops Mg31, Mg160, Mg163 and Mg304 were sampled and investigated in this study. Several samples were provided by the late Volkmar Trommsdorff; all samples labelled with the number 09 were collected during fieldwork in 2009.

Our work focuses on the garnet peridotite and chlorite harzburgite [the chlorite peridotite of Trommsdorff (1990)]. Chlorite harzburgite is the dominant rock type in the Gagnone area: key outcrops are Mg31, Mg163 and Mg304 (Fig. 1). The first two outcrops consist of foliated chlorite harzburgite and dunite that include dike-like boudinaged rodingite (Fig. 2a and b) showing red garnet-rich cores and black amphibole rims (blackwalls). Inside the chlorite harzburgite body Mg163, eclogites and coarse-grained calc-silicate rocks (derived from ophicarbonate precursors) are also present together with rodingites. Many foliated harzburgites and dunites display syntectonic olivine, chlorite and orthopyroxene. This three-phase assemblage is locally joined by magnesite and F-bearing titanian clinohumite. The olivine–orthopyroxene–chlorite foliation of the harzburgite flows around boudinaged metarodingite and mafic eclogite, testifying that the metarodingite and eclogite were more competent than the host ultramafic rock at the time of eclogitization (Fig. 2a and b). Outcrop Mg304 mostly consists of undeformed chlorite harzburgite with randomly oriented centimetre-sized orthopyroxene grains in a matrix of olivine and subordinate chlorite (Fig. 2c); these rocks also display fresh F–Ti clinohumite and magnesite. Undeformed harzburgite domains are locally present in deformed chlorite harzburgite. In outcrops Mg31, Mg161, Mg162 and Mg163, chlorite harzburgite and olivine-rich (dunitic) domains form layered structures; locally dunite cuts the harzburgite in structures comparable with those observed in mantle peridotites affected by reactive porous melt flow and peridotite replacement by dunite channels. Retrograde field features are represented by the black amphibole haloes around rodingites, related to amphibolite-facies rehydration of these rocks (Fig. 2b; Evans *et al.*, 1979), by talc, tremolite and cummingtonite growth in ultramafic rocks, and by red anthophyllite veins cutting all structures in dunite and chlorite harzburgite.

As noted in several previous studies (e.g. Evans & Trommsdorff, 1978), garnet peridotite is mainly exposed at outcrop Mg160, on the western side of Cima di Gagnone, along the cliff just south of Passo Scaiee (Fig. 1). The outcrop mostly consists of deformed grey chlorite harzburgite. Foliated peridotite with green clinopyroxene, pink garnet, olivine and orthopyroxene (Fig. 2d) forms the core of the body. Neither eclogite nor rodingite have been observed in outcrop, although many rodingite blocks occur in the fallen debris below the outcrop. In the Mg160 peridotite body, the foliation involves the garnet-bearing assemblage and appears to be syn-eclogitic (Fig. 2d). Pink garnet

occurs in centimetre-thick and several centimetre-long layers; coarse centimetre-sized crystals locally present in these rocks may correspond to veins or fluid-related pockets and conduits. The garnet-bearing layers are parallel to the foliation (Fig. 2d) and are also enriched in green clinopyroxene: these domains are peculiar to outcrop Mgl60. Formation of garnet + clinopyroxene-rich rock volumes can originate from tectonic dismemberment of previous pyroxenites, which are locally preserved as green bands that are a centimetre thick and a few centimetres long (Fig. 2e). As a consequence, the garnet-rich domains in the Mgl60 Gagnone garnet peridotite can be related to shearing and deformation of a layered mantle precursor. Fine-grained garnet grains also crystallize in domains distant from the clinopyroxene- and garnet-rich rock domains. The green and red garnet peridotite grades into a grey chlorite and amphibole-bearing harzburgite that corresponds to a retrograde overgrowth of the garnet-bearing rocks (Evans & Trommsdorff, 1978; see petrography section) and that constitutes a significant part of this peridotite body.

SAMPLE PETROGRAPHY AND MICROSTRUCTURES

Chlorite harzburgite

Eight chlorite harzburgite and associated dunite samples were investigated for their petrography, bulk-rock major and trace element compositions, and mineral chemistry (Mg304 92-1; Mg304 92-2; Mg304-09-03; Mg31-09-01; Mgl63-09-05; Mgl63-09-06D; Mgl63-09-06H; Mgl63-09-07). Table 1 summarizes the mineral assemblages and the metamorphic events recognized in these rocks. Chlorite harzburgite occurs in deformed (Fig. 2b) and relatively undeformed varieties (Figs 2c and 3a). The latter (Mg304 92-1; Mg304 92-2) display coarse-grained textures with randomly oriented idiomorphic orthopyroxene, olivine, interstitial chlorite locally associated with minor modal amounts of F-bearing Ti-clinohumite, magnesite and diopside (also detected by X-ray diffraction of sample Mg304 92-2). Fluorine-bearing titanian clinohumite intergrown with orthopyroxene and olivine (Fig. 3b) corresponds to clinohumite described by Evans & Trommsdorff (1983) in their samples labelled Mg304. Magnesite is another phase that may belong to the peak assemblage of the chlorite harzburgites. Common opaque minerals are magnetite and chromite, frequently associated with sulfides (pentladite and pyrrhotite). In samples Mg304 92-1 and Mg304 92-2 sulfides occur either as inclusions (of several hundred micrometres in size) in olivine and orthopyroxene, or as smaller grains (up to 100 μm) between high-pressure silicates (Supplementary Data Fig. S1; all supplementary data are available for downloading at http://www.petrology.oxfordjournals.org). Electron microscope studies of Ti-clinohumite from sample Mg304 92-1 revealed the presence of relict monophase inclusions of antigorite, talc and chlorite (Fig. 3c). Talc and chlorite inclusions are also present in olivine and orthpyroxene. These features point to serpentine, chlorite and talc assemblages that pre-date the eclogite-facies paragenesis. Olivine and orthopyroxene host abundant multiphase inclusions, the morphology and also textural position of which strongly resemble those of primary fluid-derived inclusions in the Almirez chlorite harzburgite (Scambelluri *et al.*, 2001). In sample Mg304 92-1, detailed electron microscopy has revealed the occurrence of fine-grained (replacive) orthopyroxene that partly overgrows and replaces the coarse olivine associated with the coarse orthopyroxene and chlorite that form the main rock structure and rock-forming assemblage.

The foliated chlorite harzburgite displays abundant platy olivine associated with orthopyroxene (generally less abundant than olivine) and chlorite (Fig. 3d). Minor amounts of diopside were detected through X-ray powder diffraction of sample Mg31-09-01. In deformed samples the chlorite is syn-tectonic and parallels the main foliation (Fig. 3d). These rocks correspond to the chlorite peridotite 1 of Trommsdorff (1990). In outcrops Mg31 and Mgl63 the peridotite foliation parallels the high-pressure foliation of eclogite and metarodingite that wraps around eclogitic boudins; this indicates that the chlorite assemblage represents the peak high-pressure paragenesis. Some deformed chlorite harzburgites display relict coarse othopyroxene porphyroclasts in a chlorite–olivine–orthopyroxene rock matrix (Fig. 3e), suggesting that deformation probably post-dates the growth of coarse, randomly oriented ortopyroxene, probably in the same undeformed structures as shown in Fig. 3a. Both deformed and undeformed chlorite harzburgite from outcrops Mg31, Mgl63 and Mg304 thus contain primary chlorite coexisting with olivine and orthopyroxene in the main metamorphic assemblage. Dunite layers associated with the chlorite harzburgite consist of dominant platy olivine and minor chlorite parallel to the foliation. In the chlorite harzburgite (deformed and undeformed) and dunite, tremolitic amphibole occurs as coarse- and fine-grained retrograde needles overgrowing, in association with talc and cummingtonite, the peak assemblage (Fig. 3f).

Garnet peridotite

Twelve garnet peridotites and their retrogressed varieties (Mgl60 96-1; Mgl60 96-2; Mgl60 4-8; Mgl60 4-3; Mgl60 4-5; Mgl60-09-02; Mgl60-09-05; Mgl60-09-06C; Mgl60-09-07; Mgl60-09-10; Mgl61 92-1; Mgl61 92-1B) were investigated for their petrography, bulk-rock and mineral composition. The selected samples cover the whole peridotite history, from pre-eclogitic stages to retrogression. The mineral assemblages and the evolution of these rocks are given in Table 1. All samples are foliated, with olivine, orthopyroxene, clinopyroxene, garnet and

Table 1: Mineral assemblages and key minerals of prograde, peak and post-peak stages recognized in each sample

Sample		Mineral assemblages	Index minerals		
			Pre-eclogitic	Eclogitic	Post-eclogitic
Chlorite harzburgite					
Mg304 92-1	Undeformed	Ol, Opx, Chl, F-TiCl, Mt, Chr, Sulf, Cpx, Serp, Tlc, Tr, Cm	Ser, Tlc, Chl	Ol, Opx, Chl, F-TiCl	Tlc, Tr, Cm, Chl
Mg304 92-2	Undeformed	Ol, Opx, Chl, Mgs, Mt, Chr, Sulf, Dol, Tlc, Tr, Cm		Ol, Opx, Chl, Mgs	Tlc, Tr, Cm, Chl, Dol
Mg304 09-03	Undeformed	Ol, Opx, Chl, Tlc, Tr, Cm, Mt, Sulf		Ol, Opx, Chl	Tlc, Tr, Cm, Chl
Mg31 09-01	Foliated	Ol, Opx, Chl, Tlc, Tr, Cm, Opaque		Ol, Opx, Chl	Tr, Tlc
Mg163 09-06H	Foliated	Ol, Chl, Opx, Tlc, Tr, Cm, Opaque		Ol, Opx, Chl	Tlc, Tr, Chl, Cm
Mg163 09-07	Foliated	Ol, Chl, Opx, Tlc, Tr, Cm, Opaque		Ol, Opx, Chl	Tlc, Tr, Cm, Chl
Mg163 09-05	Foliated	Ol, Chl, Opx, Tlc, Tr, Cm, Opaque		Ol, Opx, Chl	Tlc, Tr, Cm, Chl
Mg163 09-06D	Foliated (R)	Ol, Tlc, Tr, Chl, Mgs, Opx, Cm, Dol, Opaque		Ol, Chl, Opx, Mgs	Tlc, Tr, Chl, Cm, Dol
Garnet peridotite					
Mg160 96-1	Foliated grt-rich	Ol, Opx, Mg-Hbl, Grt, Cpx, Chl, Mt, Sp, Tr	Opx, Cpx	Ol, Opx, Mg-Hbl, Grt, Cpx, Ilm	Mg-Hbl, Opx, Sp, Chl, Tr
Mg160 96-2	Foliated grt-rich	Ol, Opx, Mg-Hbl, Grt, Cpx, Mt, Chl, Ilm, Sp, Tr	Opx, cpx, TiCl	Ol, Opx, Mg-Hbl, Grt, Cpx, Ilm	MgHbl, Opx, Sp, Chl, Tr
Mg160 4-8	Foliated grt-rich	Ol, Opx, Mg-Hbl, Grt, Cpx, Mt, Chl, Ca-amph, Tr, Tlc	Chl, Opx, Ca-amp, Cpx	Ol, Opx, Mg-Hbl, Grt, Cpx	Mg-Hbl, Opx, Sp, Chl, Tr, Tlc
Mg161 92-1	Foliated grt-rich	Ol, Opx, Mg-Hbl, Grt, Cpx, Mt, Ilm, Sulf, Chl,Tr	Opx, cpx, TiCl	Ol, Opx, Mg-Hbl, Grt, Cpx, Ilm	Mg-Hbl, Opx, Sp, Chl, Tr
Mg161 92-1B	Foliated grt-rich	Ol, Opx, Mg-Hbl, Grt, Cpx, Mt, Sp	Opx, Cpx	Ol, Opx, Mg-Hbl, Grt, Cpx	Mg-Hbl, Opx, Sp, Chl
Mg160 09-10G	Foliated grt-rich	Ol, Opx, Mg-Hbl, Grt, Cpx, Chl, Mt, Tlc		Ol, Opx, Mg-Hbl, Grt, Cpx	Mg-Hbl, Opx, Sp, Chl
Mg160 09-10	Foliated	Ol, Opx, Mg-Hbl, Grt, Cpx, Chl, Mt, Tlc		Ol, Opx, Mg-Hbl, Grt, Cpx	Mg-Hbl, Opx, Sp, Chl
Mg160 09-02	Foliated	Ol, Opx, Mg-Hbl, Grt, Cpx, Chl, Mt, Ca-amph, Tr, Chl, Tlc		Ol, Opx, Mg-Hbl, Grt, Cpx	Ca-amph, Tr, Chl, Tlc
Mg160 09-05	Foliated (R)	Ol, Opx, Mg-Hbl, Chl, Mt, Ca-amph, Tr, Tlc		Ol, Opx, Mg-Hbl	Ca-amph, Tr, Chl, Tlc
Mg160 09-06C	Foliated (R)	Ol, Opx, Mg-Hbl, Chl, Mt, Ca-amph, Tr, Tlc		Ol, Opx, Mg-Hbl	Ca-amph, Tr, Chl, Tlc
Mg160 09-07	Foliated (R)	Ol, Opx, Mg-Hbl, Chl, Mt, Ca-amph, Tr, Tlc		Ol, Opx, Mg-Hbl	Ca-amph, Tr, Chl, Tlc

Ol, Olivine; Opx, orthopyroxene; Cpx, clinopyroxene; Grt, garnet; Mg-Hbl, Mg-hornblende; TiCl, Ti-clinohumite; F-TiCl, fluorine-bearing Ti-clinohumite; Chl, chlorite; Mgs, magnesite, Dol, dolomite, Ser, serpentine; Tlc, talc; Mt, magnetite; Chr, chromite, Sulf, sulfides, Opaque, undistinguished opaque minerals; Tr, tremolite, Cm, cummingtonite; Ca-amph, calcic amphibole; (R), retrogressed sample.

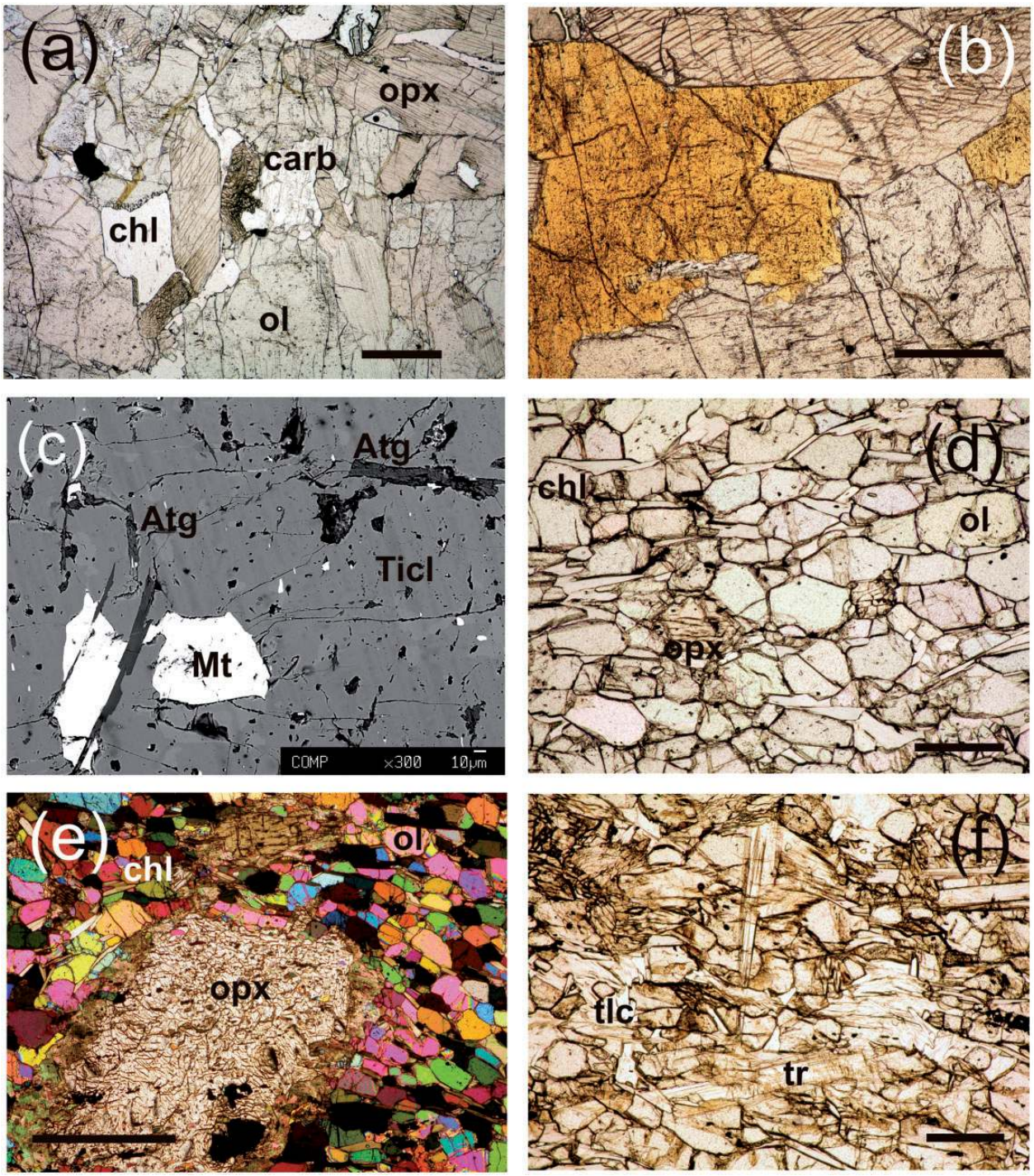

Fig. 3. Photomicrographs of chlorite harzburgites. In (a, b, d–f) scale bars represent 500 μm. (a) Undeformed chlorite harzburgite (see Fig. 2c) showing coarse orthopyroxene and olivine coexisting with chlorite. Carbonate (magnesite) and F-bearing Ti-clinohumite can be present in the assemblage (samples Mg304 92-1 and Mg304 92-2; from outcrop Mg304). (b) Detail of sample Mg304 92-1, showing coarse F-bearing Ti-clinohumite coexisting with orthopyroxene and olivine. Clinohumite hosts inclusions of antigoritic serpentine, illustrated in the scanning electron microscope image (c). (d) Platy olivine, oriented orthopyroxene and chlorite flattened along the main high-pressure foliation (sample Mg3l 09-0l; from outcrop Mg3l; see Fig. 2a and b). (e) Coarse relict orthopyroxene replaced by a high-pressure olivine, chlorite, orthopyroxene foliation (from northern end of outcrop Mgl63), showing that an earlier stage of low-strain crystallization can be followed by deformation. (f) Retrograde tremolite (tr) and talc (tlc) overgrowing the high-pressure olivine, chlorite, orthopyroxene foliation.

amphibole (Mg-hornblende) oriented parallel to the main foliation. Opaque minerals are rarer compared with the chlorite harzburgites; they occur as tiny grains and in most cases are oxides; sulfides have been observed only locally. The most frequent oxide is ilmenite intergrown with olivine at the expense of former Ti-clinohumite. The Gagnone garnet peridotite can display high modal amounts of garnet (from about 15 to 25 vol. %) in some layered domains (e.g. Mgl60-09-10G; Fig. 2d) close to domains where modal garnet is much less (e.g. Mgl60-09-10). Garnet develops as a coarse poikiloblastic phase growing parallel to the foliation and enclosing oriented rock-forming minerals (Figs 2d and 4a, b). Poikiloblastic garnet can host mono-mineralic inclusions of pre-peak mineral phases, although it equilibrated with the matrix minerals. The oldest minerals recognizable in garnet correspond to fine-grained, sub-microscopic mono-phase inclusions of orthopyroxene, chlorite, Ca-amphibole and spinel, identified by scanning electron microscopy (Fig. 4c). These minerals evidence a low-pressure hydrated assemblage that pre-dates development of the chlorite-free, garnet-bearing foliation. The large garnet poikiloblasts also include coarse to medium-sized olivine, ortho- and clinopyroxene deformed in old foliations and folds (Fig. 4a), which probably postdate the fine-grained chlorite-bearing assemblage. Pfiffner & Tromsdorff (1998) and Morten & Trommsdorff (2003) have reported the presence of coarse prograde Ca-amphibole inclusions inside the poikilitic garnet. In our study, we did not find such coarse Ca-amphibole inclusions in garnet; the only pre-garnet amphibole (not analyzed because of its small size) recognized is represented by the above-described fine-grained inclusions shown in Fig. 4c. From a textural point of view, coarse Mg-hornblende appears to be stable during eclogite-facies metamorphism and during retrogression. This amphibole type occurs both as syn-tectonic idiomorphic crystals parallel to the main foliation (Fig. 4d) and as a secondary phase replacing the medium to coarse clinopyroxene inclusions in poikiloblastic garnet and the clinopyroxene crystals along the foliation. Several samples (e.g. Mgl60 96-1, Mgl60 96-2) also display olivine intergrown with vermicular ilmenite (Fig. 4e), a microstructure attributed to the breakdown of precursor Ti-clinohumite (Evans & Trommsdorff, 1983).

A large part of outcrop Mgl60 consists of chlorite harzburgite, which replaces former garnet-peridotite (e.g. Mgl60-09-02; Mgl60-09-05; Mgl60-09-06C; Mgl60-09-07). In these samples the garnet rims are overgrown by retrograde symplectites (kelyphites) with fine-grained lamellae of orthopyroxene, amphibole and spinel. In the most transformed domains, garnet is fully replaced by post-kinematic chlorite that is randomly oriented and does not follow the main foliation (Fig. 4f). This implies static retrograde re-hydration of garnet-bearing rocks to form post-peak chlorite harzburgite [the chlorite peridotite 2 of Trommsdorff (1990)]. Formation of this retrograde chlorite harzburgite variety might have destroyed much of the eclogitic garnet-facies assemblages in the area. Textures thus indicate that these rocks types are different from the chlorite harzburgite 1 described above.

ANALYTICAL METHODS

Bulk-rocks

Bulk-rock major element analyses were performed by lithium metaborate–tetraborate fusion inductively coupled plasma (ICP) (major elements) techniques at the Actlabs Laboratories (Western Ontario, Canada; http://www.actlabs.com). Trace element concentrations [Li, Cd, Co, Ni, Cu, As, Rb, Sr, Y, Zr, Nb, Cs, Ba, rare earth elements (REE), Hf, Ta, Pb, Th, U and W] were determined by inductively coupled plasma mass spectrometry (ICP-MS) using a Thermo Finnigan Element2 High Resolution system at Géosciences Montpellier (University Montpellier 2, France). Most elements were measured in low-resolution mode ($m/\Delta m$ ~400), except for Co, Ni, and Cu that were analysed in medium-resolution mode ($m/\Delta m$ ~4000) and As, measured in high-resolution mode ($m/\Delta m$ ~10 000). The analytical procedure has been described by Ionov *et al.* (1992) and Godard *et al.* (2000). The method involves dissolution of 100 mg aliquots in an $HF–HClO_4$ mixture and dilution of the solution by a factor of 2000. Indium and bismuth were used as internal standards during ICP-MS measurements. Calibration was based on Merck multi-element standard solutions, except for Nb and Ta. To avoid memory effects owing to the introduction of concentrated Nb–Ta solutions in the instrument, Nb and Ta concentrations were determined by using, respectively, Zr and Hf as internal standards. This technique is similar to that described by Jochum *et al.* (1990) for the determination of Nb by spark-source mass spectrometry. To assess the analytical method, we determined the trace element concentrations of UBN, a serpentinite that contains high Ba ($27 \pm 1{\cdot}8$ ppm) and relatively low Eu (83 ± 10 ppb) (GEOREM, http://georem.mpch-mainz.gwdg.de/). The values obtained are $87{\cdot}3 \pm 1{\cdot}7$ ppb Eu and $26{\cdot}2 \pm 0{\cdot}3$ ppm Ba, comparable with the recommended values of Govindaraju (1994) (Ba = 97 ppm; Eu = 0·08 ppm), confirming that the analytical method provides reliable data. Detection limits, procedural blanks and values obtained for the rock standards are reported in Supplementary Data Appendix 1.

Mineral compositions

Major element mineral compositions were determined by electron probe microanalysis using the JEOL 8200 Superprobe at the Dipartimento di Scienze della Terra, University of Milano; quantitative elemental analyses were performed by wavelength-dispersive analysis at

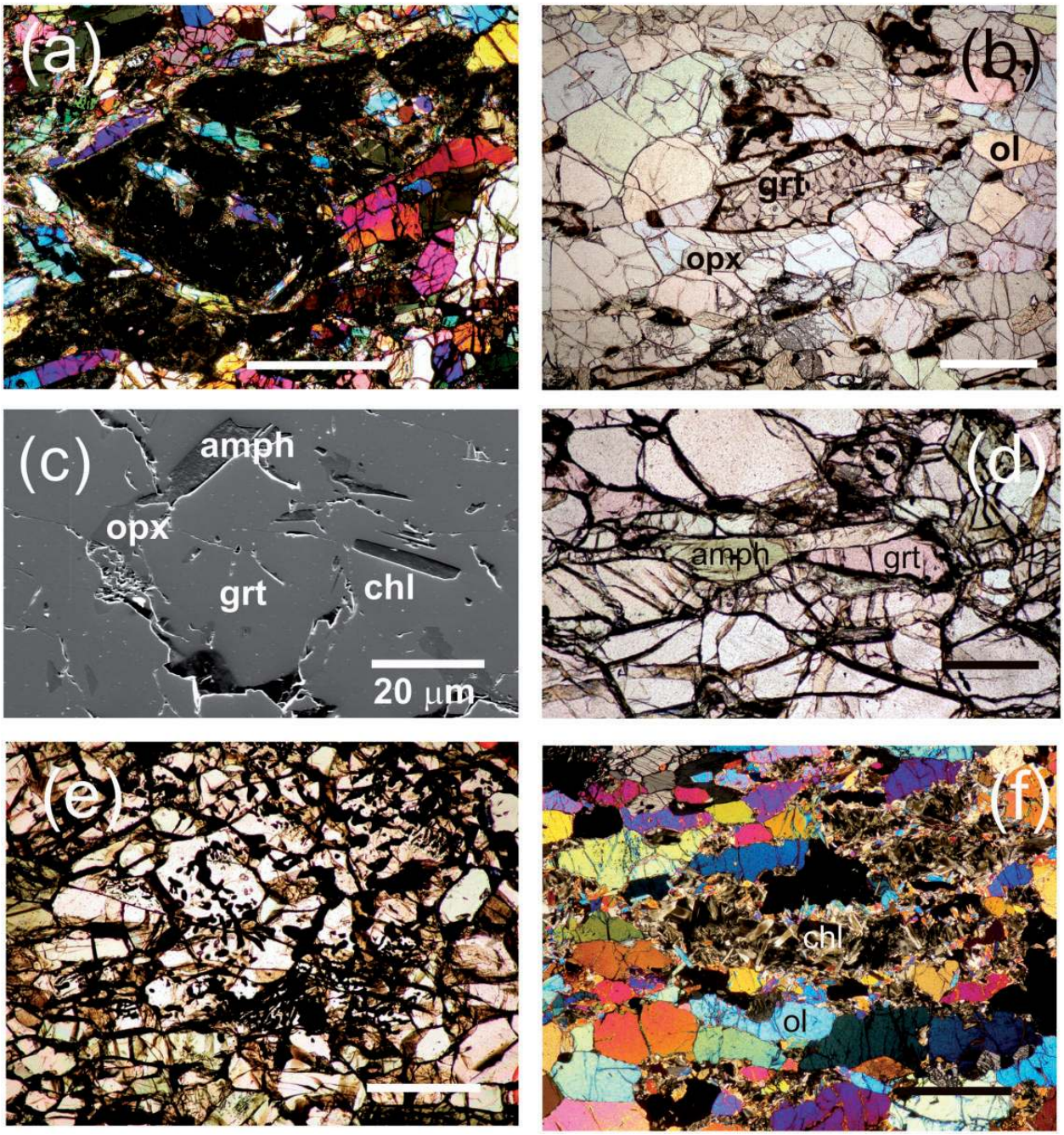

Fig. 4. Photomicrographs of garnet peridotites. In (a, b, d–f) scale bars represent 500 μm. (a) Poikiloblastic garnet overgrowing an orthopyroxene, olivine and clinopyroxene foliation (sample Mgl60 96-1). (b) High-pressure foliation in the garnet peridotite. (c) Inclusions of prograde chlorite, amphibole and orthopyroxene hosted in a poikilobastic garnet (sample Mgl60 4-8). (d) Mg-hornblende along the garnet-bearing high-pressure foliation. (e) Olivine plus vermicular ilmenite pseudomorphous after Ti-clinohumite. (f) Randomly oriented, retrograde chlorite replacing garnet in garnet peridotite sample Mgl60 09-02.

15 kV and 60 nA. Natural silicates were used as standards: Mg–Al–Si on pyrope, Fe on almandine, Ca on grossular, Mn on rhodonite, Cr on chromite, and Ti on ilmenite. A PhiRhoZ routine was used for matrix correction. Scanning electron microscopy and analyses of mineral inclusions in olivine were carried out at the University of Genova in energy-dispersive mode with a SEM VEGA3 TESCAN operating at 15 kV and equipped with an EDAX APOLLO XSDD energy-dispersive X-ray spectrometer. The accelerating potential was 15 kV, the beam current

20 nA, the beam diameter ~2 μm and counting time 100 s. Natural mineral and glass standards were employed.

Mineral trace element analyses were conducted by laser ablation (LA)-ICP-MS with a Geolas Pro 2006 193 nm ArF excimer laser coupled to an Elan DRC-e ICP-MS instrument at the University of Bern. Instrument optimization procedures, analytical strategies and data reduction closely followed those reported by Spandler *et al.* (2011) and Pettke *et al.* (2012). Beam sizes were chosen as large as possible (up to 120 μm diameter) to lower the limits of detection, calculated using the new formulation in Pettke *et al.* (2012). External standardization was against the NIST SRM610 glass, employing values from Jochum *et al.* (2011) and Spandler *et al.* (2011). Internal standardization used major element concentrations determined by electron microprobe analysis measured in mineral domains close to the laser spots (CaO for clinopyroxene, garnet and amphibole; MgO for olivine, orthopyroxene, Ti-clinohumite, chlorite and magnesite). Data reduction employed the SILLS program (Guillong *et al.*, 2008). Ablation rates were tuned to *c.* 0·15 μm per pulse via attenuation of the laser output beam; the laser repetition rate was 10 Hz. Background intervals were about 1 min, and signal intervals were set such as to avoid contributions from inclusions. Uncertainties on the external reproducibility are of the order of 1–2% (2SD) unless signal intensities were low, where counting statistics uncertainties increase to a few tens of per cent near limits of detection. Analytical accuracy was regularly monitored by measurement of GSD-1g basalt glass, accepting that mineral standard reference materials (SRM) to be used here as secondary standards are not available to date. These data show that for some less frequently analysed elements, including B, As and Sb, overall accuracy is often limited by homogeneity (e.g. Eggins & Shelley, 2002) and/or knowledge of the reference element concentrations in the external standard reference material [for a detailed evaluation see, e.g. Spandler *et al.* (2011)] and may increase to 10% 2SD uncertainty.

RESULTS

Bulk-rock compositions

Major elements

The major element compositions of the Gagnone peridotites are reported in Table 2 and illustrated in Figs 5 and 6. These figures also show, when available, the data by Pfiffner (1999). The analyzed samples have variable loss on ignition (LOI), ranging from very low values to maximum values of 5·66 wt % for a chlorite harzburgite. The volatile-free compositions plotted in Figs 5 and 6 show the variation of major (CaO, Al_2O_3) and trace (V, Sc, Li) elements vs MgO, which are consistent with the trends reported in the literature. The entire sample set is characterized by significant compositional variability, showing a continuous range from very depleted compositions, with low CaO (0·3–1·3 wt %) and Al_2O_3 (0·18–1·76 wt %), to compositions enriched in CaO and Al_2O_3 up to values exceeding the Primitive Mantle (PM; values after McDonough & Sun, 1995). The highest CaO (4–4·5 wt %) and Al_2O_3 (5–6 wt %) pertain to the garnet-rich peridotite. Such high values indicate that CaO and Al_2O_3 were added to the peridotite system. In Figs 5 and 6 these oxides display negative correlations with MgO that varies from 35 wt % in garnet-rich rocks to 47 wt % in dunitic samples. The large spread in bulk-rock MgO is not accompanied by a comparable variation of the bulk-rock Mg number of all the investigated peridotites, showing rather constant values (Mg# 0·89–0·91; Table 1). Several chlorite harzburgite and dunite samples analyzed here, together with samples reported by Pfiffner (1999), plot below the CaO, Al_2O_3 (and Na_2O) depletion trend shown in Fig. 5 (see arrows in the figure). These anomalously low abundances, recorded by several samples, probably reflect previous serpentinization, which caused preferential loss of these components owing to pyroxene replacement by Ca-, Al- and alkali-free serpentine.

Trace elements

Variations in V, Sc and Li within the analyzed sample suite are shown in Fig. 6 together with the available data of Pfiffner (1999). All samples display negative correlations between MgO and the fusible trace elements Sc and V; the most refractory elements Co, Ni and Cr (not shown in Fig. 6) positively correlate with MgO. These variations are consistent with the major element trends of Fig. 5. The Sc contents of some chlorite harzburgites plot below the depletion trends shown by the majority of samples; as for CaO and Al_2O_3, these anomalously low contents can be related to pyroxene replacement by serpentine, causing loss of such pyroxene-hosted components.

The REE compositions of the Gagnone peridotites are reported in Table 1 and in Fig. 7a and c. The garnet-bearing peridotites have flat heavy REE (HREE) to middle REE (MREE) patterns, with moderate depletion in light REE (LREE). The absolute concentrations range from 0·22 to 0·4 times PM for the LREE, and from 0·31 to 1·39 PM for MREE to HREE. The highest REE concentrations are characteristic of the garnet-rich peridotites showing the highest CaO, Al_2O_3, Na_2O, Sc, V, Ti and lowest MgO (samples Mg160-09-10G; Mg160-4-8; Mg161-92-1). Intermediate REE contents occur in garnet peridotites with intermediate CaO, Al_2O_3 and Na_2O (Mg160-96-2; Mg160-09-06C); the lowest REE contents occur in samples with the lowest CaO, Al_2O_3 and Na_2O (Mg160-09-10; Mg160-09-07; Mg160-09-02; Mg160-09-05). A direct relation between REE content and degree of major element depletion and/or melt–rock reaction is therefore established in Figs 5–7. However, this is not coupled to variable LREE/MREE fractionation, because

Table 2: Bulk-rock major and trace element analyses of garnet peridotites and chlorite harzburgites

	Mg160 09-10G Grt per	Mg160 96-1 Grt per	Mg160 96-2 Grt per	Mg160 4-8 Grt per	Mg161 92-1 Grt per	Mg160 09-02 Grt per	Mg160 09-05 Grt per	Mg160 09-06C Grt per	Mg160 09-07 Grt per	Mg160 09-10 Grt per	Mg163 09-05 Chl Hz	Mg163 09-07 Chl Hz	Mg31 09-01 Chl Hz	Mg163 09-06D Dunite	Mg163 09-06H Chl Hz	Mg304 92-1 Chl Hz	Mg304 92-2 Chl Hz	Mg304 09-03 Chl Hz
SiO_2	44·35	44·93	43·81	44·91	45·22	43·81	43·24	43·30	42·32	43·45	42·99	42·50	44·66	41·40	42·16	44·75	43·00	42·38
Al_2O_3	5·06	5·31	3·90	4·87	5·49	2·74	2·18	2·72	2·36	2·82	1·52	0·74	0·93	1·34	1·76	0·18	0·68	0·77
Fe_2O_3	8·92	8·75	8·76	8·62	8·26	8·84	9·09	8·78	8·82	9·12	8·89	8·79	9·23	9·55	9·54	10·62	8·82	8·59
MnO	0·15	0·14	0·13	0·13	0·14	0·13	0·13	0·13	0·13	0·12	0·13	0·13	0·14	0·12	0·14	0·06	0·07	0·13
MgO	36·38	35·33	40·15	36·48	36·05	40·91	40·88	39·72	40·94	41·04	42·78	45·56	42·47	41·15	41·87	42·81	39·76	45·09
CaO	4·28	4·07	2·88	4·02	4·21	2·50	2·17	2·62	2·12	2·24	1·13	0·03	0·08	0·08	1·33	1·11	2·88	0·18
Na_2O	0·18	0·21	0·16	0·35	0·22	0·16	0·03	0·03	0·10	0·10	0·03	0·01	0·02	0·01	0·01	0·03	0·03	<0·01
K_2O	0·03	<0·01	<0·01	0·02	<0·01	0·04	0·03	0·03	0·05	0·03	0·03	0·02	0·02	0·03	0·06	0·05	<0·01	0·02
TiO_2	0·19	0·20	0·11	0·15	0·18	0·09	0·04	0·10	0·16	0·10	0·02	0·03	0·02	0·09	0·04	0·02	0·02	0·03
P_2O_5	0·01	0·01	0·01	0·02	<0·01	0·01	0·01	0·01	0·01	0·01	0·01	0·01	0·01	0·01	0·01	<0·01	<0·01	0·01
Cr_2O_3	0·33	n.d.	n.d.	0·34	n.d.	0·40	0·37	0·35	0·34	0·37	0·39	0·39	0·38	0·40	0·36	n.d.	n.d.	0·40
LOI	0·00	0·00	0·00	0·35	0·00	0·10	2·02	2·74	1·25	0·00	1·71	1·25	0·86	5·66	2·54	0·13	5·08	1·36
Total	99·34	98·59	99·65	100·26	99·46	99·73	100·20	100·50	98·59	98·76	99·62	99·46	98·82	99·84	99·81	99·77	100·30	98·95
Mg #	0·89	0·89	0·90	0·89	0·90	0·90	0·90	0·90	0·90	0·90	0·91	0·91	0·90	0·90	0·90	0·89	0·90	0·91
Li	1·804	n.d.	1·95	2·19	2·00	2·46	4·36	2·99	3·14	2·08	4·74	6·52	3·26	3·30	3·02	2·86	1·76	4·67
Mo	0·085	n.d.	0·023	0·048	0·031	3·269	0·330	0·391	0·087	3·038	4·035	0·812	0·077	0·104	0·208	0·047	0·039	0·118
Cd	0·050	n.d.	0·038	0·045	0·051	0·038	0·028	0·029	0·025	0·042	0·052	0·021	0·031	0·023	0·038	0·011	0·015	0·016
Sb	0·023	n.d.	0·019	0·038	0·028	0·028	0·095	0·113	0·193	0·030	0·047	0·072	0·098	0·078	0·055	0·018	0·013	0·081
W	0·127	n.d.	0·083	0·169	0·099	0·095	0·436	0·821	0·377	0·071	0·223	0·251	0·384	0·928	0·935	0·403	0·288	0·203
Sc	17·67	n.d.	14·72	17·70	18·58	13·02	11·30	13·00	9·14	11·22	10·95	7·07	8·15	7·12	9·15	3·61	5·79	7·66
V	83·98	n.d.	72·78	84·81	90·56	60·78	51·98	59·95	55·22	55·18	60·94	36·56	36·58	43·18	59·60	27·25	36·03	28·72
Co	88	n.d.	94	85	87	97	100	97	83	99	105	111	107	113	87	119	105	110
Ni	1407	n.d.	1550	1353	1377	1636	1678	1605	1408	1601	1753	1886	1850	1844	1426	2104	1988	1919
Cu	28·28	n.d.	31·11	28·69	67·13	25·42	14·00	8·86	18·87	5·43	1·44	2·04	2·26	1·48	2·15	11·56	7·50	1·77
Zn	44·67	n.d.	49·55	44·78	44·16	48·10	47·35	46·35	40·48	52·36	47·22	51·51	61·52	64·50	42·57	78·84	78·54	49·61
As	0·733	n.d.	0·676	1·628	1·105	0·636	2·377	2·561	17·634	0·715	0·738	1·732	1·964	0·519	0·710	1·769	1·055	1·146
Rb	0·168	n.d.	0·133	0·293	0·155	0·432	0·283	0·380	0·335	0·277	0·172	0·228	0·108	0·158	0·172	0·054	0·052	0·092
Sr	18·94	n.d.	14·54	18·37	19·60	11·58	13·43	9·628	14·7	10·7	3·061	0·756	0·596	0·411	2·532	2·035	5·414	1·067
Y	5·26	n.d.	2·96	4·21	5·33	1·89	1·43	2·40	1·91	1·67	0·511	0·124	0·257	0·171	0·800	0·450	1·349	0·232
Zr	6·53	n.d.	5·19	6·75	6·95	3·24	0·81	1·38	1·65	4·19	0·635	0·697	0·473	0·177	0·257	0·208	0·269	0·165
Nb	0·223	n.d.	0·350	0·541	0·247	0·224	0·233	0·380	0·265	0·121	0·453	1·020	0·090	0·536	0·254	0·484	0·183	0·177
Cs	0·026	n.d.	0·025	0·034	0·023	0·040	0·047	0·050	0·037	0·022	0·013	0·026	0·025	0·021	0·022	0·015	0·014	0·012
Ba	1·560	n.d.	1·339	2·670	1·991	2·319	0·936	1·249	2·122	1·746	0·389	0·469	2·461	0·957	0·854	0·611	0·832	0·966
La	0·239	n.d.	0·196	0·233	0·257	0·155	0·159	0·137	0·150	0·142	0·054	0·049	0·040	0·022	0·039	0·041	0·085	0·040
Ce	0·764	n.d.	0·618	0·735	0·846	0·463	0·378	0·381	0·440	0·440	0·158	0·120	0·093	0·055	0·166	0·128	0·329	0·091
Pr	0·133	n.d.	0·106	0·126	0·150	0·074	0·049	0·063	0·000	0·075	0·024	0·015	0·011	0·007	0·000	0·021	0·061	0·012
Nd	0·847	n.d.	0·668	0·795	0·936	0·434	0·240	0·380	0·391	0·470	0·132	0·065	0·050	0·033	0·167	0·116	0·358	0·065
Sm	0·348	n.d.	0·254	0·304	0·382	0·154	0·079	0·158	0·000	0·181	0·037	0·015	0·015	0·009	0·000	0·034	0·118	0·022
Eu	0·159	n.d.	0·114	0·134	0·175	0·064	0·046	0·069	0·000	0·076	0·013	0·004	0·006	0·004	0·000	0·011	0·033	0·008
Gd	0·639	n.d.	0·427	0·541	0·736	0·254	0·151	0·289	0·000	0·277	0·054	0·020	0·025	0·015	0·000	0·048	0·164	0·032
Tb	0·122	n.d.	0·075	0·101	0·137	0·044	0·028	0·054	0·040	0·047	0·010	0·003	0·005	0·003	0·013	0·009	0·029	0·006
Dy	0·942	n.d.	0·544	0·744	0·987	0·331	0·225	0·414	0·289	0·324	0·075	0·019	0·037	0·022	0·110	0·062	0·211	0·037
Ho	0·200	n.d.	0·114	0·164	0·208	0·071	0·053	0·090	0·060	0·064	0·018	0·004	0·009	0·006	0·023	0·014	0·045	0·008
Er	0·541	n.d.	0·306	0·437	0·553	0·192	0·149	0·247	0·171	0·168	0·056	0·014	0·030	0·020	0·080	0·046	0·129	0·025
Tm	0·086	n.d.	0·047	0·068	0·084	0·031	0·025	0·039	0·027	0·025	0·010	0·003	0·006	0·004	0·014	0·008	0·022	0·004
Yb	0·562	n.d.	0·300	0·439	0·553	0·200	0·171	0·254	0·180	0·154	0·076	0·022	0·057	0·040	0·097	0·065	0·152	0·035
Lu	0·096	n.d.	0·051	0·075	0·094	0·034	0·032	0·044	0·031	0·025	0·015	0·005	0·013	0·011	0·018	0·012	0·026	0·007
Hf	0·231	n.d.	0·192	0·257	0·281		0·072	0·101	0·110	0·136	0·014	0·017	0·011	0·007	0·014	0·006	0·007	0·005
Ta	0·013	n.d.	0·016	0·019	0·018	0·009	0·006	0·010	0·022	0·006	0·008	0·030	0·005	0·073	0·017	0·038	0·012	0·007
Pb	1·61	n.d.	1·75	2·34	2·16	1·35	1·34	1·32	1·80	1·44	0·57	0·72	1·22	0·59	0·64	0·73	0·54	0·59
Th	0·014	n.d.	0·012	0·014	0·013	0·017	0·011	0·011	0·017	0·013	0·012	0·032	0·029	0·008	0·012	0·103	0·128	0·022
U	0·004	n.d.	0·005	0·018	0·006	0·009	0·007	0·021	0·013	0·007	0·038	0·027	0·007	0·046	0·023	0·033	0·030	0·042

n.d., not determined.

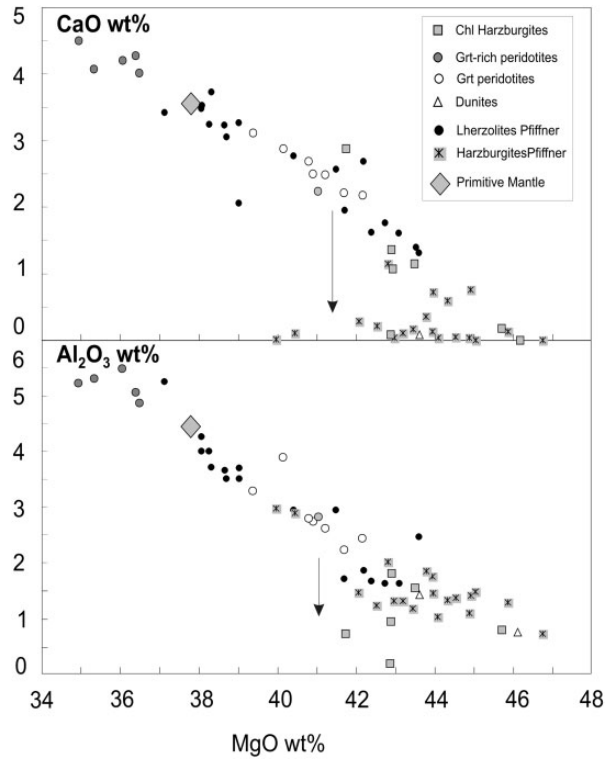

Fig. 5. Bulk-rock CaO and Al_2O_3 (wt %) vs MgO in garnet peridotites and chlorite harzburgites, together with analyses of the same rock types reported by Pfiffner (1999).

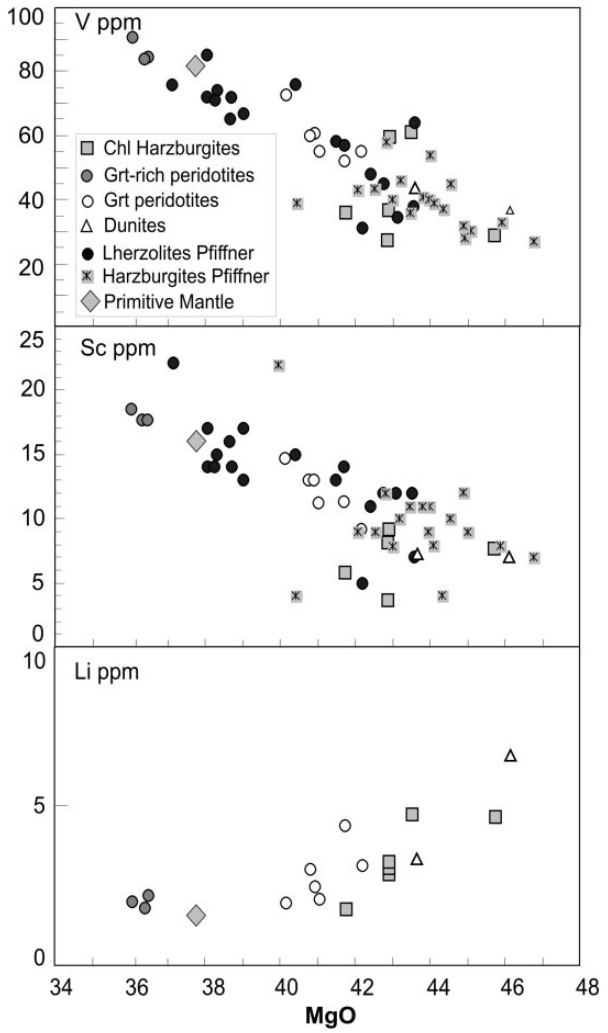

Fig. 6. Bulk-rock variations in V, Sc and Li (ppm) vs MgO (wt %) in garnet peridotites and chlorite harzburgites, together with analyses of the same rock types reported by Pfiffner (1999).

all garnet peridotites exhibit similar moderate LREE depletion (Ce_N/Sm_N 0·53–0·73; Ce_N/Yb_N 0·36–0·75), lower than the fractionation recorded by other, variably depleted, alpine Apennine peridotites (see Discussion).

Chlorite peridotites display much lower absolute REE abundances than garnet peridotites (< 1 PM). Overall, these rocks have spoon-shaped REE patterns, with depletion from HREE to MREE and a slight enrichment in LREE relative to MREE. This is a feature common to all samples except Mg304 92-2, which displays much higher REE contents and a negative Eu anomaly.

The complete set of trace elements analysed in the Gagnone peridotites is reported in the primitive mantle normalized trace element patterns of Fig. 7 together with the average compositions of present-day serpentinized abyssal peridotites from the Mid-Atlantic Ridge, the Hess Deep, Newfoundland and the Mariana fore-arc (Kodolányi *et al.*, 2012). The bulk-rock contents of B and Be plotted in Fig. 7 have been estimated using a mass-balance calculation, based on the trace element composition of single rock-forming minerals combined with the modal amounts of these phases in representative samples. Features common to all the Gagnone samples are prominent positive anomalies in the fluid-mobile elements B, Pb, As, Sb, Be, Li and, to a minor extent, Cs, U and Sr. High contents of Pb, As, Sb and B are a striking feature of the Gagnone rocks. U has variable concentrations in garnet peridotites (from 0·2 to about 1 PM); it is more homogeneous and above 1 PM in the chlorite harzburgites. Arsenic in Gagnone has significantly high concentrations, and in the case of sample Mgl60 09 07, up to 300 times the PM. Another key enrichment involves Li, ranging from 1·8 to 6·5 ppm and positively correlated with MgO (Fig. 6). Another main difference between garnet peridotite and chlorite harzburgite is indicated by the positive anomalies in Ti, Ta and Nb shown by the chlorite harzburgites.

Mineral compositions

Major elements

Microprobe analyses were performed on the main rock-forming minerals of the chlorite harzburgites (orthopyroxene, olivine, chlorite and Ti-clinohumite) and garnet

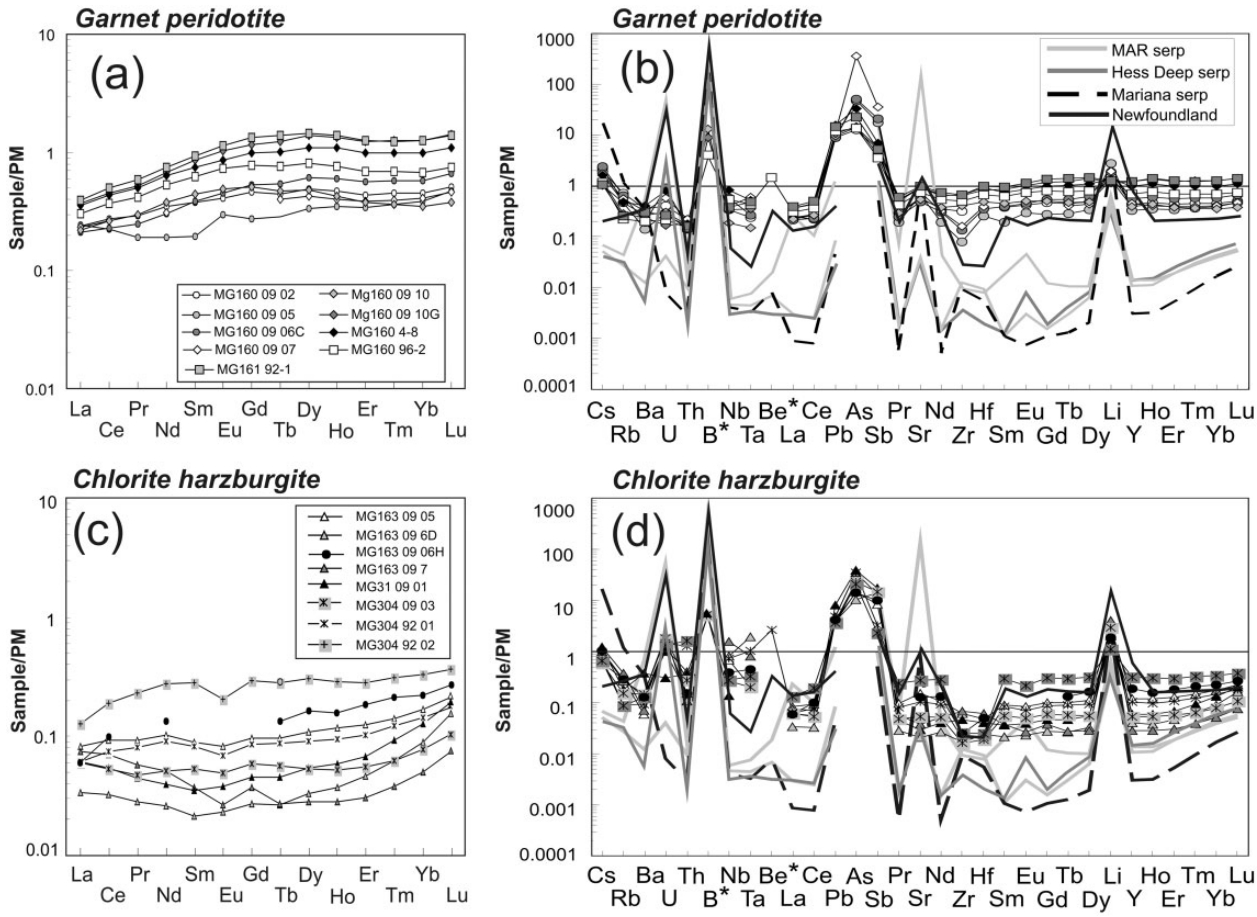

Fig. 7. Primitive Mantle normalized bulk-rock REE and trace element patterns of the Gagnone garnet peridotites (a, b) and chlorite harzburgites (c, d). Shown for comparison are the compositions of present-day oceanic serpentinites from various geotectonic settings: passive margin (Newfoundland), mid-ocean ridge (MAR and Hess Deep), and Marianas forearc [data from Kodolányi *et al.* (2012)]. The bulk-rock B and Be contents were estimated with a mass-balance calculation, using the trace element composition of single rock-forming minerals combined with the modal amounts of these minerals in representative samples.

lherzolites (clino- and orthopyroxene, garnet, olivine and amphibole). The full dataset of major and trace element compositions of the rock-forming minerals of two chlorite harzburgites (Mg304 92-1, Mg304 92-2) and five garnet peridotites (Mgl60 4-8, Mgl60 96-1, Mgl60 96-2, Mgl61 92-1, Mgl61 92-1B) is reported in the Supplementary Data. Compositional variations are shown in Figs 8–12.

In the chlorite harzburgites, orthopyroxene displays negative Si–Mg correlations (Fig. 8), has very low Al_2O_3 (maximum 0·03 wt %), and $X_{Mg} = 0·89$ is the same as that of the coexisting olivine. The fluorine-bearing titanian clinohumite belonging to the peak assemblage in these rocks has $X_{Mg} = 91$, 0·94–1·56 wt % TiO_2 and up to 2·12 wt % F. Comparable compositions were reported by Evans & Trommsdorff, 1983 for Ti-clinohumite in these rock types from Gagnone. The composition of chlorite from the peak assemblage is reported in Supplementary Data Table 1; this chlorite is Cr-bearing and contains 1·14–1·27 wt % Cr_2O_3.

In garnet peridotite, the analysed minerals display variable compositions; clinopyroxene, in particular, shows the largest heterogeneity. Clinopyroxene is characterized by negative Ca–Al and Ca–Na correlations; however, systematic core–rim variations cannot be distinguished in the Ca–Al and Ca–Na trends, as clinopyroxene cores and rims display the same range of compositional variations (Fig. 8). Comparable trends of Na and Al decrease coupled with Ca increase were related by Evans & Trommsdorff (1978) to core–rim variations in clinopyroxene and attributed to Mg-hornblende growth upon pyroxene hydration. This may also reflect a lack of full equilibration of this mineral during metamorphic recrystallization. Orthopyroxene shows negative Si–Al and Si–Mg trends; the variation of Al versus Si is common to all samples and seems to be related to a change in the Tschermak component, although (as observed in clinopyroxene) this is not clearly related to core–rim variations. The variations along the negative Si–Mg trend seem to be related to the bulk

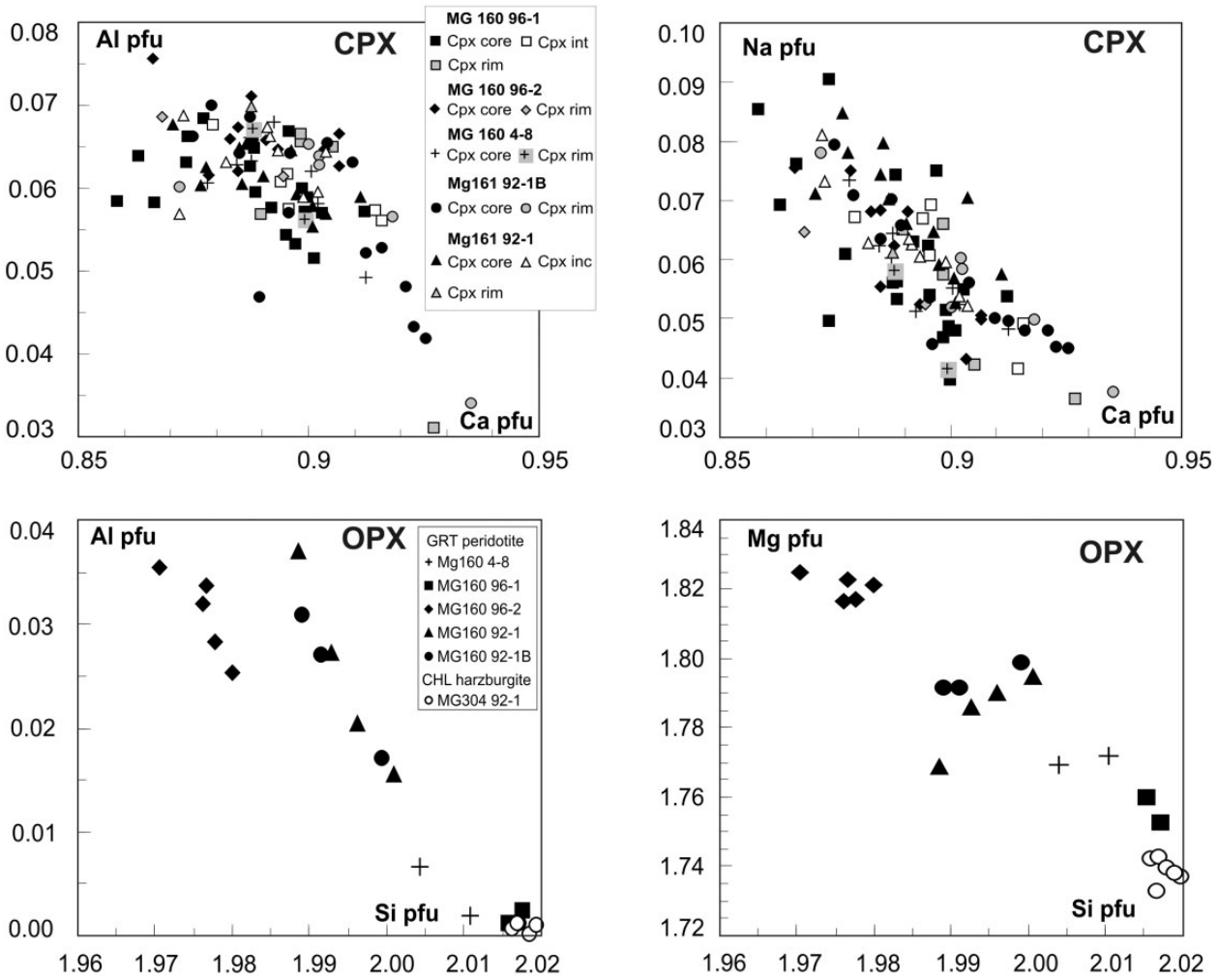

Fig. 8. Major element compositions of clino- and orthopyroxene from the Gagnone peridotites.

samples. Garnet is pyrope-rich, with 61–68% pyrope end-member, 20–25% almandine, 11–13% grossular and 1% spessartine. Figure 9 shows that large poikiloblastic garnet has flat core-to-rim patterns showing small variations in major element concentrations. Garnet from sample Mgl60 96-1A shows a small core-to-rim decrease in pyrope accompanied by an increase in almandine (Fig. 9), whereas grossular and spessartine do not show significant changes. The olivine composition is forsterite 90–92. The amphibole compositions are shown in Fig. 10, where the different amphibole types recognized on a textural basis are distinguished. Amphibole parallel to the main foliation and stable in the eclogitic garnet-bearing assemblage corresponds to Mg-hornblende and/or tschermakitic hornblende (see also Evans & Trommsdorff, 1978). This amphibole is compositionally similar to the retrograde amphibole overgrowing clinopyroxene along the main foliation and as coarse inclusions inside poikiloblastic garnet. In practice the composition of syn-tectonic eclogitic amphibole and of pseudomorphic amphibole after clinopyroxene is similar. Very different is the composition of retrograde amphibole overgrowing the foliation and shown in Fig. 10 as late-stage amphibole 3: this corresponds to tremolite ($X_{Mg} = 0{\cdot}95$) and is frequently associated with talc, chlorite, cummingtonite and other retrograde phases representing the late-stage evolution of these rocks. The transition from early (peak and early retrograde) hornblende to late-stage tremolite is accompanied by strong decrease in Al and Na, particularly in tetrahedral and octahedral Al. Again, the distinction from peak syn-tectonic amphibole in amphibole pseudomorphs after clinopyroxene is not easy on compositional grounds. Two major generations of amphibole are clearly shown in Fig. 10.

Trace elements

The comprehensive LA-ICP-MS trace element dataset for olivine, orthopyroxene, clinopyroxene, garnet, chlorite, amphibole, F-bearing Ti-clinohumite and chlorite from

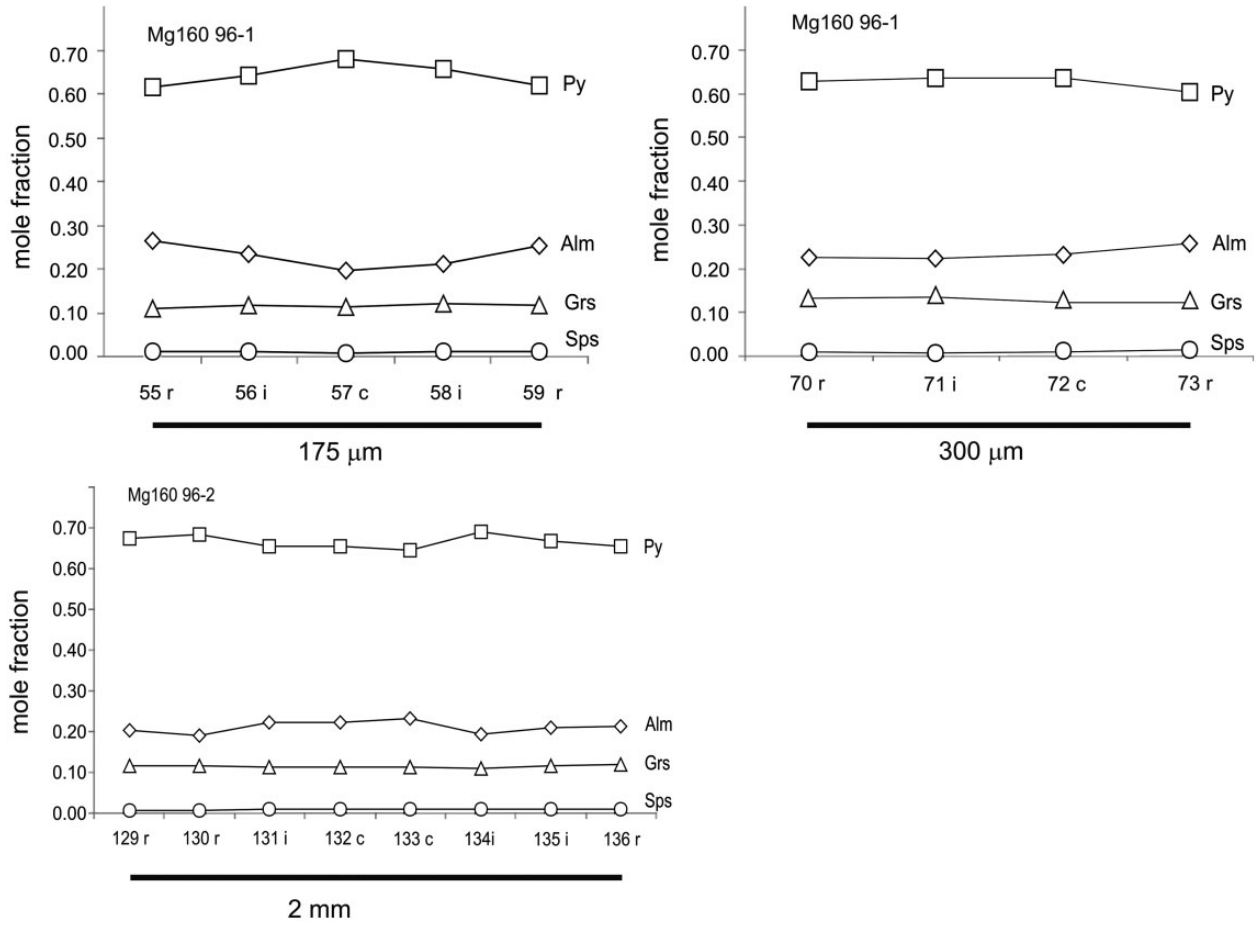

Fig. 9. Major element core–rim compositional profiles of garnets.

chlorite harzburgite (Mg304 92-1, Mg304 92-2) and garnet peridotite samples (Mg160 96-1, Mg160 96-2, Mg160 4-8, Mg161 92-1, Mg161 92-1B) is reported in the Supplementary Data. Data are plotted in Figs 11 and 12. As a whole, the rock-forming minerals show patterns and enrichments comparable with those shown by the bulk-rocks with respect to inferred serpentinite protoliths.

Orthopyroxene is the major REE host in the chlorite harzburgites. Its REE patterns are concave upwards, showing relatively high HREE (maximum 0·3 Lu_N), MREE depletion with respect to HREE (Gd_N about 0·01) and variable LREE, with enrichment of up to $La_N = 0{\cdot}07$ (Fig. 11). The REE patterns of orthopyroxene broadly reflect those of the bulk-rocks (Fig. 6) and there is no clear distinction between the composition of coarse orthopyroxene stable with olivine plus chlorite in the peak pressure assemblage and the fine-grained orthopyroxene replacing olivine (Fig. 11). In terms of other trace elements, orthopyroxene shows the same fluid-mobile element enrichments as the bulk-rocks, notably for B, Be, As, Sb and Pb, and less so for Th and U. In light of potential serpentinite protoliths, some of these enrichments (e.g. Be, As, Sb) are particularly high. With respect to the bulk-rocks and to other high-pressure phases, orthopyroxene shows different and much lower U_N/Th_N ratios. Olivine and Ti-clinohumite from the chlorite harzburgites do not show appreciable REE contents (Fig. 11). As for orthopyroxene, these minerals have high U, B, As, Sb and Li; additionally, Ti-clinohumite hosts high Ta and Nb. Chlorite is a poor host for all the trace elements discussed above (see Supplementary Data); most elements are below detection or are below the PM concentration. The distribution of trace elements among the rock-forming minerals of a representative chlorite harzburgite sample (Mg304 92-1) is reported in Fig. 13. The mineral proportions (olivine 67%, orthopyroxene 25%, chlorite 5%, F-bearing Ti-clinohumite 3%) were estimated by optical microscopy and the major element compositions of the bulk-rock and constituent minerals. The modal estimate corresponds well to that of Evans & Trommsdorff (1983) for their sample MG304 (olivine 60%, orthopyroxene 25%, chlorite 2%, F-bearing Ti-clinohumite 5%, Mg cummingtonite 3%, accessory minerals 3%). For the mass balance shown in Fig. 13a we adopted the average trace element composition of each

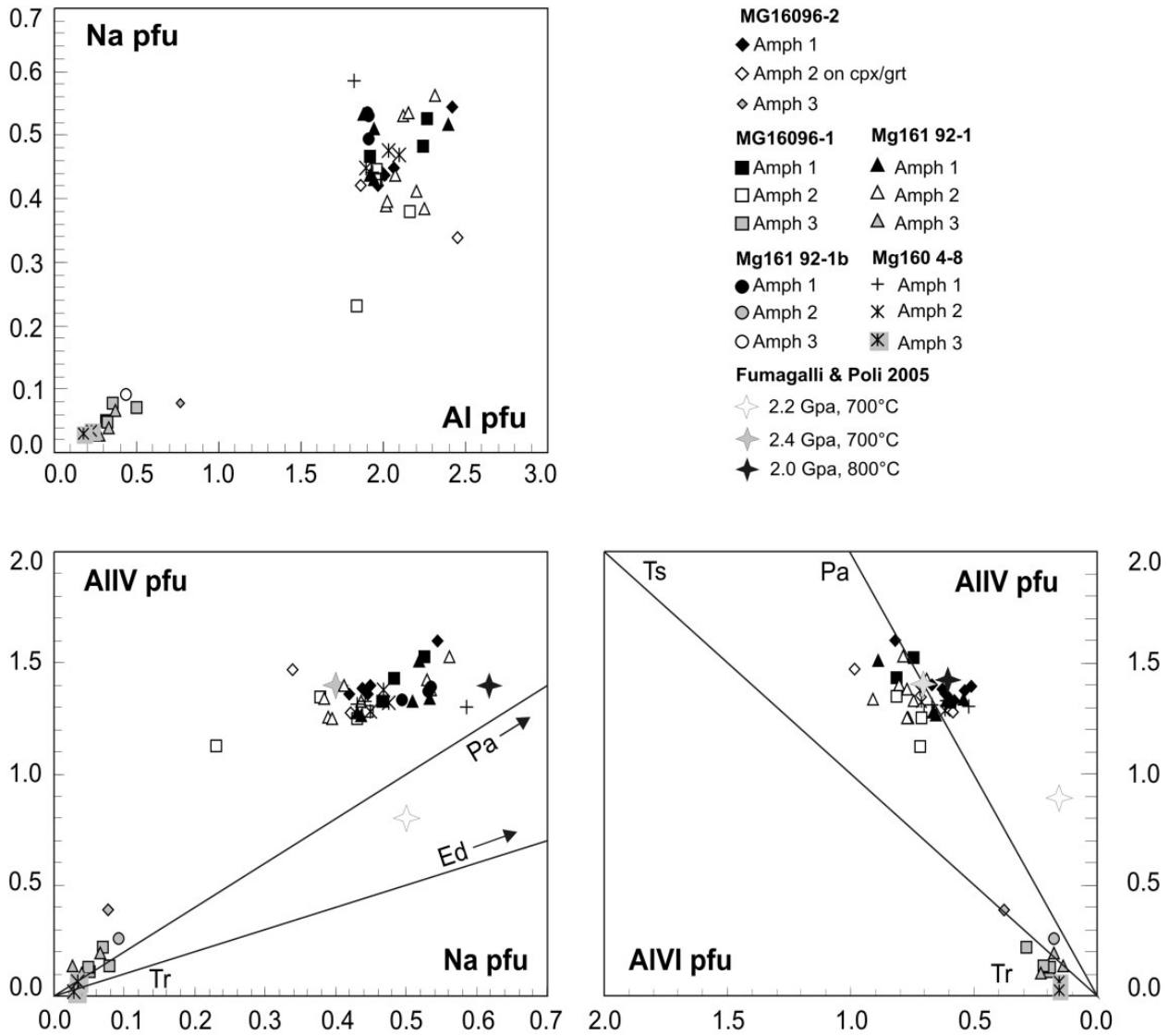

Fig. 10. Major element compositions of Mg hornblende and of retrograde tremolite from garnet peridotites. Plotted for comparison are experimental high-pressure amphibole compositions from Fumagalli & Poli (2005).

rock-forming mineral (see Supplementary Data) and the bulk sample composition (Table 2). Precise budgeting is hampered by the fine-grained size of some rock domains, by the presence of sulfides (not included in the mass-balance calculation) and by the occurrence of tiny polyphase inclusions in olivine and orthopyroxene. Concerning sample Mg304 92-1, Fig. 13a shows that orthopyroxene and olivine are the main hosts of most trace elements, whereas clinohumite is the main host of Hf, Nb and Ta. Only the elements Li, Hf, Sb, Ta, Nb and Th are fully hosted by the analysed minerals; the remaining elements [REE, large ion lithophile elements (LILE) and chalcophile] are unbalanced. The sulfide minerals pentlandite and pyrrhotite probably store As; the remaining elements might be hosted in fine-grained accessory phases or in microscopic polyphase inclusions and in non-analyzed retrograde minerals. The mass-balance diagram of Fig. 13a shows that the use of only either bulk-rock or *in situ* mineral analyses may not be decisive in assessing element storage in the chlorite harzburgites and in achieving reliable constraints on subduction zone processes. Rather, the combined use of such analyses is necessary.

Clinopyroxene, garnet and Mg-hornblende are the main REE repositories in the garnet peridotites. Clinopyroxene has LREE-depleted REE patterns and shows a very heterogeneous HREE distribution (Fig. 12) that clearly reflects the lack of widespread achievement of equilibrium with garnet. There are no clear textural relationships between HREE-rich and HREE-poor clinopyroxene, as they can occur at the core as well as in the rim domains

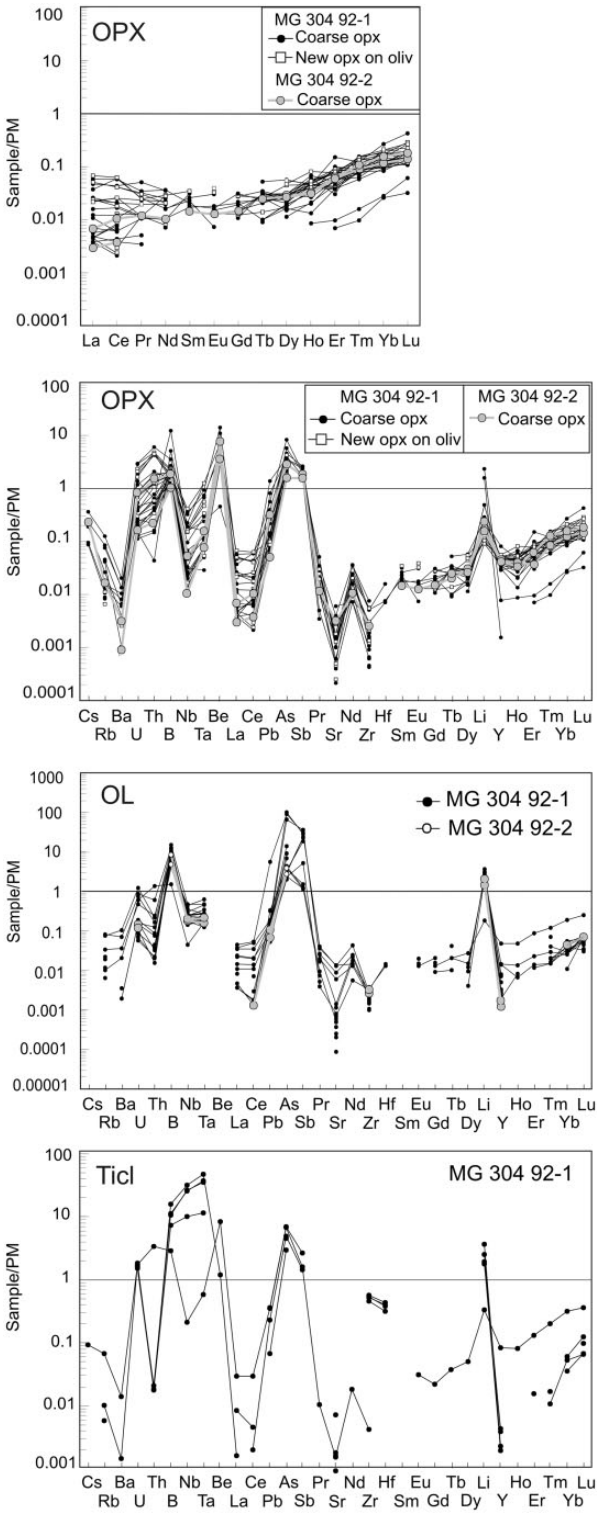

Fig. 11. Primitive Mantle normalized REE and trace element patterns of orthopyroxene, olivine and Ti-clinohumite from chlorite harzburgites.

of clinopyroxene crystals along the eclogitic foliation and in clinopyroxene inclusions inside poikiloblastic garnet. Clinopyroxene with high HREE contents (Lu_N around 5 PM) probably formed prior to garnet crystallization, whereas the entire spread of decreasing HREE contents down to 0·02 Lu_N could reflect progressive equilibration with garnet. Garnet shows the classic REE pattern with high HREE and LREE depletion as a result of equilibration with clinopyroxene and amphibole. Orthopyroxene from garnet peridotites has low absolute REE contents; unlike the orthopyroxene of the chlorite harzburgites, it shows continuous REE depletion from HREE to LREE. Mg-hornblende occurring as syn-tectonic crystals and as pseudomorphs after eclogitic clinopyroxene is characterized by similar REE patterns, with low HREE contents (Lu_N ranges from 0·3 to less than 1 PM), enrichment in MREE and depletion in LREE (Fig. 12). The HREE depletion of this amphibole reflects its equilibrium with garnet and its stability in the eclogite assemblage. The syn-tectonic and the pseudomorphic Mg-hornblende are clearly different from late-stage retrograde tremolite, with much higher HREE contents reflecting an absence of stable garnet during their crystallization.

The whole range of trace element compositions measured in the rock-forming minerals from the garnet peridotites is shown in the Primitive Mantle-normalized trace element patterns of Fig. 12. Like the bulk-rocks, all the minerals are enriched in fluid-mobile elements. Clinopyroxene and Mg-hornblende host the highest amounts of B, Be, Pb, As, Sb and Li. Pb, As and Sb can be as high as tens and up to a hundred times PM. Significant but less prominent enrichments in these elements, although in minor absolute amounts, also occur in the companion phases garnet and orthopyroxene (Fig. 12). Clinopyroxene thus hosts significant amounts of As, which appears to inversely correlate with HREE. The clinopyroxene grains showing the highest Lu_N around 4 PM (i.e. unstable with the eclogitic garnet) have relatively low amounts of As (1–3 times PM; see the thick gray lines in the trace element clinopyroxene plot of Fig. 12). In contrast, clinopyroxene grains with the lowest Lu_N and equilibrated with garnet can have the highest As contents (up to 30 times PM; see the thick light gray line in Fig. 12). Amphibole has the highest As contents. Another interesting feature concerns the Be enrichment of all Gagnone minerals relative to the bulk-rock compositions of potential serpentinite (or serpentinized mantle) precursors. In all minerals Be is distinctly higher than, or similar to PM; that is, two orders of magnitude higher than the potential protolith reservoirs. The trace element budget of the main rock-forming minerals of garnet peridotite sample Mg160 4/8 is illustrated in Fig. 13b. As for chlorite harzburgite, the mineral volume estimates employed for the mass-balance calculation are based on thin-section observation, bulk-rock and mineral

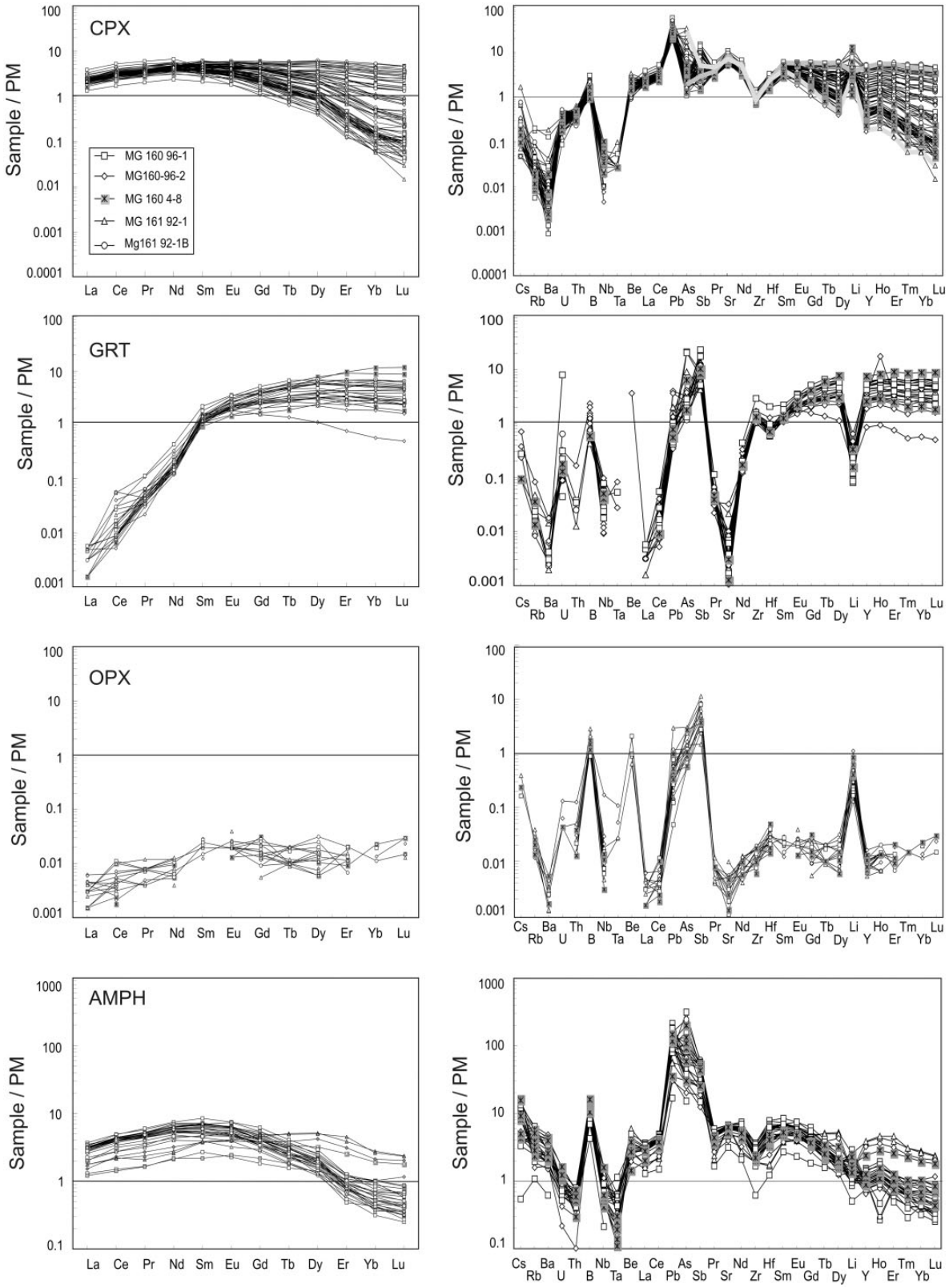

Fig. 12. Primitive Mantle normalized REE and trace element patterns of the main high-pressure minerals from garnet peridotites. The trace element patterns of clinopyroxene include two wide gray lines: the dark gray line refers to pre-eclogitic clinopyroxene with a flat HREE pattern, showing lower As than the eclogitic clinopyroxene stable with garnet characterized by HREE depletion represented by the wide light gray line. (See discussion on serpentinization environments for further explanation.)

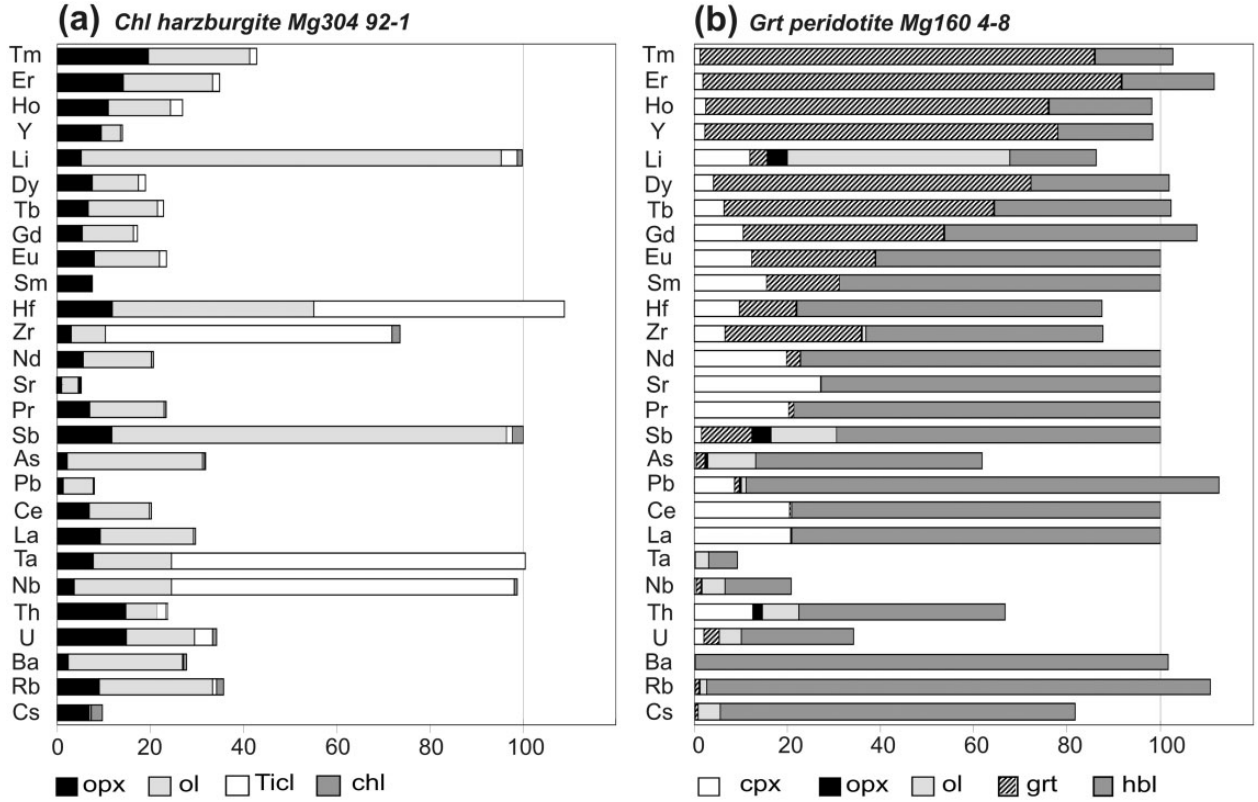

Fig. 13. Trace element distribution among the rock-forming minerals in chlorite harzburgite and garnet peridotite. The modal abundances of minerals in the two samples were obtained based on petrographic and mass-balance calculations using mineral and bulk-rock major element compositions. (a) Chlorite harzburgite Mg304 92-1. Th and Sb exceeded 120% and have been recalculated to 100. Low Sr and As can be hosted by non-analyzed sulfides and magnesite, respectively. The remaining unbalanced trace elements can be explained by storage in microphases and/or in fluid-related inclusions. (See text for further explanation.) (b) Garnet peridotite Mg160 4-8. La, Sr, Sb, Ce, Pr, Sm and Eu exceeded 120% and have been recalculated to 100.

major element composition (olivine 55%, garnet 15%, amphibole 15%, orthopyroxene 10%, clinopyroxene 5%) and the average trace element composition of each mineral involved (see Supplementary Data). For the garnet peridotite, the trace element distribution is well constrained and this shows that amphibole is the major repository for most fluid-mobile elements and LILE. Garnet, clinopyroxene and orthopyroxene compete with amphibole to host the REE. Notable exceptions are Nb, Ta, Th and U. These can be hosted by minor, non-analysed phases. The unbalanced high field strength elements (HFSE) can be hosted by the ilmenite intergrown with olivine at the expense of earlier Ti-clinohumite (Fig. 4e).

DISCUSSION

Textural and geochemical evidence for the polyphase history of the Gagnone peridotites

The crustal plus mantle rock association from Gagnone consists of ultramafic lenses inside pelitic gneisses and micaschists (Fig. 1). The ultramafic bodies in turn host eclogites, metarodingites and ophicarbonates. These rocks display pervasive foliations consisting of oriented garnet and clinopyroxene in eclogite and garnet peridotite, and of olivine, orthopyroxene and chlorite in harzburgite. This foliation was acquired during high-pressure metamorphism and is affected by polyphase folding related to the exhumation history of the mélange, after peak Alpine metamorphism dated at 43–35 Ma (Gebauer *et al.*, 1992; Becker, 1993; Pfiffner & Trommsdorff, 1998).

Chlorite harzburgite evolution

The majority of ultramafic pods at Gagnone are of chlorite harzburgite, which well preserves the textures and the mineral assemblages acquired during eclogite-facies recrystallization (Table 1). Undeformed massive rocks (e.g. outcrop Mg304; samples Mg304 92-1, MgG304 92-2, Mg304 09-03) display intergrowths of coarse idiomorphic olivine and orthopyroxene with interstitial chlorite. Fluorine-bearing Ti-clinohumite, oxides, sulfides and locally magnesite occur as stable phases in the peak assemblage. The presence of sulfide as inclusions in the high-pressure silicates and as interstitial grains suggests that

sulfides were present before peak metamorphism and were also added and/or remobilized during subduction recrystallization.

At Cerro del Almirez (Betic Cordillera) chlorite harzburgite with a broadly comparable granofels texture and paragenesis has been inferred to have been derived from subduction dehydration of antigorite serpentinite (Trommsdorff *et al.*, 1998; Padròn-Navarta *et al.*, 2010c). Derivation of the Gagnone harzburgite from serpentinized peridotite is also indicated by the presence of relict antigorite, talc and chlorite preserved inside the high-pressure minerals (Fig. 3c; Table 1). Serpentine, chlorite and talc were part of a prograde assemblage that, as at Almirez, dehydrated to the olivine- and orthopyroxene-bearing eclogitic paragenesis. The main difference between the harzburgites from the two localities is in the absence of tremolite and the likely presence of clinopyroxene in the peak assemblage of Gagnone. This implies that the transition from antigorite to olivine + orthopyroxene at Gagnone occurred at pressures above *c.* 2 GPa, as indicated by experimental work (Padròn-Navarta *et al.*, 2010a) and computed phase diagrams (Lòpez Sànchez-Vizcaìno *et al.*, 2005).

The foliated chlorite harzburgite does not retain widespread relics of the prograde assemblages. In these rocks the stability of olivine + orthopyroxene + chlorite at peak conditions is shown by flattening of these phases along the main high-pressure foliation that is consistent with the high-pressure foliation in associated eclogite and metarodingite (e.g. outcrops Mg31, Mgl63; Fig. 3d). The harzburgite foliation wraps around the boudinaged metarodingite and eclogite and flows in the boudin necks (Fig. 2a and b); this indicates that at some stage the ultramafic rocks were hydrated and more deformable than the associated mafic rocks. Comparable structures occur in Alpine high-pressure antigorite serpentinites (Scambelluri *et al.*, 1995); this observation reinforces the hypothesis that the chlorite harzburgite formed at a higher grade at the expense of ductile serpentinized ultramafic rocks. In undeformed and deformed chlorite harzburgite the peak assemblage is statically overgrown by retrograde talc, tremolite and cummingtonite (locally associated with dolomite), forming randomly oriented acicular aggregates.

The above textural features thus point to a serpentinized mantle protolith for the Gagnone harzburgite.

Garnet peridotite evolution

Garnet peridotite displays a syn-tectonic olivine + orthopyroxene + clinopyroxene + garnet + Mg-hornblende high-pressure assemblage. Intergrowths of olivine and ilmenite indicate the former presence of Ti-clinohumite. Opaque minerals mostly correspond to oxides, sulfides occur only locally and, in general, opaque minerals are much rarer than in the chlorite harzburgite. Mg-hornblende lines the garnet-bearing foliation and appears stable in the high-pressure paragenesis. The peak poikiloblastic garnet encloses foliated pieces of the precursor rock. It also hosts tiny inclusions of Ca-amphibole, chlorite and orthopyroxene (Fig. 4c), providing evidence for a prograde amphibole + chlorite paragenesis and indicating that peak crystallization of the garnet peridotite occurred beyond the stability of antigorite and chlorite (Evans & Trommdorff, 1978; Fumagalli & Poli, 2005; Grove *et al.*, 2006; Dvir *et al.*, 2011; Till *et al.*, 2012). The peak assemblage is clearly distinguishable from retrograde ones, in which post-tectonic, randomly oriented chlorite overgrows garnet and coexists with tremolitic amphibole 3 (Fig. 3f) and cummingtonite. Retrogression of the garnet peridotite thus leads to development of late-stage chlorite harzburgite different in origin and texture from the chlorite harzburgite described above.

The modal amount of garnet ranges from 15 to 25% by volume. In the field, the garnet-rich peridotite shows a high modal abundance of green clinopyroxene, probably derived from dismemberment and high-pressure recrystallization of clinopyroxenite veins related to the precursor mantle history of these rocks (Fig. 2e). This feature is also suggested by the bulk-rock compositions of the garnet-rich peridotite, which have Al_2O_3, CaO and Na_2O contents higher than primitive mantle abundances (Fig. 5). This indicates that the protolith of the garnet peridotite from outcrop Mgl60 hosted clinopyroxenite veins and/or layers (Fig. 2e).

The high-pressure paragenesis defined on textural grounds can be further verified by testing if the REE distribution among minerals reflects attainment of chemical equilibrium. The REE patterns point to equilibration between garnet, orthopyroxene and part of the clinopyroxene and Mg-hornblende. The HREE-rich composition of the garnet is counterbalanced by the HREE depletion of orthopyroxene. Regarding clinopyroxene, not all analyzed grains display HREE depletion. The large spread in HREE composition of clinopyroxene, particularly the occurrence of flat HREE to MREE patterns (Fig. 11), points to the inheritance of compositions pre-dating garnet formation and reveals a process of continuous clinopyroxene (re)crystallization during equilibration with eclogite-facies garnet, as shown by the increasing HREE depletion of clinopyroxene. The garnet peridotite thus preserves clinopyroxene that retains the pre-eclogitic REE composition of precursor mantle clinopyroxene.

Hornblende stability at peak conditions in the Gagnone garnet peridotite was discussed by Evans & Trommsdorff (1978), who proposed that Mg-hornblende could derive from re-hydration of higher-grade pyroxene + olivine + garnet rocks. We observe a HREE-depleted composition for the majority of the Mg-hornblende, pointing to equilibration with garnet. Amphibole showing high HREE contents (Fig. 12) generally replaces garnet. The

distribution of Sc, Lu and Y between garnet–clinopyroxene and garnet–hornblende is similar. Figure 14 shows that clinopyroxene and Mg-hornblende with low Lu, Sc and Y share an equilibrium distribution with garnet, having much higher contents in these elements. This type of Mg-hornblende achieved equilibrium with garnet under eclogite-facies conditions. On the other hand, clinopyroxene and Mg-hornblende with intermediate to high Lu, Sc and Y compositions are in disequilibrium with garnet; this is particularly the case of Mg-hornblende 2, which overgrows clinopyroxene and garnet. Based on this combined evidence, we favour the idea that part of the observed Mg-hornblende formed during peak metamorphism in coexistence with ol + grt + opx + cpx, thus implying a maximum pressure at 3 GPa (Niida & Green, 1999; Fumagalli & Poli, 2005).

Pressure–temperature conditions

Pressure–temperature estimates for the high-pressure rocks from Gagnone are available for eclogite, meta-rodingite and garnet peridotite, and are lacking for chlorite harzburgite. Concerning eclogite and metarodingite, Evans *et al.* (1979) reported temperature conditions from 690 to 807°C; this relatively large spread is due to different K_d values for Fe–Mg garnet–clinopyroxene partitioning and to the input of different pressure values in the geothermometer equation. The first estimates for the garnet peridotite were by Evans & Trommsdorff (1978), based on the pyroxene solvus, Fe–Mg garnet–clinopyroxene exchange and Al solubility in orthopyroxene, and suggested temperatures of 800°C and minimum pressures of 2 GPa. Essentially the same values (800°C and 2·5 GPa) were obtained by Pfiffner (1999) using a larger sample dataset.

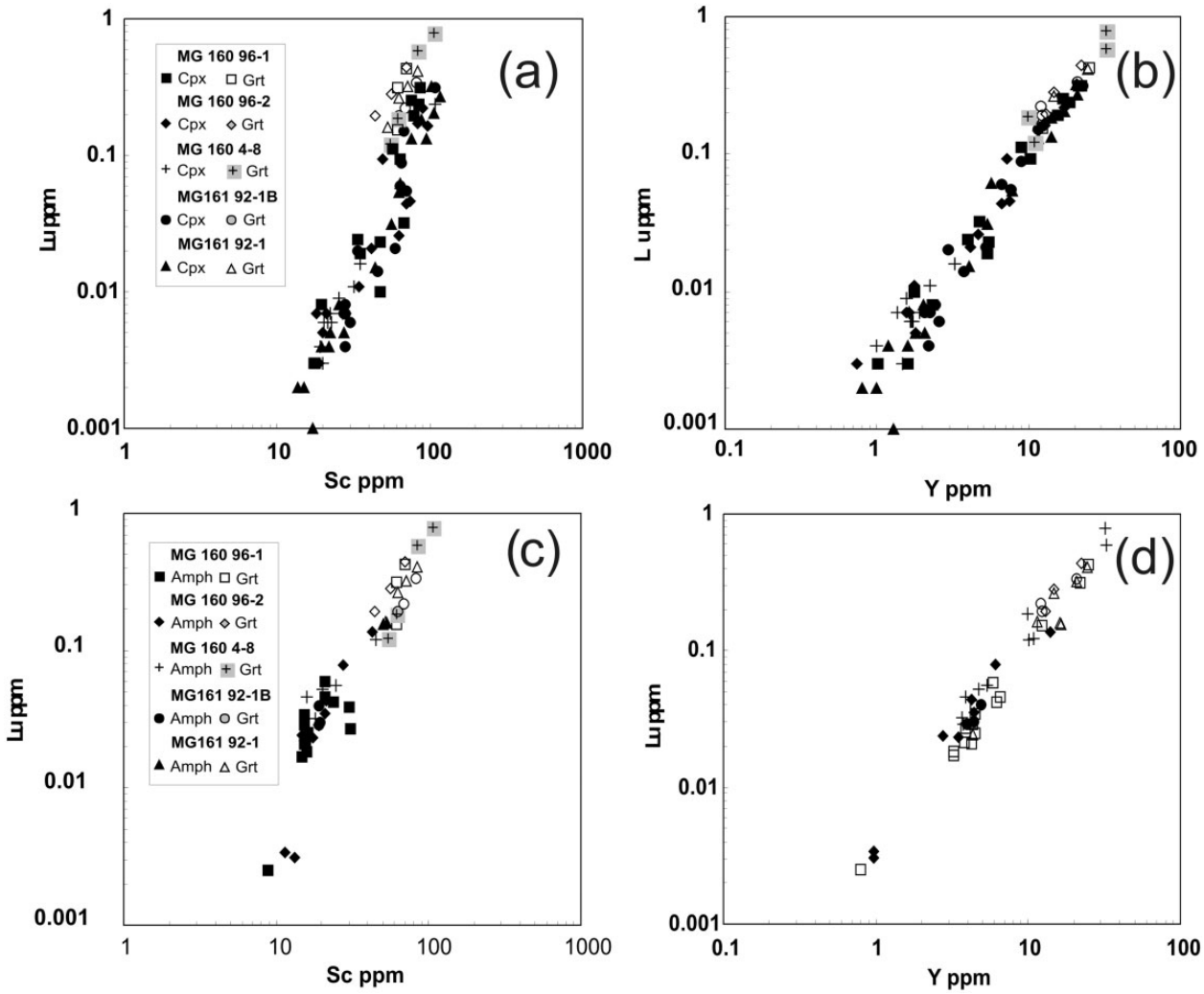

Fig. 14. Trace element compositions of garnet, clinopyroxene and Mg-hornblende from garnet peridotites.

More recent estimates by Nimis & Trommsdorff (2001) yielded a slightly lower temperature of 740°C and pressure up to 3 GPa. According to Evans *et al.* (1979), garnet peridotite, eclogite and metarodingite could have recrystallized together at peak conditions of 800°C and pressures around 2·5 GPa. Applying the calibrations involving garnet, clinopyroxene and orthopyroxene to equilibrium pairs and grains in mutual contact in apparent textural equilibrium, we obtained for the garnet peridotite the average temperature values reported in Table 3. The temperatures estimated from two-pyroxene solvus thermometry correspond to 800 ± 50°C (Brey & Köhler, 1990), 790 ± 50°C (Nimis & Taylor, 2000), 974°C (Taylor, 1998) and 800 ± 15°C (single orthopyroxene for the two-pyroxene solvus; Brey & Köhler, 1990). In such cases, the good performance of the Brey & Köhler (1990) geothermometer can be related to the low Na content of the clinopyroxene (0·03–0·08 a.p.f.u.), which is much lower than the critical values of 0·19–0·25 a.p.f.u. above which this thermometer overestimates the temperature [see discussion by Nimis & Grutter (2010, 2012)]. On the other hand, the geothermometer of Taylor (1998) yielded for Gagnone significantly higher temperatures than the other methods. Temperature values around 800°C have also been obtained using garnet–clinopyroxene (811°C; Ellis & Green, 1979) and garnet–orthopyroxene (781°C; Harley, 1984). The above values (see Table 2) are therefore comparable with previous geothermometry of the Gagnone high-pressure rocks.

To achieve independent estimates for garnet peridotite, to retrieve the possible pressure–temperature conditions for the high-pressure crystallization of chlorite harzburgite and to discuss the different assemblages and pressure–temperature conditions as a function of the major element bulk-rock compositions, we calculated phase diagram sections (pseudosections) for garnet peridotite and chlorite harzburgite using the program Perplex (Connolly, 1990). The results of these calculations are compared with the natural mineral parageneses achieved on the basis of the textural study and of the mineral and bulk-rock compositions. The correctness of the phase relations presented in Fig. 15 for garnet peridotite and chlorite harzburgite, and the exact P–T location of phase boundaries are affected by the choice of the fluid with an H_2O activity = 1 and by the adopted mineral compositions. The presence of CO_2 in the fluid could be expected; this would shift all dehydration curves to lower temperatures. Also worth mentioning is the lack of a Cr component in the calculations; the choice of clinochlore for the calculations does not account for Cr storage in this mineral, which enhances chlorite stability towards higher temperatures. The presence of Cr, moreover, stabilizes the spinel-bearing assemblage and favours the coexistence of garnet and spinel over a significant range of pressure–temperature conditions (Ziberna *et al.*, 2013). Also of note is the low Al content of serpentine (Supplementary Data), which leads to a restricted stability field for antigorite in the pseudosections (see Padròn-Navarta *et al.*, 2013).

Table 3: Geothermometry of three representative garnet peridotite samples

Garnet peridotite sample	Mg161 92-1b	Mg160 96-1	Mg160 96-2
Two-pyroxene solvus			
Brey & Köhler (1990)	785	756	842
Brey & Köhler (1990), opx	795	800	807
Nimis & Taylor (2000)	775	772	841
Taylor (1998)	974	933	1016
Garnet–clinopyroxene			
Ellis & Green (1979)	837	812	775
Garnet–orthopyroxene			
Harley (1984)	837	791	755

For garnet peridotite we adopted the SiO_2–Al_2O_3–MgO–FeO–CaO–Na_2O–H_2O (CNFMASH) system considering both garnet-rich (sample Mg160-09-10G) and normal peridotite compositions (sample Mg160-09-10). The solid solution models adopted for garnet, clinopyroxene, orthopyroxene and olivine are from Holland & Powell (1998); the solid solution model of Dale *et al.* (2000) was used for amphibole. The results for garnet-rich and normal garnet peridotite compositions are shown in Fig. 15a and b; the two compositions do not result in significantly different topologies and temperature boundaries for the main mineral assemblages. The main boundaries are the antigorite-out and chlorite-out reactions, respectively located at ~600°C and 800–830°C in both bulk systems. The stability field (between 600 and 750°C and below 2 GPa) of orthopyroxene + olivine + chlorite + amphibole, representative of the crystallization conditions of the prograde inclusion assemblage hosted in poikiloblastic garnet (Fig. 4c), should be noted. The peak olivine, orthopyroxene + clinopyroxene + garnet + amphibole paragenesis is stable in a pressure–temperature domain bordered by the temperature-dependent chlorite-out curve at about 800°C and by the pressure-dependent garnet-in (1–1·2 GPa) and amphibole-out (2·8–3 GPa) curves. The computed stability field for the peak assemblage fits the temperature estimates made by Evans & Trommsdorff (1978) and by Pfiffner (1999) for the Gagnone garnet peridotites, and is slightly higher in temperature than the estimates of Nimis & Trommsdorff (2001). Importantly, the chlorite and amphibole stability fields in the pseudosections of Fig. 15a and b are in good agreement with the experimental phase relations achieved

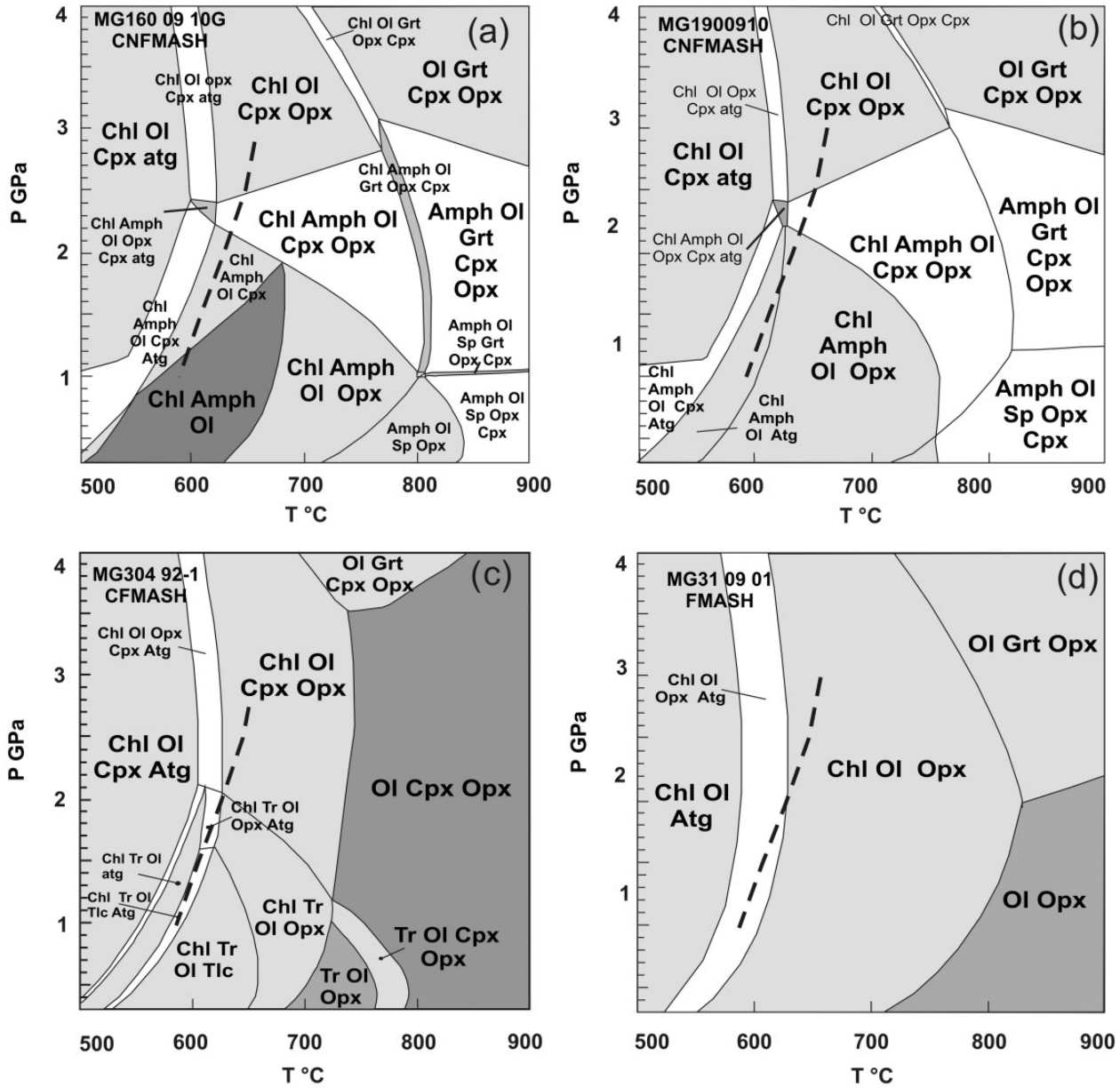

Fig. 15. Pressure–temperature–composition diagrams (pseudosections) for specific compositions of garnet peridotite [(a) garnet-rich sample Mgl60 09-10G; (b) garnet peridotite sample Mgl60 09-10] and chlorite harzburgite (Mg3l 09-0l). For the chlorite harzburgite Ca-poor (c) and Ca-free systems (d) have been adopted. The Ti-clinohumite-out curve (black dashed line) is after Lòpez-Sànchez Vizcaìno *et al.* (2005).

for hydrous fertile peridotites (Fumagalli & Poli, 2005) and for peridotite C–O–H systems (Malaspina & Tumiati, 2012). A discrepancy exists between the pseudosections of Fig. 15a and b and the experimental phase relations as regards the location of the spinel to garnet transition, which was experimentally determined at *c.* 1·4–1·5 GPa at 700–800°C and at 1·8–2 GPa at 1200°C for fertile peridotite CMAS compositions (O'Neil, 1981; Klemme & O'Neil, 2000). Although not crucial to the present study, the difference might be due to the presence of Fe^{2+} in the calculated pseudosections (Fig. 15a and b), shifting the spinel to garnet transition to about 0·2–0·3 GPa lower pressure for a characteristic mantle Mg# of 0·9 (O'Neil, 1981; Klemme & O'Neil, 2000).

The compositions of amphiboles crystallized during the experimental runs at 700–800°C and pressure above 2 GPa for peridotite compositions enriched in a basaltic component [the bulk composition labelled px by Fumagalli & Poli (2005)] compare well with the compositions of the Gagnone Mg-hornblende (Fig. 10). Although we cannot exclude the possibility that these rocks underwent high-pressure crystallization above the amphibole

stability (i.e. $P > 3$ GPa), here we favour the scenario in which the Gagnone garnet peridotite records high-pressure conditions above 800°C and 2–3 GPa, in line with trace element equilibrium between grt, cpx and amph, and with the presence of relict prograde chl + amph as mineral inclusions in grt. The major dehydration stages monitored by the garnet peridotites are therefore the antigorite- and chlorite-out reactions.

The chlorite harzburgite pseudosection was computed using the Ca-bearing system SiO_2–Al_2O_3–MgO–FeO–CaO–H_2O (Fig. 15c) and the composition of sample Mg304 92-1 (1·11 wt % CaO) and the Ca-absent system SiO_2–Al_2O_3–MgO–FeO–H_2O (Fig. 15d) using the Ca-poor bulk composition of sample Mg31 09-01. The solid solution models of Holland & Powell (1998) were adopted for all phases involved. The topology of the Ca-bearing system of Fig. 14c shows the stability of the antigorite-bearing assemblages, ending between 600 and 650°C, and of chlorite-bearing assemblages, terminating at about 750°C. The latter boundary probably provides the upper temperature limit for crystallization of these rocks. Interesting to note are the stability fields of chlorite + tremolite + olivine + orthopyroxene and, at lower pressure of chlorite + tremolite + olivine + talc. The topology of the Ca-bearing system for Gagnone is comparable with that derived by Lòpez Sànchez-Vizcaìno *et al.* (2005) for the Almirez chlorite harzburgites having a maximum 5 wt % magnetite. In contrast to Almirez, where tremolite is stable in the peak paragenesis, the absence of peak tremolite and the likely presence of clinopyroxene (detected by X-ray diffraction in Mg31 09 01) in the Gagnone harzburgite indicates minimum pressures of about 2 GPa. At lower pressure, the stability of talc + tremolite corresponds to the formation of the retrograde assemblages that statically overgrew the peak paragenesis (see Fig. 3f). A minimum temperature of 630°C for the eclogite-facies crystallization of the Gagnone harzburgite is provided by the antigorite-out reaction. This estimate also fits the breakdown reaction of F-free Ti-clinohumite calculated by Lòpez Sànchez-Vizcaìno *et al.* (2005, fig. 9) and the transition to F-bearing Ti-clinohumite that has been well documented in Gagnone by Evans & Trommsdorff (1983) and in this study (see Supplementary Data). The maximum temperature conditions are provided by the chlorite-out reaction, located at about 720°C for the Ca-bearing system and at about 800°C for Ca-absent system.

Based on the phase diagram sections of Fig. 15, it thus appears that the maximum peak temperature achieved for the chlorite harzburgite (720–800°C) may represent a minimum temperature for crystallization of the garnet peridotite peak assemblage. This leads to the following possibilities: (1) the two systems have equilibrated at the same peak pressure–temperature conditions, which must be around 800°C and 3 GPa, after dehydration of antigorite serpentine and chlorite in the garnet peridotites and of essentially antigorite in the chlorite harzburgite; (2) the two peridotite bodies now exposed at Gagnone have decoupled during peak subduction metamorphism, recording different peak pressure–temperature conditions; that is, a maximum of 800°C for the chlorite harzburgite and higher temperature conditions for the garnet peridotite. The difference in peak temperature conditions could be even higher if the garnet peridotite effectively crystallized in the stability field of the anhydrous olivine–garnet–clinopyroxene–orthopyroxene assemblage above the amphibole-out curve.

Both hypotheses could be realistic. However, a geodynamic model in which the Gagnone crust–mantle assemblage could correspond to a mélange in which the various ultramafic bodies might have attained different peak metamorphic conditions during subduction, and could have been tectonically emplaced together at HP–UHP conditions prior to exhumation, awaits careful investigation. Such a scenario is currently envisaged for subduction channels or in mélanges atop subduction slabs (Cloos, 1982; Engi *et al.*, 2001; Gerya *et al.*, 2002; Bebout, 2007; Federico *et al.*, 2007; Malatesta *et al.*, 2012). What still remains undefined is the timing of tectonic coupling between the gneiss–micaschist country rocks and the ultramafic lenses, whether during subduction burial or during exhumation. We discuss this aspect in the following sections.

The Gagnone peridotites: protoliths, evidence for fluid processes and exchange with the crust during subduction

Inheritance from the mantle protoliths

The Gagnone peridotites display a large variability of bulk-rock major and trace element compositions, as shown by the trends illustrated in Figs 5 and 6. The diagrams document decrease of Al_2O_3, CaO, SiO_2, Sc and V (Table 1) and increase in Ni, Co and (more slightly) FeO_{tot} with increasing MgO. These trends are associated with a constant Mg# for all bulk-rocks (Table 1) and broadly constant Mg# of olivine and orthopyroxene with increasing modal amounts of olivine (i.e. from garnet peridotite to harzburgite to dunitic varieties; Supplementary Data). Several studies on abyssal and ophiolitic peridotites have recently pointed out that comparable bulk-rock trends, decoupled from evident changes in mineral compositions, cannot be produced solely by peridotite partial melting (Niu *et al.*, 1997; Asimow, 1999; Godard *et al.*, 2000, 2008; Rampone *et al.*, 2004). Rather, these variations are better explained by combined processes of open-system partial melt extraction, melt percolation and peridotite–melt reaction causing dissolution of pyroxene and crystallization of olivine (Godard *et al.*, 2000, 2008; Rampone *et al.*, 2004). These processes affected large domains of the ophiolitic mantle now exposed in the Alps;

evidence for this is provided by field and petrological studies showing the formation of replacive dunite and harzburgite layers and/or anastomosing channels in peridotites, and by textural observation of olivine replacements after clino- and orthopyroxene (Piccardo, 2003; Müntener *et al.*, 2004; Rampone *et al.*, 2008). As in the other Alpine peridotite masses, Gagnone thus records the early stages of melting and melt–rock reaction that led to the compositional heterogeneity recorded by these rocks. Melt percolation in the early evolutionary stages of the Gagnone peridotites is suggested by the field occurrence of dunite layers parallel to or cutting the harzburgites. Further evidence for melt–rock reaction is provided by the REE patterns of the Gagnone peridotites, chlorite harzburgite in particular. The latter is characterized by flat to spoon-shaped REE patterns, similar to those documented in ophiolites and abyssal peridotites, and attributed to open-system peridotite melting and melt percolation, with the LREE contents buffered by the percolating melts and the HREE contents controlled by the melting reactions (Godard *et al.*, 2000, 2008). Similarly, garnet peridotites have REE patterns with LREE less fractionated than MREE and HREE with respect to other Alpine peridotites (e.g. Erro–Tobbio, Rampone *et al.*, 2004; Rampone & Borghini, 2008); this relative LREE enrichment could also result from melt–peridotite interaction. In summary, melt–rock reaction prior to serpentinization (see Kodolányi *et al.*, 2012) probably accounts for a prominent and variable part of geochemical variability recorded in the ultramafic rocks investigated here.

Another key aspect concerning the inherited mantle features of Gagnone is the presence of pyroxenite layers or veins, as clearly recorded by the garnet peridotite outcrop Mgl60 (Figs 1 and 2). In this body, the occurrence of garnet- and clinopyroxene-rich domains within the peridotite can be due either to pyroxene enrichment during percolation of pyroxenite liquids, or, more simply, to tectonic transposition and recrystallization of pyroxenite layers during Alpine deformation. This caused the peridotite enrichment in Ca, Al and alkalis above the primitive mantle values, as shown in Fig. 5 by the garnet-rich peridotite samples. As for other Alpine massifs, prior to serpentinization the Gagnone mantle was thus characterized since its early history by compositional heterogeneities owing to melt–rock reactions and was locally veined by pyroxenite.

Serpentinized protoliths for the Gagnone peridotites

The presence of rodingite, serpentine, talc and chlorite relics in F-bearing Ti-clinohumite (Fig. 3b) and of a three-phase assemblage analogous to that developed in the Bétic de-serpentinized peridotites (Trommsdorff *et al.*, 1998) strongly suggest that at least the Gagnone chlorite harzburgite was derived from serpentinized mantle rocks. A serpentinized precursor for the garnet peridotite is less clear from field and petrological evidence; the main indication is provided by olivine + ilmenite pseudomorphs after Ti-clinohumite (Fig. 4e), a mineral characteristic of Alpine high-pressure serpentinized peridotites. Further indication of pre-peak serpentinization is shown by the loss of Ca, Al and alkalis in some chlorite harzburgite samples falling outside the CaO–MgO and Al_2O_3–MgO variation trends (Fig. 5), a feature that can be related to clinopyroxene dissolution and/or replacement during serpentinization. A fall in the bulk-rock concentration of Al_2O_3, CaO and Na_2O in these samples indicates that serpentinization might have been locally intense. However, the high forsterite content of much of the olivine from Gagnone suggests that serpentinization was not so strong as to produce abundant magnetite and fayalite-rich olivine.

Serpentinized protoliths are also indicated by the bulk-rock trace element compositions of all Gagnone peridotites (Fig. 7). As discussed above, the bulk peridotite compositions range from 1 PM to below PM concentrations for a large number of elements (e.g. REE). On the other hand, enrichment in the fluid-mobile elements B, Pb, As, Sb, Sr, U and Li characterizes the compositions of all rocks and of peak metamorphic minerals (Figs 7, 11 and 12). A key point concerns the uptake of such elements, which may occur at any time during the pressure–temperature history of these rocks. Figure 13a shows that for chlorite harzburgite, the bulk trace element content is not fully balanced by the high-pressure mineral phases and that other trace element sinks (sulphides, fluid-related inclusions, interstitial accessory phases, retrograde minerals) must be envisaged. The use of bulk-rock compositions alone can thus be misleading in assessing the timing of element uptake in the Gagnone rocks. Detection of significant amounts of the above-mentioned fluid-mobile elements in all the high-pressure minerals from Gagnone, as documented by *in situ* mineral analyses (Figs 11 and 12), is therefore crucial to assess if enrichment pre-dates, or is coeval with, the high-pressure metamorphism. The Gagnone peridotites share with present-day abyssal serpentinites positive bulk-rock anomalies in B, Pb, Sr, U and Li, and comparable trends in U–Th fractionation (Kodolányi *et al.*, 2012). The relatively high U contents and, importantly, the U/Th fractionation shown by the Gagnone peridotites may therefore be inherited from an oceanic serpentinization stage. Several researchers have documented considerable variations in the U contents of present-day abyssal serpentinites, from below PM values (0·023 ppm; McDonough & Sun, 1995) to enrichments of hundreds of times PM, which result in relatively high U/Th ratios (Niu, 2004; Paulick *et al.*, 2006; Kodolányi *et al.*, 2012). According to Kodolányi *et al.* (2012), the U content of present-day serpentinites is high in the most altered, near-surface samples, and is lower in less altered rocks. Uranium enrichment, in addition to redox conditions during alteration, might also be related to the extent of serpentinization. In Fig. 7, the

garnet peridotite displays variable bulk U contents, varying from 0·17 to about 1 PM; U is higher and more uniform in chlorite harzburgite, where it is in the range of 1–2 times PM. This may indicate variable alteration intensities of the protoliths: lower and heterogeneous in the case of the garnet peridotite and higher for the chlorite harzburgite.

A similar interpretation can be drawn based on the B and Li contents of high-pressure minerals from the Gagnone peridotites (Fig. 16). In Fig. 16a, the boron and lithium contents of olivine, orthopyroxene and Ti-clinohumite are intermediate between unaltered mantle olivine and metamorphic olivine and orthopyroxene of de-serpentinized Almirez harzburgites (Scambelluri *et al.*, 2004a). As for Almirez, the rock-forming minerals at Gagnone inherit B and Li from the serpentinized protolith, and the variable contents shown by chlorite harzburgite and garnet peridotite minerals may again reflect different degrees of pre-eclogitic alteration (Fig. 16a).

Even more striking are the conspicuously elevated As concentrations of the Gagnone bulk-rocks and eclogite-facies minerals (Fig. 16b). Arsenic in the Gagnone peridotites is hosted by pentlandite and pyrrhotite (as shown in Table 1 for chlorite harzburgite samples labelled Mg304) and by the high-pressure silicates. We cannot exclude the possibility that anomalies in As and in other fluid-mobile elements could be due to the fluid-related inclusions. However, the systematic detection of these elements in all high-pressure minerals in all samples is clear evidence for As storage in silicate minerals. Recent work has documented high bulk-rock As abundances in supra-subduction zone high-pressure serpentinites (Hattori & Guillot, 2003, 2007; Deschamps *et al.*, 2011, 2012), where it occurs as As(V) absorbed by high-pressure antigorite (Hattori *et al.*, 2005). Appreciable As has also been detected in serpentinite from the accretionary wedges of Cuba and the Dominican Republic (Deschamps *et al.*, 2011, 2012). The positive correlation of B and As in Fig. 16b suggests, as for boron, that arsenic enrichment could represent a marker for serpentinized peridotite protoliths. In Gagnone, the presence of appreciable As and B in high-pressure minerals thus indicates that serpentinization pre-dated the eclogite-facies dehydration. It is worth emphasizing that the anhydrous eclogitic minerals still retain appreciable B, Li, As and Sb (Fig. 16) and recycle these elements deep into the mantle.

We thus confirm an origin from variably serpentinized protoliths of all eclogite-facies peridotites at Cima di Gagnone. Our dataset supports the early idea of Evans & Trommsdorff (1978) and we definitely claim that these peridotites truly represent the products of the evolution and dehydration of hydrated mantle in subduction zones.

Serpentinization environments

The fluid-mobile trace element enrichments documented here may not necessarily be the result of a single event of

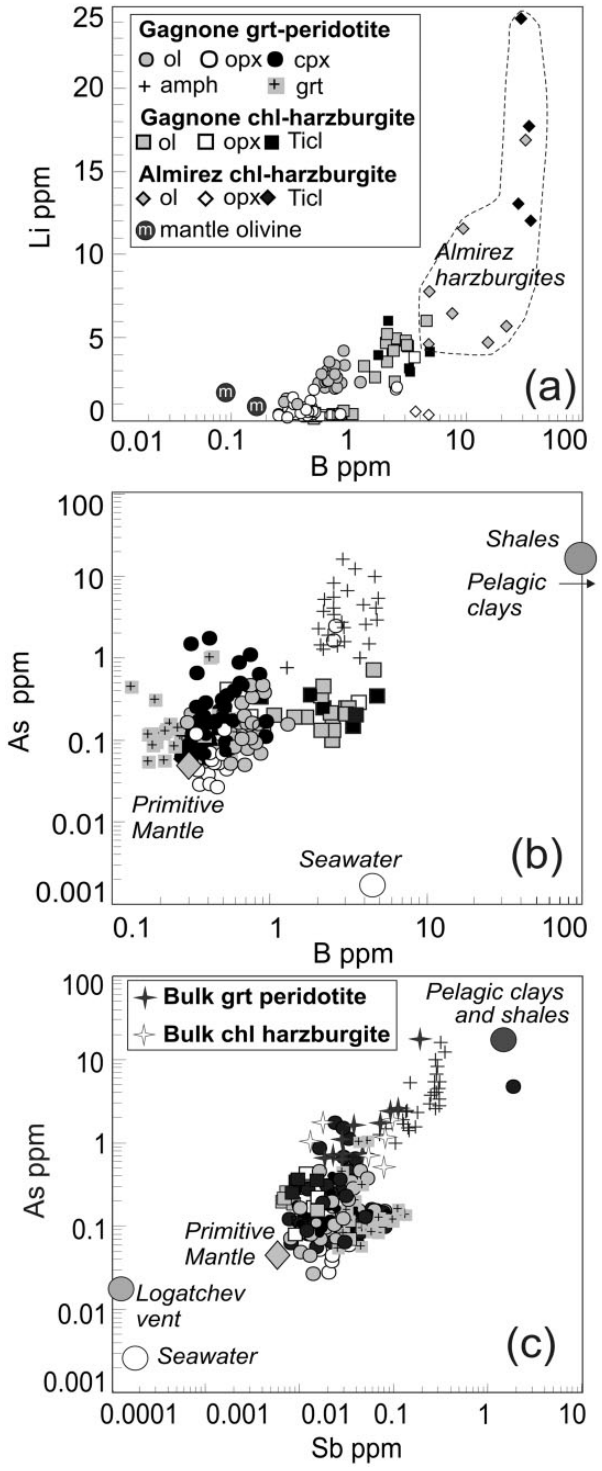

Fig. 16. Variation of Li–B (a), As–B (b) and As–Sb (c) for rock-forming minerals and bulk-rocks [only in (c)] from Gagnone. Plotted for comparison are: the compositions of rock-forming minerals in the Almirez harzburgites (Scambelluri *et al.*, 2004a); the compositions of pelagic clays and shales (Li, 1991); the primitive mantle (McDonough & Sun, 1995); the composition of seawater (Li, 1984; Smith *et al.*, 1995) and Logatchev hydrothermal vent fluid (Schmidt *et al.*, 2007).

seafloor to sub-seafloor alteration, but may be the result of multiple hydration stages in various environments. The positive anomalies in B, Pb, Sr, U and Li and high U/Th ratios can be fully to partly attributed to interaction with seawater and seawater-derived fluids during oceanic serpentinization (Table 4), as suggested by comparison with modern abyssal serpentinites and with ophiolites (Niu, 2004; Scambelluri *et al.*, 2004a; Boschi *et al.*, 2008; Vils *et al.*, 2009; Deschamps *et al.*, 2011, 2012; Kodolányi *et al.*, 2012).

In the Gagnone peridotites, element influx from reservoirs other than seawater is suggested by Be concentrations exceeding PM values (1·5–2·65 PM; Fig. 7) and by prominent positive anomalies of As and Sb recorded by the bulk-rocks and by the high-pressure silicate minerals. Bulk Be estimates in several reservoirs [0·0002 ppb in seawater (Li, 1984); 0·07 ppm in primitive mantle (Palme & O'Neill, 2004); 1·5–2·8 ppm in the continental crust (Rudnick & Gao, 2004); 2·6 and 3 ppm in pelagic clays and shales, respectively (Li, 1991)] indicate that this element is prevalently hosted in crustal and sedimentary rocks; its recycling from slab sediments to arc lavas has been shown by several researchers (Tera *et al.*, 1986; Morris *et al.*, 1990). At Gagnone, Be is higher than PM in all the major rock-forming minerals (clinopyroxene, amphibole, orthopyroxene and garnet from garnet peridotite) and in orthopyroxene of the chlorite harzburgite (Figs 11 and 12). Bulk Be estimates (calculated according to mineral compositions and abundances; Fig. 7) are two orders of magnitude higher than the reference values of oceanic serpentinites (Vils *et al.*, 2011; Kodolányi *et al.*, 2012). Although Be is less soluble in fluids than most fluid-mobile elements (e.g. Kessel *et al.*, 2005), the high Be contents of the Gagnone peridotites probably suggest input from fluids that exchanged with sediments.

Elevated As and Sb contents of bulk-rocks and high-pressure silicate minerals from Gagnone also appear consistent with sedimentary (or crust-derived) input. In the Gagnone ultramafic rocks these elements can also be hosted in sulfides since the early evolutionary (mantle) stages. However, the higher modal abundance of sulfides in chlorite harzburgite with respect to garnet peridotite suggests a relationship with serpentinization and its intensity. Moreover, the presence of interstitial sulfides in undeformed chlorite harzburgite suggests S remobilization and/or input along with As and Sb during subduction recrystallization. Together with the systematic presence of prominent positive anomalies in As and Sb in eclogitic minerals, this evidence points to mobility prior to high-pressure metamorphism. This hypothesis is reinforced by recent S isotope work on Alpine high-pressure serpentinized peridotites, pointing to input of heavy sulfur during prograde subduction metamorphism and hydration of mantle rocks (Shimizu *et al.*, 2013). The textural relationships of sulfides in chlorite harzburgite and, importantly, the widespread abundance of As and Sb in high-pressure minerals, suggest their influx during rock serpentinization.

In contrast to the elements discussed above, As occurs in low amounts in many present-day oceanic serpentinites and is high in serpentinites from accretionary wedges or from supra-subduction settings affected by fluids that exchanged with sediments (Hattori *et al.*, 2005; Deschamps *et al.*, 2012). Figure 16b shows that the majority of the Gagnone high-pressure minerals have As contents above the primitive mantle value (grey diamond in Fig. 16b) and trend towards the composition of pelagic sedimentary reservoirs (Li, 1991). Arsenic in seawater is one to four orders of magnitude lower than in the Gagnone peridotites, and this again calls for contamination by a sedimentary reservoir. Comparable conclusions

Table 4: Geological events, processes and element gains or losses recorded by the Gagnone peridotites

Evolutionary stage	Processes	Geochemical features and element exchange + income in rocks; - release to fluids
Mantle	Pyroxenite intrusion; melt percolation, melt–peridotite reaction; formation of reactive harzburgite and dunite layers	Acquisition of the major and trace element variability of rocks
Oceanic	MORB dike intrusion in peridotite; peridotite reaction with seawater-derived fluids, variable extent of alteration and serpentinization; rodingitization of mafic dikes	+ H_2O, CO_2, U, Sr, B, Pb, S
Prograde	Tectonic coupling of peridotite and gneiss, mélange formation; further fluid influx and peridotite hydration and alteration	+ H_2O, CO_2, As, Sb, Be, B, Pb, Sr, S
Peak	Dehydration of antigorite and chlorite, fluid release and formation of high-pressure assemblages in garnet peridotite and chlorite harzburgite; possible uptake in mélange of the garnet peridotite bodies	+ As (?), REE (?); - H_2O, CO_2, As, Sb, Pb, B, Sr

are suggested by the positive As–Sb correlation illustrated in Fig. 16c, showing that bulk-rocks and minerals from Gagnone plot between primitive mantle and pelagic sedimentary reservoirs. The As and Sb contents of seawater (Li, 1984) and of hydrothermal fluids from present-day oceans (e.g. Logatchev vent, Schmidt *et al.*, 2007) are too low to have affected the As and Sb budget of the Gagnone peridotites. Deschamps *et al.* (2011) measured comparable amounts of As and Sb in serpentinites from accretionary complexes from Cuba and the Dominican Republic, and attributed this relative enrichment to fluid-mediated exchange with sediments. In Gagnone, As enrichment during subduction is, moreover, suggested by the change in As contents of clinopyroxene from garnet peridotites. In Fig. 12 the pre-eclogitic clinopyroxene (with flat MREE and HREE patterns; wide dark gray line) has much higher As than oceanic serpentinites, but as a whole it has lower contents than eclogitic clinopyroxene stable with garnet (HREE-depleted patterns; wide light gray line). This feature suggests that clinopyroxene records progressive As influx and enrichment upon protracted clinopyroxene crystallization during continuing subduction, with the largest As input during the eclogite-facies event.

The major and trace element dataset presented here provides strong evidence that the Gagnone peridotites record a multistage history of early mantle melt infiltration, hydration and serpentinization, encompassing the following evolutionary stages (Table 4). A first oceanic stage included melt percolation and later serpentinization when close to the ocean floor, probably causing partial enrichment in B, U, Sr, Pb and Li. A second stage was related to prograde subduction and percolation of sediment-equilibrated fluids, which further enriched the ultramafic rocks in trace elements such as Be, As and Sb, with the most prominent metasomatism occurring near or at peak pressure conditions. We suggest that the association of ultramafic–mafic lenses with paragneisses (and possibly orthogneisses, too) was established at the subduction interface during the protracted history of prograde to peak to early retrograde evolution of the Cima Lunga Unit. The Cima di Gagnone rock association may thus represent an excellent example of a kilometre-scale mélange atop a subducting slab. Our preferred scenario is illustrated in Fig. 17 (redrawn after Trommsdorff, 1990); this emphasizes that mantle from the oceanic slab (and probably also from the upper plate) can tectonically mix with sediments and crustal rocks from the beginning of subduction to form the mélange associations currently exposed in the area.

Element redistribution and recycling

An increasing number of studies suggest that the plate boundary in subduction zones consists of kilometre-thick, hydrated, soft layers (Peacock, 1993; Bostock *et al.*, 2002; Van Keken, 2003) in which slices of the downgoing slab and of the overlying mantle become tectonically mixed (Bebout, 2007; Spandler *et al.*, 2008; Marschall & Shumacher, 2012). In these layers atop the subducted slab ('subduction channels' and/or mélanges) fluid flux and tectonic stresses are strongly focused, and these domains are now viewed as very active environments in which deformation, and fluid and mass transfer are enhanced. Moreover, fluid ascent from the slab facilitates hydration of the forearc mantle and of the hanging-wall mantle above the slab: this determines water and fluid-mobile element storage in such hydrated mantle domains and their transfer to subarc depths (Hyndman & Peacock, 2003; Savov *et al.*, 2005; Scambelluri & Tonarini, 2012). The Gagnone peridotites are exhumed examples of such environments, recording exchange of mantle materials with crust-derived fluids during chemical and tectonic interaction with (meta)sediments on the subduction pathway to depth. Because these peridotites are the dehydration products of variably serpentinized protoliths, they also provide information about element distribution among high-pressure minerals deriving from dehydration processes and about the elemental budget finally retained by the residual anhydrous minerals and recycled into the mantle.

Figure 18a–e shows the distribution of several fluid-mobile elements between the high-pressure minerals of the garnet peridotites and chlorite harzburgites from Gagnone. The partition coefficients have been computed adopting the average compositions of minerals from each sample (see Supplementary Data Table 1). Cs, Rb and Ba are reported for only clinopyroxene and Mg-hornblende (Fig. 18d) because olivine, orthopyroxene and garnet are poor repositories and display large variations in these elements, precluding reliable average estimates. Figure 18a–d shows that in the garnet peridotites clinopyroxene and amphibole are the main hosts of Cs, Rb, Ba, Sr,U, Th, Pb and HFSE. Lithium preferentially enters clinopyroxene. Boron, As and Sb partition fairly equally among clinopyroxene, garnet and orthopyroxene. Amphibole has a much higher affinity for the LILE (Cs, Rb, Ba), together with B, As, Sb and HFSE, thus working as a fluid-mobile element sink. In the chlorite harzburgites (Fig. 16d), B, As and Sb are preferentially hosted by olivine, whereas F-bearing Ti-clinohumite stores the HFSE. Boron retention in residual rocks is significantly accomplished by olivine, as documented in previous studies of natural rocks (Scambelluri *et al.*, 2004*a*, 2004*b*) and in experiments (Tenthorey & Hermann, 2004). Fluid-mobile element concentrations in chlorite are low or below detection (Supplementary Data), making this phase irrelevant to the trace element transfer process.

Amphibole is therefore fundamental for fluid-mobile element storage in the garnet peridotites and is the last hydrous phase surviving at Gagnone; its breakdown along a subduction geotherm (Schmidt & Poli, 1998; Fumagalli & Poli, 2005) at higher P–T (1000°C, 3 GPa) may occur via

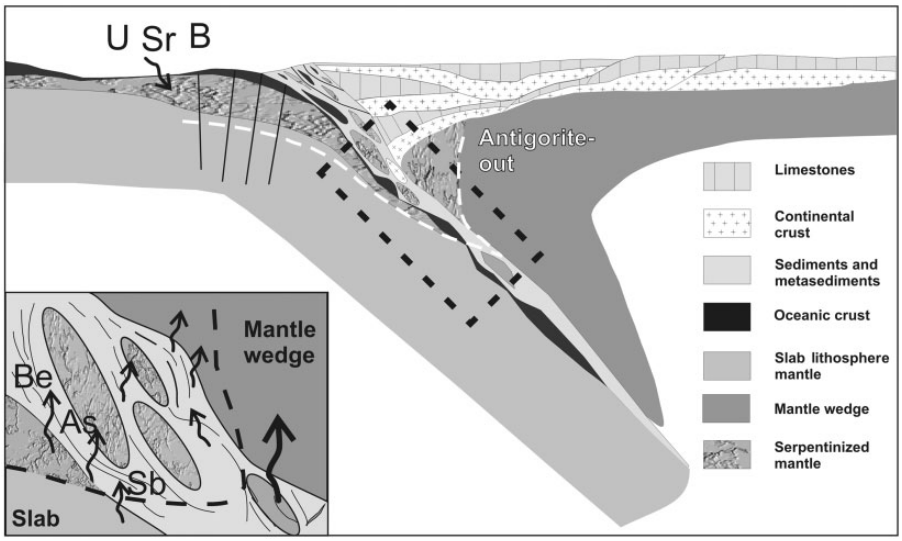

Fig. 17. Tectonic sketch (not to scale) showing the evolution of the Gagnone peridotites. Redrawn after Trommsdorff (1990).

the dehydration reaction amphibole + orthopyroxene = clinopyroxene + olivine + garnet + water (Tumiati *et al.*, 2012). To evaluate the trace element budget still stored in the rock after amphibole breakdown, the modal amount of amphibole in garnet peridotite sample Mg160 4-8 was estimated and the trace element budget of amphibole was subtracted from the bulk-rock composition. The selected sample contains 0·35 wt % water (Table 1), an amount comparable with the 0·4 wt % water reported for the same sample by Evans & Trommsdorff (1978). The modal abundance of amphibole estimated by optical microscopy is 17–18 vol. %, in good agreement with the 20% modal amphibole that corresponds to the 0·35–0·4 wt % water content of this rock sample. Combining these estimates with the average composition of Mg-hornblende from Mg160 4-8, the amphibole-free composition is computed and reported in Fig. 18f, which shows sample Mg160 4-8 together with its dehydrated counterpart after extraction of 15% and 20% modal amphibole (grey and open circles, respectively). This gross comparison suggests that most Rb, Ba and Pb are below 0·01 PM in the computed amphibole-free compositions, which implies that these elements can be largely removed from the system at the amphibole-out reaction. In contrast, U, Th, B, Nb, Ta, Be and As remain relatively unchanged. If true, this would imply that, for instance, the gross content of 3 ppm B and 1·6 ppm As of the garnet peridotites may decrease to about 2 and 0·8 pmm, respectively, thus significantly affecting the budget of these 'crustal' elements in the deep mantle. Even higher amounts of these trace element are recycled into the mantle by the chlorite harzburgites, whose budget remains virtually unaffected by chlorite disappearance, thus ensuring an influx of 3·5 ppm B and about 1 ppm As, largely exceeding the primitive mantle concentrations.

Comparison with other Alpine garnet peridotites: evidence for partial melting at Gagnone?

Orogenic garnet peridotites frequently occur as lenses tectonically embedded in crustal rocks. This geological association has been related to tectonic erosion of the supra-subduction zone mantle by the subducting crust (Brueckner, 1998; Nimis & Morten, 2000; Zhang *et al.*, 2000; Beyer *et al.*, 2006; Malaspina *et al.*, 2009), or to tectonic mixing (mélanges) atop the slab (Zheng, 2012). These mantle rocks are frequently metasomatized by fluids and/or melts derived from crustal rocks and can act as proxies of crust-to-mantle element exchange in subduction zones down to 200 km depth (Zhang *et al.*, 2000; Rampone & Morten, 2001; Beyer *et al.*, 2006; Malaspina *et al.*, 2006, 2009; Scambelluri *et al.*, 2006, 2008). The Ulten Zone (Eastern Alps) is another Alpine locality at which garnet peridotite lenses are embedded in Hercynian high-pressure crustal units (Morten & Obata, 1990). In this setting, continental crust and mantle were tectonically coupled at eclogite-facies conditions, when migmatized layers of the continental slab tectonically enclosed slices of the overlying hanging-wall mantle (Tumiati *et al.*, 2003). The latter transformed into garnet + amphibole ± carbonate ± phlogopite peridotite whose geochemical characteristics reflect infiltration of C–O–H, trace element-enriched, metasomatic fluids of crustal origin. These fluids originated from migmatitic melts, either by silica-consuming reactions with mantle rocks (Scambelluri *et al.*, 2006) or by a process of exsolution, related to *in situ* crystallization of the migmatitic melts (Rampone & Morten, 2001).

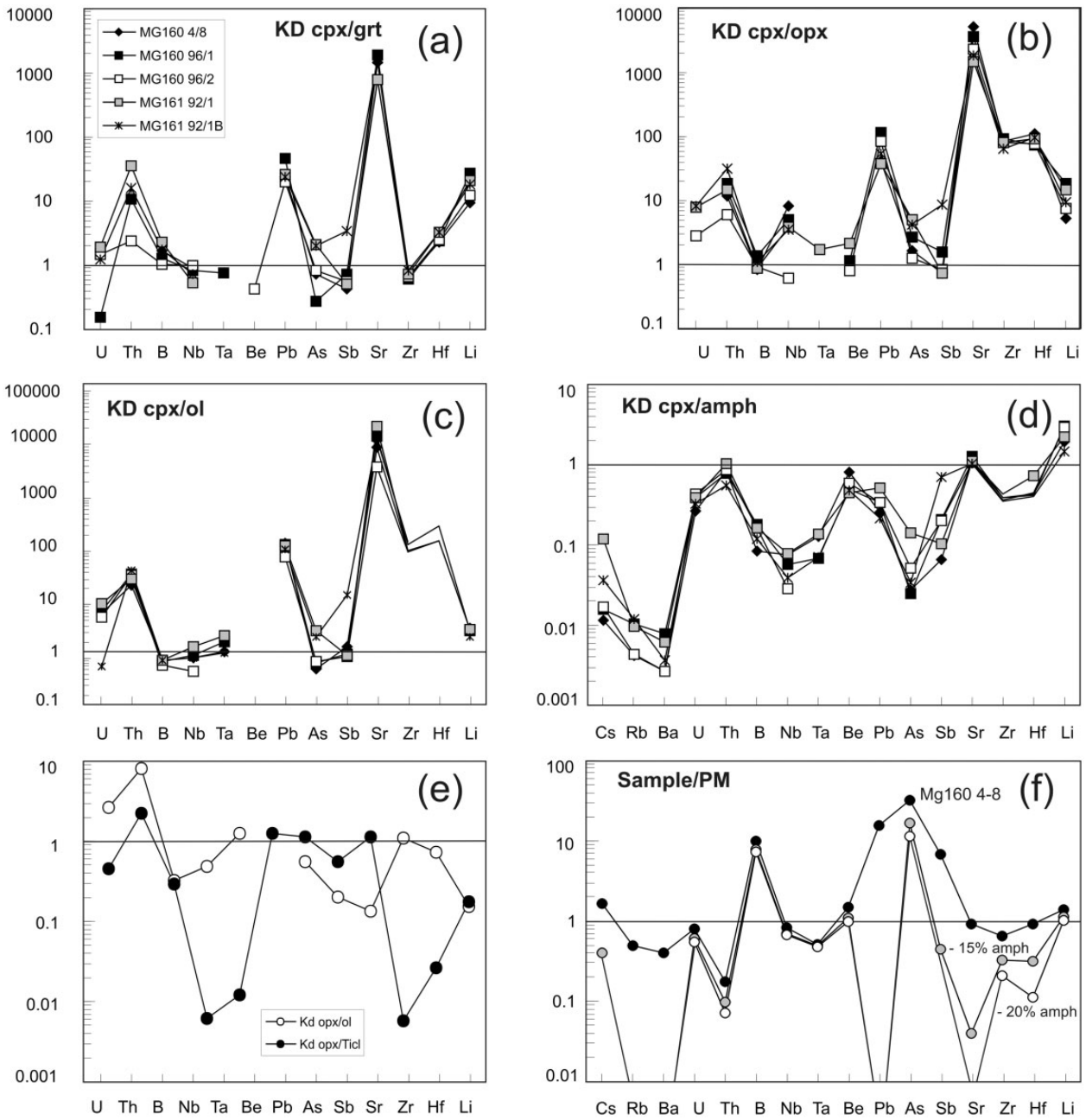

Fig. 18. (a–e) Calculated K_D describing element distribution between the key mineral phases of the garnet peridotites and chlorite harzburgites. (f) Primitive Mantle normalized composition of garnet peridotite sample Mgl60 4-8 with and without amphibole.

Although different in many aspects related to fluid evolution (Ulten records fluid influx; Gagnone records dehydration), the Ulten and Gagnone peridotites can be compared in terms of mineral assemblages, location (top of the slab) and broad pressure–temperature conditions (850°C, $P < 3$ GPa; Nimis & Morten, 2000). A major difference is that partial melting affects the Ulten country rock gneisses. Comparison of the Gagnone and Ulten peridotites can help to clarify the trace element imprint acquired by mantle rocks in the presence and absence of partial melting of the crust. The Ulten bulk-rocks, clinopyroxene and amphibole (the main LILE and LREE repositories) store higher amounts of Cs, Rb, Ba, Th, U and La than the Gagnone garnet peridotite; the difference can be 3–10 times in the case of Cs and Rb, and 10–50 times in the case of Ba, U and Th (Fig. 19).

Analysis of the trace element composition of fluids and melts experimentally produced from metapelite in the

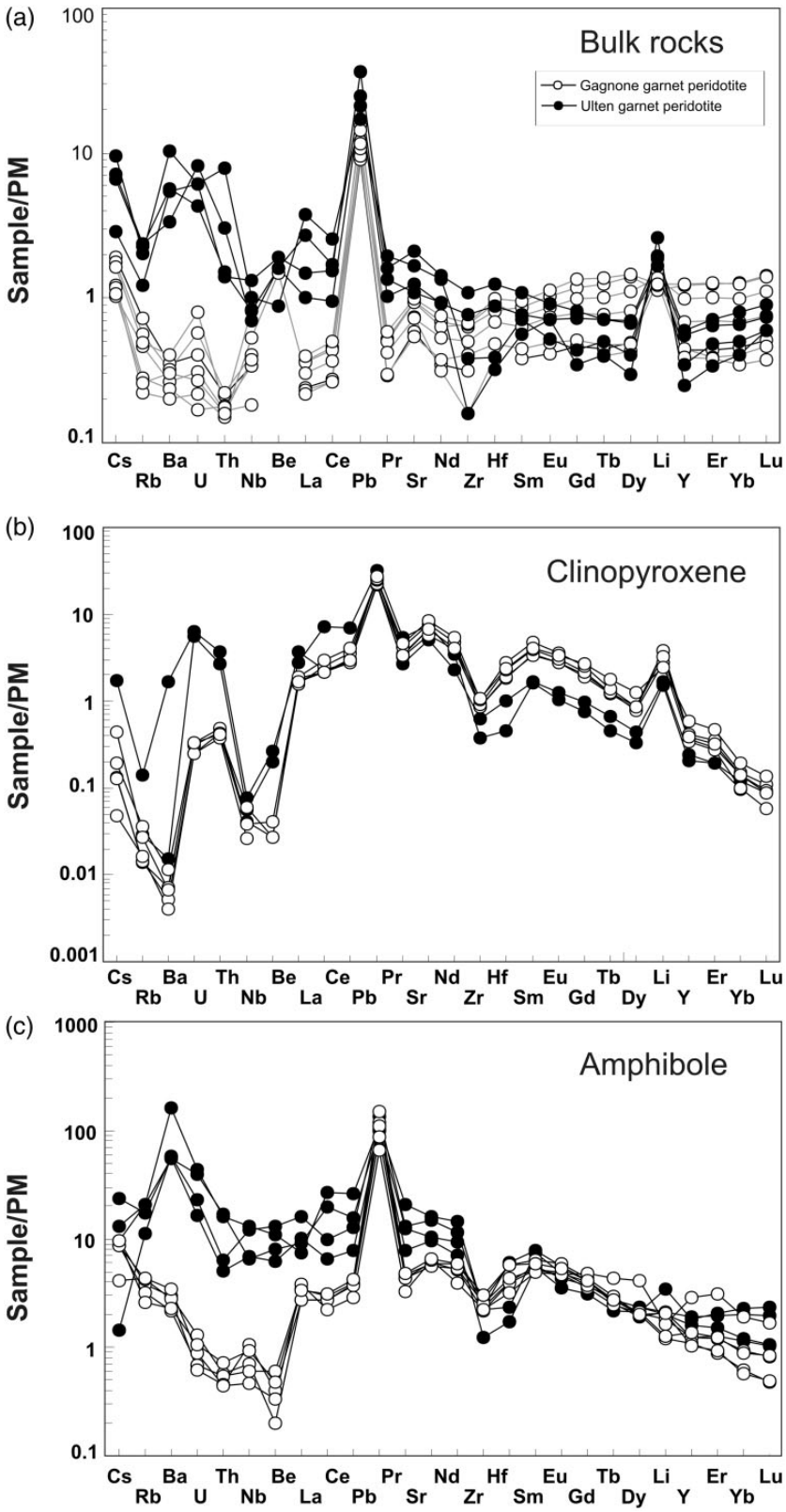

Fig. 19. Comparison of the Primitive Mantle normalized trace element patterns of bulk-rocks (a), clinopyroxene (b) and amphibole (c) from Gagnone and Ulten Zone garnet peridotites. Ulten data are from Scambelluri *et al.* (2006) and Sapienza *et al.* (2009).

600–750°C temperature range shows that silicate melts have much higher trace element contents than fluids (Hermann & Green, 2001; Spandler *et al.*, 2007; Hermann & Spandler, 2008). The melt/fluid partition coefficients are 5–10 for Rb and Cs, around 50 for Sr and Ba, and above 100 for U and Th (Spandler *et al.*, 2007). Potentially, a melt-derived fluid (as in the case of Ulten) may inherit from the silicate melt a trace element budget higher than a dehydration fluid. The Ulten–Gagnone bulk-rock ratios for Cs, Rb and Ba (3·3–11 for Cs, Rb; 10–50 for Ba; Fig. 19) are roughly comparable with the melt/fluid partition coefficients of Spandler *et al.* (2007), whereas the ratios for U and Th are much lower (maximum values around 50) than melt/fluid coefficients of Spandler *et al.* (2007). Despite the fact that the comparison presented here is very rough, the data suggest that the higher trace element load of the Ulten fluid indicates inheritance from a partial melt, in accordance with previous interpretations (Rampone & Morten, 2001; Scambelluri *et al.*, 2006; Sapienza *et al.*, 2009).

The above evidence suggests that in Gagnone the crustal rocks did not experience partial melting (consistent with field evidence) and that the agent metasomatizing the ultramafic bodies during subduction was an aqueous fluid equilibrated with the crustal host-rocks. In particular, the garnet peridotite, recording chlorite breakdown to garnet during peak metamorphism, retains significant amounts of fluid-mobile trace elements that would be removed in the case of melting. This indicates that the eclogite-facies breakdown of chlorite ($T > 750$°C, $P < 3$ GPa) was not accompanied by peridotite melting. In turn, the chlorite breakdown fluid should have enhanced melting of the surrounding gneiss. Absence of gneiss melting can thus be interpreted to indicate that the high-pressure coupling of garnet peridotite with the gneisses took place after chlorite breakdown.

CONCLUSIONS

(1) The garnet peridotite and chlorite harzburgite from Cima di Gagnone are derived from hydrated peridotites involved in Alpine subduction. The pressure–temperature estimates presented here agree with previously published studies and suggest temperature conditions in the range of 750–850°C and pressures below 3 GPa. The pseudosection modelling shows that the maximum temperature conditions experienced by the chlorite harzburgites coincide with the minimum temperatures recorded by the garnet peridotites. This suggests that either these rocks recrystallized cofacially in the same temperature range of about 800°C, or that the various bodies were decoupled during subduction, as achieved in subduction mélanges or in tectonically active plate interface boundaries.

(2) A large part of the major element and REE compositional variability of the Gagnone peridotite suite was acquired during mantle evolution. Transition from fertile garnet peridotite to depleted chlorite harzburgite to dunite is not simply the result of different degrees of partial melting. Rather, the bulk-rock and mineral compositions suggest that reactive melt flow during the pre-subduction history also influenced the variability now observed in Gagnone.

(3) The geochemical fingerprint of the Gagnone peridotites is characterized by enrichments in fluid-mobile elements above primitive mantle values for B, Pb, As, Sb, Cs, Li, U and Be. The bulk trace element compositions of these rocks suggest multiple processes of hydration and serpentinization. The similarity between the Gagnone peridotites and present-day oceanic serpentinites in terms of U, Pb, B, Li and Sr suggests that uptake of these elements could have partly occurred during an initial stage of serpentinization driven by seawater-derived fluids, confirming the early interpretation of these rocks by Evans & Trommsdorff (1978). Moreover, positive anomalies in Be, As and Sb (well above the budgets of seawater and hydrothermal vents) require involvement of aqueous fluids equilibrated with crustal (metasedimentary) reservoirs during prograde subduction metamorphism, possibly when the peridotites were tectonically coupled with (meta)sediments.

(4) The above-envisaged additional stage of prograde to peak hydration of the Gagnone peridotites in top-slab mélange environments is revealed by the trace element compositions of peak eclogitic minerals in the garnet peridotite and chlorite harzburgite. These minerals are most enriched in fluid-mobile elements, clearly implying that enrichment pre-dated peak subduction dehydration.

(5) Retention of fluid-mobile elements in anhydrous residual minerals at Gagnone points to recycling to the deep mantle of B, Li, As and Sb in amounts that largely exceed primitive mantle values. Recycling of such HP–UHP materials will thus introduce geochemical anomalies into the Earth's mantle.

(6) Comparison with other eclogite-facies garnet peridotites of the Eastern Alps (Ulten Zone) metasomatized by fluids evolved from migmatitic melts released from the associated crustal rocks shows that Cs, Rb, Ba, U, Th and LREE are significantly lower in the Gagnone peridotites and high-pressure minerals. This evidence suggests that the crustal sequences hosting the Gagnone peridotite pods did not experience partial melting. Garnet peridotites, despite experiencing chlorite dehydration to garnet assemblages, still retain significant amounts of fluid-mobile elements, which would be removed efficiently by a partial melting process. Consequently, the Gagnone garnet peridotites did not cross the wet peridotite solidus during chlorite breakdown, as recently also suggested by experiment.

We conclude that the ultramafic bodies of Gagnone represent a prime example of mantle peridotites recording a

multistage (ocean floor and prograde) history of mantle peridotite hydration and subduction dehydration in a subduction channel plate interface setting.

ACKNOWLEDGEMENTS

Volkmar Trommsdorff, Trommi to his friends, was a master and leader in metamorphic petrology, Alpine geology and, not least, in Alpine ski. He was the father of petrological research on hydrated and carbonated peridotites and on metamorphic fluids. He lectured with great enthusiasm on the wonders of metamorphic petrology and his work lives on through the students he taught. Bernard Evans and Trommi were the first to propose that subduction dehydration of serpentinized mantle was relevant for the genesis of orogenic peridotites and for the subduction-zone water cycle; an idea still timely 35 years later. Trommi was a great friend and an excellent teacher—critical but also full of ideas. We dedicate this work to him. We thank Bernard Evans and an anonymous reviewer for their valuable constructive comments, and Jöerg Hermann for editorial handling and for his sharp and helpful remarks. They all improved this paper significantly. Laura Negretti and Andrea Risplendente are gratefully acknowledged for technical help during microprobe analysis and electron microscopy.

FUNDING

M.S. and E.R. acknowledge the Italian Ministero dell'Istruzione, dell'Università e della Ricerca (Progetti di ricerca di Rilevante Interesse Nazionale COFIN project 2009XRH8JJ 'Transfer of light elements in subduction zone peridotites') and the University of Genova for funding.

SUPPLEMENTARY DATA

Supplementary data for this paper are available at *Journal of Petrology* online.

REFERENCES

Alt, J. C. & Shanks, W. C. (2006). Stable isotope compositions of serpentinite seamounts in the Mariana forearc: Serpentinization processes, fluid sources and sulfur metasomatism. *Earth and Planetary Science Letters* **242**, 272–285.

Alt, J. C., Garrido, C. J., Shanks, W. C., Turchyn, A., Padròn-Navarta, J. A., Lòpez-Sànchez-Vizcaino, V., Gòmez Pugnaire, M. T. & Marchesi, C. (2012). Recycling of water, carbon, and sulfur during subduction of serpentinites: A stable isotope study of Cerro del Almirez, Spain. *Earth and Planetary Science Letters* **327–328**, 50–60.

Angiboust, S., Agard, P., Raimbourg, H., Yamato, P. & Huet, B. (2011). Subduction interface processes recorded by eclogite-facies shear zones (Monviso, W. Alps). *Lithos* **127**, 222–238.

Asimow, P. D. (1999). A model that reconciles major- and trace element data from abyssal peridotites. *Earth and Planetary Science Letters* **169**, 303–319.

Barnes, J. D. & Straub, S. M. (2010). Chlorine stable isotope variations in Izu–Bonin tephra: implications for serpentinite subduction. *Chemical Geology* **272**, 62–74.

Bebout, G. E. (2007). Metamorphic chemical geodynamics of subduction zones. *Earth and Planetary Science Letters* **260**, 373–393.

Becker, H. (1993). Garnet peridotite and eclogite Sm–Nd mineral ages from the Lepontine dome (Swiss Alps): new evidence for Eocene high-pressure metamorphism in the Central Alps. *Geology* **21**, 599–602.

Beyer, E. E., Griffin, W. L. & O'Reilly, S. Y. (2006). Transformation of Archaean lithospheric mantle by refertilization: evidence from exposed peridotites in the Western Gneiss Region, Norway. *Journal of Petrology* **47**, 1611–1636.

Bonifacie, M., Busigny, V., Mével, C., Philippot, P., Agrinier, P., Jendrzejewski, N., Scambelluri, M. & Javoy, M. (2008). Chlorine isotopic composition in seafloor serpentinites and high-pressure metaperidotites. Insights into oceanic serpentinization and subduction processes. *Geochimica et Cosmochimica Acta* **72**, 126–139.

Boschi, C., Dini, A., Frueh Green, G. L. & Kelley, D. S. (2008). Isotopic and element exchange during serpentinization and metasomatism at the Atlantis Massif (MAR 30°N): Insights from B and Sr isotope data. *Geochimica et Cosmochimica Acta* **72**, 1801–1823.

Bostock, M. G., Hyndman, R. D., Rondenay, S. & Peacock, S. M. (2002). An inverted continental Moho and serpentinization of the forearc mantle. *Nature* **417**, 536–538.

Brey, G. P. & Köhler, T. (1990). Geothermobarometry in four-phase lherzolites II. New thermobarometers, and practical assessment of existing thermobarometers. *Journal of Petrology* **31**, 1353–1378.

Brouwer, F. M., Burri, T., Engi, M. & Berger, A. (2005). Eclogite relics in the Central Alps: Regional distribution, metamorphic PT-evolution, Lu-Hf ages, and genetic implications on the formation of tectonic mélange zones. *Schweizerische Mineralogische Petrographische Mitteilungen* **85**, 147–174.

Brueckner, H. K. (1998). Sinking intrusion model for the emplacement of garnet-bearing peridotites into continent collision orogens. *Geology* **26**, 631–634.

Cannat, M., Mével, C., Maia, M., Deplus, C., Durand, C., Gente, P., Agrinier, P., Belarouchi, A., Dubuisson, G., Humler, E. & Reynolds, J. (1995). Thin crust, ultramafic exposures, and rugged faulting patterns at the Mid-Atlantic Ridge (22°–24°N). *Geology* **23**, 49–52.

Cimmino, F., Messiga, B. & Piccardo, G. B. (1979). Ti-clinohumite-bearing assemblages within antigoritic serpentinites of the Voltri Massif (Western Liguria): inferences on the geodynamic evolution of piemontese ultramafic sections. *Ofioliti* **4**, 97–120.

Cloos, M. (1982). Flow mélanges: Numerical modelling and geologic constraints on their origin in the Franciscan subduction complex, California. *Geological Society of America Bulletin* **93**, 330–345.

Connolly, J. A. D. (1990). Multivariable phase diagrams: an algorithm based on generalized thermodynamics. *American Journal of Science* **290**, 666–718.

Dale, J., Holland, T. & Powell, R. (2000). Hornblende–garnet–plagioclase thermobarometry: a natural assemblage calibration of the thermodynamics of hornblende. *Contributions to Mineralogy and Petrology* **140**, 353–362.

Deschamps, F., Guillot, S., Godard, M., Chauvel, C., Andreani, M. & Hattori, K. H. (2010). *In situ* characterization of serpentinites from forearc mantle wedges: timing of serpentinization and behavior of

fluid-mobile elements in subduction zones. *Chemical Geology* **269**, 262–277.

Deschamps, F., Guillot, S., Godard, M., Andreani, M. & Hattori, K. H. (2011). Serpentinites act as sponges for fluid-mobile elements in abyssal and subduction zone environments. *Terra Nova* **23**, 171–178.

Deschamps, F., Godard, M., Guillot, S., Chauvel, C., Andreani, M., Hattori, K., Wunder, B. & France, L. (2012). Behavior of fluid-mobile elements in serpentines from abyssal to subduction environments: Examples from Cuba and Dominican Republic. *Chemical Geology* **312–313**, 93–117.

Dobrzhinetskaya, L., Green, H. W. & Wang, S. (1996). Alpe Arami: A peridotite massif from depths of more than 300 kilometers. *Science* **271**, 1841–1845.

Dobson, D. P., Meredith, P. G. & Boon, S. A. (2002). Simulation of subduction-zone seismicity by dehydration of serpentine. *Science* **298**, 1407–1410.

Dvir, O., Pettke, T., Fumagalli, P. & Kessel, R. (2011). Fluids in the peridotite–water system up to 6 GPa and 800°C: new experimental constrains on dehydration reactions. *Contributions to Mineralogy and Petrology* **161**, 829–844.

Eggins, S. M. & Shelley, J. M. G. (2002). Compositional heterogeneity in NIST SRM 610–617 glasses. *Geostandards Newsletter* **26**, 269–286.

Ellis, D. J. & Green, D. H. (1979). An experimental study of the effect of Ca upon the garnet–clinopyroxene Fe–Mg exchange equilibria. *Contributions to Mineralogy and Petrology* **71**, 13–22.

Engi, M., Berger, A. & Roselle, G. T. (2001). Role of the tectonic accretion channel in collisional orogeny. *Geology* **29**, 1143–1146.

Ernst, W. G. (1977). Mineralogic study of eclogitic rocks from Alpe Arami Lepontine Alps, Southern Switzerland. *Journal of Petrology* **18**, 371–398.

Evans, B. W. (2010). Lizardite versus antigorite serpentinite: Magnetite, hydrogen, and life(?). *Geology* **38**, 879–882.

Evans, B. W. & Trommsdorff, V. (1978). Petrogenesis of garnet lherzolite, Cima di Gagnone, Lepontine Alps. *Earth and Planetary Science Letters* **40**, 333–348.

Evans, B. W. & Trommsdorff, V. (1983). Fluorine hydroxyl titanian clinohumite in alpine recrystallized garnet peridotite: compositional controls and petrologic significance. *American Journal of Science* **283-A**, 355–369.

Evans, B. W., Trommsdorff, V. & Richter, W. (1979). Petrology of an eclogite–metarodingite suite at Cima di Gagnone, Ticino, Switzerland. *American Mineralogist* **64**, 15–31.

Evans, B. W., Trommsdorff, V. & Goles, G. G. (1981). Geochemistry of high-grade eclogites and metarodingites from the Central Alps. *Contributions to Mineralogy and Petrology* **76**, 301–311.

Faccenda, M., Burlini, L., Gerya, T. & Mainprice, D. (2008). Fault-induced seismic anisotropy by hydration in subducting oceanic plates. *Nature* **455**, 1097–1100.

Federico, L., Crispini, L., Scambelluri, M. & Capponi, G. (2007). Ophiolite mélange zone records exhumation in a fossil subduction channel. *Geology* **35**, 499–502.

Fontana, E., Panseri, M. & Tartarotti, P. (2008). Oceanic relict textures in the Mount Avic serpentinites, Western Alps. *Ofioliti* **33**, 105–118.

Freese, K., Trommsdorff, V. & Kunze, K. (2003). Olivine [100] normal to foliation: Lattice preferred in prograde garnet peridotite formed at high H_2O activity, Cima di Gagnone (Central Alps). *Contributions to Mineralogy and Petrology* **145**, 75–86.

Froitzheim, N., Schmid, S. M. & Frey, M. (1996). Mesozoic paleogeography and the timing of eclogite facies metamorphism in the Alps: a working hypothesis. *Eclogae Geologicae Helvetiae* **89**, 81–110.

Fumagalli, P. & Poli, S. (2005). Experimentally determined phase relations in hydrous peridotites to 6·5 GPa and their consequences on the dynamics of subduction zones. *Journal of Petrology* **46**, 555–578.

Fumasoli, M. W. (1974). Geologie des Gebietes nordlich und sudlich der Jorio–Tonale-Linie im Westen von Gravedona (Como, Italia). Dissertation thesis, Universität Zurich, 230 pp.

Garrido, C. J., López Sánchez-Vizcaíno, V., Gómez-Pugnaire, M. T., Trommsdorff, V., Alard, O., Bodinier, J.-L. & Godard, M. (2005). Enrichment of HFSE in chlorite–harzburgite produced by high-pressure dehydration of antigorite–serpentinite: implications for subduction magmatism. *Geochemistry, Geophysics, Geosystems* **6(1)**, http://dx.doi.org/10.1029/2004GC000791.

Gebauer, D. (1996). A *P–T–t* path for an (ultra?-) high-pressure ultramafic/mafic rock-association and its felsic country-rocks based on SHRIMP dating of magmatic and metamorphic zircon domains. Example: Alpe Arami (Central Swiss Alps). *Earth Processes: Reading the Isotopic Code. American Geophysical Union, Geophysical Monographs* **95**, 309–328.

Gebauer, D., Grunenfelder, M., Tilton, G., Trommsdorff, V. & Schmid, S. (1992). The geodynamic evolution of garnet-peridotites, garnet-pyroxenites and eclogites of Alpe Arami and Cima di Gagnone (Central Alps) from Early Proterozoic to Oligocene. *Schweizerische Mineralogische und Petrographische Mitteilungen* **72**, 107–111.

Gebauer, D., Schertl, H. P., Brix, M. & Schreyer, W. (1997). 35 Ma old ultrahigh-pressure metamorphism and evidence of very rapid exhumation in the Dora Maira Massif, Western Alps. *Lithos* **41**, 5–24.

Gerya, T. V., Stöckhert, B. & Perchuk, A. L. (2002). Exhumation of high-pressure metamorphic rocks in a subduction channel: A numerical simulation. *Tectonics* **21(6)**, 1056, doi:1029/2002TC001406.

Godard, M., Jousselin, D. & Bodinier, J.-L. (2000). Relationships between geochemistry and structure beneath a palaeo-spreading centre: A study of the mantle section in the Oman Ophiolite. *Earth and Planetary Science Letters* **180**, 133–148.

Godard, M., Lagabrielle, Y., Alard, O. & Harvey, J. (2008). Geochemistry of the highly depleted peridotites drilled at ODP Sites 1272 and 1274 (Fifteen–Twenty Fracture Zone, Mid-Atlantic Ridge): implications for mantle dynamics beneath a slow spreading ridge. *Earth and Planetary Science Letters* **267**, 410–425.

Govindaraju, K. (1994). 1994 compilation of working values and sample description for 383 geostandards. *Geostandard Newsletters* **18(Special Issue)**, 1–158.

Grove, T. L., Chatterjee, N., Parman, S. W. & Medard, E. (2006). The influence of H_2O on mantle wedge melting. *Earth and Planetary Science Letters* **249(1–2)**, 74–89.

Guillong, M., Meier, D. L., Allan, M. M., Heinrich, C. A. & Yardley, B. W. D. (2008). SILLS: A MATLAB-based program for the reduction of laser ablation ICP–MS data of homogeneous materials and inclusions. In: Sylvester, P. (ed.) *Laser Ablation ICP-MS in the Earth Sciences: Current Practices and Outstanding Issues. Mineralogical Association of Canada, Short Course Series* **40**, 328–333.

Guillot, S., Hattori, K. H., De Sigoyer, J., Nägler, T. & Auzende, A.-L. (2001). Evidence of hydration of the mantle wedge and its role in the exhumation of eclogites. *Earth and Planetary Science Letters* **193**, 115–127.

Harley, S. L. (1984). An experimental study of the partitioning of Fe and Mg between garnet and orthopyroxene. *Contributions to Mineralogy and Petrology* **86**, 353–373.

Hattori, K. H. & Guillot, S. (2003). Volcanic fronts form as a consequence of serpentinite dehydration in the forearc mantle wedge. *Geology* **31**, 525–528.

Hattori, K. H. & Guillot, S. (2007). Geochemical character of serpentinites associated with high- to ultrahigh-pressure metamorphic

rocks in the Alps, Cuba, and the Himalayas: recycling of elements in subduction zones. *Geochemistry, Geophysics, Geosystems* **8(9)**, http://dx.doi.org/10.1029/2007GC001594.

Hattori, K., Takahashi, Y., Guillot, S. & Johanson, B. (2005). Occurrence of arsenic(V) in forearc mantle serpentinites based on X-ray absorption spectroscopy study. *Geochimica et Cosmochimica Acta* **69(23)**, 5585–5596.

Healy, D., Reddy, S. M., Timms, N. E., Gray, E. M. & Brovarone, A. V. (2009). Trench-parallel fast axes of seismic anisotropy due to fluid-filled cracks in subducting slabs. *Earth and Planetary Science Letters* **283**, 75–86.

Heinrich, C. A. (1982). Kyanite-eclogite to amphibolite facies evolution of hydrous mafic and pelitic rocks, Adula nappe, Central Alps. *Contributions to Mineralogy and Petrology* **81**, 30–38.

Heinrich, C. A. (1986). Eclogite facies regional metamorphism of hydrous mafic rocks in the Central Alpine Adula nappe. *Journal of Petrology* **27**, 123–154.

Hermann, J. & Green, D. H. (2001). Experimental constraints on high pressure melting in subducted crust. *Earth and Planetary Science Letters* **188**, 149–168.

Hermann, J. & Spandler, C. (2008). Sediment melts at sub-arc depths: an experimental study. *Journal of Petrology* **49**, 717–740.

Hermann, J., Müntener, O. & Scambelluri, M. (2000). The importance of serpentinite mylonites for subduction and exhumation of oceanic crust. *Tectonophysics* **327**, 225–238.

Herwartz, D., Nagel, T. J., Munker, C., Scherer, E. E. & Froitzheim, N. (2011). Tracing two orogenic cycles in one eclogite sample by Lu–Hf garnet chronometry. *Nature Geoscience* **4**, 178–183.

Hilairet, N., Reynard, B., Wang, Y. B., Daniel, I., Merkel, S., Nishiyama, N. & Petitgirard, S. (2007). High-pressure creep of serpentine, interseismic deformation, and initiation of subduction. *Science* **318**, 1910–1913.

Holland, T. J. B. & Powell, R. (1998). An internally consistent thermodynamic data set for phases of petrological interest. *Journal of Metamorphic Geology* **16**, 309–343.

Hyndman, R. D. & Peacock, S. M. (2003). Serpentinization of the forearc mantle. *Earth and Planetary Science Letters* **212**, 417–432.

Ionov, D. A., Savoyant, L. & Dupuy, C. (1992). Application of the ICP-MS technique to trace element analysis of peridotites and theirminerals. *Geostandards Newsletters* **16**, 311–315.

Jäger, E., Niggli, E. & Wenk, E. (1967). *Rb–Sr Alterbestimmungen an Glimmern der Zentralalpen. Beitrage Geologische Karte Schweiz* **134**, 67 pp.

Jochum, K. P., Seufert, H. M. & Thirlwall, M. F. (1990). High-sensitivity Nb analysis by spark-source mass spectrometry (SSMS) and calibration of XRF Nb and Zr. *Chemical Geology* **81**, 1–16.

Jochum, K. P., Weis, U., Stoll, B., Kuzmin, D., Yang, Q. C., Raczek, I., Jacob, D. E., Stracke, A., Birbaum, K., Frick, D. A., Gunther, D. & Enzweiler, J. (2011). Determination of reference values for NIST SRM 610–617 glasses following ISO guidelines. *Geostandards and Geoanalytical Research* **35**, 397–429.

John, T., Scambelluri, M., Frische, M., Barnes, J. & Bach, W. (2011). Dehydration of subducting serpentinite: Implications for halogen mobility in subduction zones and the deep halogen cycle. *Earth and Planetary Science Letters* **308**, 65–76.

Jung, H., Green, H. W. & Dobrzhinetskaya, L. F. (2004). Intermediate-depth earthquake faulting by dehydration embrittlement with negative volume change. *Nature* **428**, 545–549.

Kelemen, P. B. & Matter, J. (2008). *In situ* mineral carbonation in peridotite for CO_2 storage. *Proceedings of the National Academy of Sciences of the USA* **105**, 17295–17300, doi:10.1073/pnas.0805794105.

Kendrick, M. A., Scambelluri, M., Honda, M. & Phillips, D. (2011). High abundance of noble gas and chlorine delivered to the mantle by serpentinite subduction. *Nature Geoscience* **4**, 807–812.

Kerrick, D. M. (2002). Serpentinite seduction. *Science* **298**, 1344–1345.

Kessel, R., Schmidt, M. W., Ulmer, P. & Pettke, T. (2005). Trace element signature of subduction-zone fluids, melts and supercritical liquids at 120–180 km depth. *Nature* **437**, 724–727.

Klemme, S. & O'Neil, H. St. C. (2000). The near solidus transition from garnet lherzolite to spinel lherzolite. *Contributions to Mineralogy and Petrology* **138**, 237–248.

Kodolányi, J., Pettke, T., Spandler, C., Kamber, B. S. & Gméling, K. (2012). Geochemistry of ocean floor and fore-arc serpentinites: constraints on the ultramafic input to subduction zones. *Journal of Petrology* **53**, 235–270.

Li, X. P., Rahn, M. K. & Bucher, K. (2004). Serpentinites of the Zermatt–Saas ophiolite complex and their texture evolution. *Journal of Metamorphic Geology* **22**, 159–177.

Li, Y. H. (1984). A brief discussion on the mean oceanic residence time of elements. *Geochimica et Cosmochimica Acta* **46**, 2671–2675.

Li, Y. H. (1991). Distribution patterns of the elements in the ocean—a synthesis. *Geochimica et Cosmochimica Acta* **55**, 3223–3240.

Lòpez Sànchez-Vizcaìno, V., Trommsdorff, V., Gòmez-Pugnaire, M. T., Garrido, C. J., Müntener, O. & Connolly, J. A. D. (2005). Petrology of titanian clinohumite and olivine at the high pressure breakdown of antigorite serpentinite to chlorite harzburgite (Almirez Massif, S Spain). *Contributions to Mineralogy and Petrology* **149**, 627–646.

Malaspina, N. & Tumiati, S. (2012). The role of C–O–H and oxygen fugacity in subduction zone garnet peridotites. *European Journal of Mineralogy* **24**, 607–618.

Malaspina, N., Hermann, J. & Scambelluri, M. (2009). Fluid/mineral interaction in UHP garnet peridotite. *Lithos* **107**, 38–52.

Malaspina, N., Hermann, J., Scambelluri, M. & Compagnoni, R. (2006). Polyphase inclusions in garnet-orthopyroxenite (Dabie Shan, China) as monitors for metasomatism and fluid-related trace element transfer in subduction zone peridotite. *Earth and Planetary Science Letters* **240**, 668–680.

Malatesta, C., Gerya, T., Scambelluri, M., Federico, L., Crispini, L. & Capponi, G. (2012). Intraoceanic subduction of 'heterogeneous' oceanic lithosphere: 2D numerical modelling. *Lithos* **140–141**, 234–251.

Marschall, H. R. & Shumacher, J. C. (2012). Arc magmas sourced from mélange diapirs in subduction zones. *Nature Geoscience* **5**, 862–867.

Marschall, H. R., Ludwig, T., Altherr, R., Kalt, A. & Tonarini, S. (2006). Syros metasomatic tourmaline: Evidence for very high-δ^{11}B fluids in subduction zones. *Journal of Petrology* **47**, 1915–1942.

McDonough, W. F. & Sun, S.-S. (1995). The composition of the Earth. *Chemical Geology* **120**, 223–253.

Menzies, M. A. & Dupuy, C. (1991). Orogenic massifs: Protolith, process and provenance. *Journal of Petrology* (Special Issue, Orogenic Lherzolites and Mantle Processes), 1–16.

Meyre, C., De Capitani, C. & Partzsc, J. H. (1997). A ternary solid solution for omphacite and its application to geothermobarometry of eclogites from the middle Adula Nappe (Central Alps, Switzerland). *Journal of Metamorphic Geology* **15**, 687–670.

Meyre, C., De Capitani, C., Zack, T. & Frey, M. (1999). Petrology of high-pressure metapelites from the Adula Nappe (Central Alps, Switzerland). *Journal of Petrology* **40**, 199–213.

Möckel, J. R. (1969). Structural petrology of the garnet peridotite of Alpe Arami (Ticino, Switzerland). *Leidse Geologische Mededelingen* **42**, 61–130.

Morris, J. D., Leeman, W. P. & Tera, F. (1990). The subducted component in island arc lavas: constraints from Be isotopes and B–Be systematics. *Nature* **344**, 31–36.

Morten, L. & Obata, M. (1990). Rare earth abundances in the eastern Alpine peridotites, Nonsberg area, Northern Italy. *European Journal of Mineralogy* **2**, 643–653.

Morten, L. & Trommsdorff, V. (2003). Metamorphism and textures of dry and hydrous garnet peridotites. In: Carswell, D. A. & Compagnoni, R. (eds) *Ultrahigh Pressure Metamorphism. European Mineralogical Union, Notes in Mineralogy* **5**, 443–466.

Müntener, O., Pettke, T., Desmurs, L., Meier, M. & Schaltegger, U. (2004). Refertilization of mantle peridotite in embryonic ocean basins: Trace element and Nd-isotopic evidence and implications for crust–mantle relationships. *Earth and Planetary Science Letters* **221**, 293–308.

Niida, K. & Green, D. H. (1999). Stability and chemical composition of pargasitic amphibole in MORB pyrolite under upper mantle conditions. *Contributions to Mineralogy and Petrology* **135**, 18–40.

Nimis, P. & Grutter, H. (2010). Internally consistent geothermometers for garnet peridotites and implications on the nature of the lithosphere, kimberlites and diamonds. *Contributions to Mineralogy and Petrology* **159**, 411–427.

Nimis, P. & Grutter, H. (2012). Discussion of 'The applicability of garnet–orthopyroxene geobarometry in mantle xenoliths', by Wu, C.-M. and Zhao, G. (Lithos, v. 125, p. 1–9). *Lithos* **142–143**, 285–287.

Nimis, P. & Morten, L. (2000). *P–T* evolution of 'crustal' garnet peridotites and included pyroxenites from Nonsberg area (upper Austroalpine), NE Italy: from the wedge to the slab. *Journal of Geodynamics* **30**, 93–115.

Nimis, P. & Taylor, W. R. (2000). Single clinopyroxene thermobarometry for garnet peridotites. Part I. Calibration and testing of a Cr-in-Cpx barometer and an enstatite-in-Cpx thermometer. *Contributions to Mineralogy and Petrology* **139**, 541–554.

Nimis, P. & Trommsdorff, V. (2001). Revised thermobarometry of Alpe Arami and other garnet peridotites from the Central Alps. *Journal of Petrology* **42**, 103–115.

Niu, Y. (2004). Bulk-rock major and trace element compositions of abyssal peridotites: implications for mantle melting, melt extraction and post-melting processes beneath mid-ocean ridges. *Journal of Petrology* **45(12)**, 2423–2458.

Niu, Y. & Hekinian, R. (1997). Basaltic liquids and harzburgitic residues in the Garrett Transform; a case study at fastspreading ridges. *Earth and Planetary Science Letters* **146**, 243–258.

O'Hara, M. J. & Mercy, E. L. (1966). Garnet peridotite and eclogite from Bellinzona, Switzerland. *Earth and Planetary Science Letters* **1**, 61–130.

O'Neil, H. St. C. (1981). The transition between spinel lherzolite and garnet lherzolite, and its use as a geobarometer. *Contributions to Mineralogy and Petrology* **77**, 185–194.

Padrón-Navarta, J. A., Hermann, J., Garrido, C. J., Lòpez Sànchez-Vizcaìno, V. & Gòmez-Pugnaire, M. T. (2010*a*). An experimental investigation of antigorite dehydration in natural silica-enriched serpentinite. *Contributions to Mineralogy and Petrology* **159**, 25–42.

Padrón-Navarta, J. A., Lòpez Sànchez-Vizcaìno, V., Hermann, J., Connolly, J. A. D., Garrido, C. J., Gòmez-Pugnaire, M. T. & Marchesi, C. (2010*b*). Element mobility from seafloor serpentinization to high-pressure dehydration of antigorite in subducted serpentinite: Insights from the Cerro del Almirez ultramafic massif (southern Spain). *Lithos* , doi:org/10.1016/j.lithos.2013.02.001.

Padrón-Navarta, J. A., Tommasi, A., Garrido, C. J., López Sánchez-Vizcaìno, V., Gómez-Pugnaire, M. T., Jabaloy, A. & Vauchez, A. (2010*c*). Fluid transfer into the wedge controlled by high-pressure hydrofracturing in the cold top-slab mantle. *Earth and Planetary Science Letters* **297**, 271–286.

Padrón-Navarta, J. A., Lòpez Sànchez-Vizcaìno, V. & Gòmez-Pugnaire, M. T. (2013). Tschermak s substitution in antigorite and consequences for phase relations and water liberation in high grade serpentinites. *Lithos* **178**, 186–196.

Palme, H. & O'Neill, H. S. C. (2004). Cosmochemical estimate of mantle composition. In: Carlson, R. W. (ed.) *Treatise on Geochemistry. The Mantle, 2.* Amsterdam: Elsevier, pp. 1–38.

Paulick, H., Bach, W., Godard, M., De Hoog, J. C. M., Suhr, G. & Harvey, J. (2006). Geochemistry of abyssal peridotites (Mid-Atlantic Ridge, 15°20'N, ODP Leg 209): Implications for fluid/rock interaction in slow spreading environments. *Chemical Geology* **234**, 179–210.

Peacock, S. M. (1993). Large-scale hydration of the lithosphere above subducting slabs. *Chemical Geology* **108**, 49–59.

Pettke, T., Oberli, F., Audetat, A., Guillong, M., Simon, A. C., Hanley, J. J. & Klemm, L. M. (2012). Recent developments in element concentration and isotope ratio analysis of individual fluid inclusions by laser ablation single and multiple collector ICP-MS. *Ore Geology Reviews* **44**, 10–38.

Pfiffner, M. (1999). Genese der hochdruckmetamorphen ozeanischen Abfolge der Cima Lunga-Einheit (Zentralalpen) PhD thesis, ETH Zurich.

Pfiffner, M. & Trommsdorff, V. (1998). The high-pressure ultramafic–mafic–carbonate suite of Cima Lunga–Adula, Central Alps: excursions to Cima di Gagnone and Alpe Arami. *Schweizerische Mineralogische und Petrographische Mitteilungen* **78**, 337–354.

Piccardo, G. B. (2003). Mantle processes during ocean formation: petrologic records in peridotites from the Alpine–Apennine ophiolites. *Episodes* **26**, 193–199.

Puga, E., Nieto, J. M., Diaz de Federico, A., Bodinier, J. L. & Morten, L. (1999). Petrology and metamorphic evolution of ultramafic rocks and dolerite dykes of the Betic Ophiolitic Association (Mulhacen Complex, SE Spain): Evidence of eo-Alpine subduction following and ocean-floor metasomatic process. *Lithos* **4**, 23–56.

Rampone, E. & Borghini, G. (2008). Melt migration and intrusion in the Erro–Tobbio peridotites (Ligurian Alps, Italy): Insights on magmatic processes in extending lithospheric mantle. *European Journal of Mineralogy* **20**, 573–585.

Rampone, E. & Morten, L. (2001). Records of crustal metasomatism in the garnet peridotites of the Ulten Zone (Upper Austroalpine, Eastern Alps). *Journal of Petrology* **42**, 207–219.

Rampone, E. & Piccardo, G. B. (2000). The ophiolite–oceanic lithosphere analogue: new insights from the Northern Apennines (Italy). In: Dilek, Y., Moores, E. M., Elthon, D. & Nicolas, A. (eds) *Ophiolites and Oceanic Crust: New Insights from Field Studies and the Ocean Drilling Program. Geological Society of America, Special Papers* **349**, 21–34.

Rampone, E., Romairone, A. & Hofmann, A. W. (2004). Contrasting bulk and mineral chemistry in depleted peridotites: evidence for reactive porous flow. *Earth and Planetary Science Letters* **218**, 491–506.

Rampone, E., Romairone, A., Abouchami, W., Piccardo, G. B. & Hofmann, W. (2005). Chronology, petrology and isotope geochemistry of the Erro–Tobbio peridotites (Ligurian Alps, Italy): Records of Late Palaeozoic litospheric extension. *Journal of Petrology* **46**, 799–827.

Rampone, E., Piccardo, G. B. & Hofmann, A. W. (2008). Multi-stage melt–rock interaction in the Mt. Maggiore (Corsica, France) ophiolitic peridotites: microstructural and geochemical evidence. *Contributions to Mineralogy and Petrology* **156**, 453–475.

Ranero, C. R., Phipps Morgan, J., McIntosh, K. & Reichert, C. (2003). Bending-related faulting and mantle serpentinization at the Middle America trench. *Nature* **425**, 367–373.

Rebay, G., Spalla, M. I. & Zanoni, D. (2012). Interaction of deformation and metamorphism during subduction and exhumation of hydrated oceanic mantle: Insights from the Western Alps. *Journal of Metamorphic Geology* **30**, 687–702.

Rost, F., Wannemaker, J. & Grigel, W. (1974). Die Ultramafitite der Alpe Arami und Croveggio Tessin (Schweiz). *Schweizerische Mineralogische und Petrographische Mitteilungen* **54**, 353–369.

Rubatto, D., Gebauer, D. & Fanning, M. (1998). Jurassic formation and Eocene subduction of the Zermatt–Saas–Fee ophiolites: implications for the geodynamic evolution of the Central and Western Alps. *Contributions to Mineralogy and Petrology* **132**, 269–287.

Rudnick, R. L. & Gao, S. (2004). Composition of the continental crust. In: Holland, H. D. & Turekian, K. K. (eds) *Treatise on Geochemistry, The Crust, 3*. Amsterdam: Elsevier, pp. 1–64.

Sapienza, G. T., Scambelluri, M. & Braga, R. (2009). Dolomite-bearing orogenic garnet peridotites witness fluid-mediated carbon recycling in a mantle wedge (Ulten Zone, Eastern Alps, Italy). *Contributions to Mineralogy and Petrology* **158**, 401–420.

Savov, I. P., Ryan, J. G., D'Antonio, M., Kelley, K. & Mattie, P. (2005). Geochemistry of serpentinized peridotites from the Mariana Forearc Conical Seamount, ODP Leg 125: Implications for elemental recycling at subduction zones. *Geochemistry, Geophysics, Geosystems* **6**, Q04J15, doi:10.1029/2004GC000777.

Scambelluri, M. & Tonarini, S. (2012). Boron isotope evidence for shallow fluid transfer across subduction zones by serpentinized mantle. *Geology* **40(10)**, 907–910.

Scambelluri, M., Pettke, T. & Van Roermund, H. L. M. (2008). Majoritic garnets monitor deep subduction fluid flow and mantle dynamics. *Geology* **36**, 59–62.

Scambelluri, M., Hermann, J., Morten, L. & Rampone, E. (2006). Melt- versus fluid-induced metasomatism in spinel to garnet wedge peridotites (Ulten Zone, Eastern Italian Alps): clues from trace element and Li abundances. *Contributions to Mineralogy and Petrology* **151**, 372–394.

Scambelluri, M., Fiebig, J., Malaspina, N., Müntener, O. & Pettke, T. (2004*b*). Serpentinite subduction: Implications for fluid processes and trace-element recycling. *International Geology Reviews* **46**, 595–613.

Scambelluri, M., Hoogerduijn Strating, E. H., Piccardo, G. G., Vissers, R. L. M. & Rampone, E. (1991). Alpine olivine- and titanian clinohumite-bearing assemblages in the Erro–Tobbio peridotite (Voltri Massif, NW Italy). *Journal of Metamorphic Geology* **9**, 79–91.

Scambelluri, M., Müntener, O., Hermann, J., Piccardo, G. B. & Trommsdorff, V. (1995). Subduction of water into the mantle: History of an alpine peridotite. *Geology* **23**, 459–462.

Scambelluri, M., Müntener, O., Ottolini, L., Pettke, T. & Vannucci, R. (2004*a*). The fate of B, Cl and Li in the subducted oceanic mantle and in the antigorite-breakdown fluids. *Earth and Planetary Science Letters* **222**, 217–234.

Scambelluri, M., Piccardo, G. B., Philippot, P., Robbiano, A. & Negretti, L. (1997). High salinity fluid inclusions formed from recycled seawater in deeply subducted alpine serpentinite. *Earth and Planeary Science Letters* **148**, 485–500.

Scambelluri, M., Bottazzi, P., Trommsdorff, V., Vannucci, R., Hermann, J., Gòmez-Pugnaire, M. T. & Lòpez-Sànchez Vizcaino, V. (2001). Incompatible element-rich fluids released by antigorite breakdown in deeply subducted mantle. *Earth and Planeary Science Letters* **192**, 457–470.

Schmid, S. M., Rück, P. & Schreurs, G. (1990). The significance of the Schams nappes for the reconstruction of the palaeotectonic evolution of the Penninic zone along the NRP20-East traverse (Grisons, Eastern Switzerland). *Mémoires de la Société Géologique de France* **156**, 263–287.

Schmidt, K., Koschinsky, A., Garbe-Schönberg, D., de Carvalho, L. M. & Seifert, R. (2007). Geochemistry of hydrothermal fluids from the ultramafic-hosted Logatchev hydrothermal field, 15°N on the Mid-Atlantic Ridge: Temporal and spatial investigation. *Chemical Geology* **242**, 1–21.

Schmidt, M. W. & Poli, S. (1998). Experimentally based water budget for dehydrating slabs and consequences for arc magma generation. *Earth and Planetary Sciences Letters* **163**, 361–379.

Schwartz, S., Allemand, P. & Guillot, S. (2001). Numerical model of the effect of serpentinites on the exhumation of eclogitic rocks: Insights from the Monviso ophiolitic massif (Western Alps). *Tectonophysics* **42**, 193–206.

Sharp, Z. D. & Barnes, J. D. (2004). Water-soluble chlorides in massive seafloor serpentinites: a source of chloride in subduction zones. *Earth and Planetary Science Letters* **226**, 243–254.

Shimizu, N., Scambelluri, M., Santiago Ramos, D. & Tonarini, S. (2013). Boron and sulfur isotopic variations during subduction of hydrated lithosphere: The Erro Tobbio case. *Mineralogical Magazine* **77(5)**, 2201.

Skemer, P., Katayama, I. & Karato, S. (2006). Deformation fabrics of the Cima di Gagnone peridotite massif, Central Alps, Switzerland: evidence of deformation at low temperatures in the presence of water. *Contributions to Mineralogy and Petrology* **152**, 43–51.

Smith, H. J., Spivack, A. J., Staudigel, H. & Hart, S. R. (1995). The boron isotopic composition of altered oceanic crust. *Chemical Geology* **126**, 119–135.

Spandler, C., Mavrogenes, J. & Hermann, J. (2007). Experimental constraints on element mobility from subducted sediments using high-*P* synthetic fluid/melt inclusions. *Chemical Geology* **239**, 228–249.

Spandler, C., Hermann, J., Faure, R. K., Mavrogenes, J. & Arculus, R. (2008). The importance of talc and chlorite 'hybrid' rocks for volatile recycling through subduction zones: evidence from the high-pressure subduction mélange of New Caledonia. *Contributions to Mineralogy and Petrology* **155**, 181–198.

Spandler, C., Pettke, T. & Rubatto, D. (2011). Internal and external fluid sources for eclogite-facies veins in the Monviso meta-ophiolite, western Alps: implications for fluid flow in subduction zones. *Journal of Petrology* **52**, 1207–1236.

Straub, S. M. & Layne, G. D. (2003). The systematics of chlorine, fluorine, and water in Izu arc front volcanic rocks: Implications for volatile recycling in subduction zones. *Geochimica et Cosmochimica Acta* **67**, 4179–4203.

Taylor, W. R. (1998). An experimental test of some geothermometer and geobarometer formulations for upper mantle peridotites with application to the thermobarometry of fertile lherzolite and garnet websterite. *Neues Jahrbuch für Mineralogie, Abhandlungen* **172**, 381–408.

Tenthorey, E. & Hermann, J. (2004). Composition of fluids during serpentinite breakdown in subduction zones: evidence for limited boron mobility. *Geology* **32**, 865–868.

Tera, F., Brown, L., Morris, J., Sacks, I. S., Klein, J. & Middleton, R. (1986). Sediment incorporation in island arc magmas: inferences from Be-10. *Geochimica et Cosmochimica Acta* **50**, 535–550.

Till, C. B., Grove, T. L. & Withers, A. C. (2012). The beginnings of hydrous mantle wedge melting. *Contributions to Mineralogy and Petrology* **163**, 669–688.

Trommsdorff, V. (1966). Progressive Metamorphose kieseliger Karbonatgesteine in den Zentralalpen zwischen Bernina und Simplon. *Schweizerische Mineralogische und Petrographische Mitteilungen* **46**, 431–460.

Trommsdorff, V. (1990). Metamorphism and tectonics in the Central Alps: The Alpine lithospheric mélange of Cima Lunga and Adula. *Memorie della Società Geologica Italiana* **45**, 39–49.

Trommsdorff, V. & Evans, B. W. (1974). Alpine metamorphism of peridotitic rocks. *Schweizerische Mineralogische und Petrographische Mitteilungen* **54**, 333–352.

Trommsdorff, V., López Sánchez-Vizcaíno, V., Gómez-Pugnaire, M. T. & Müntener, O. (1998). High pressure breakdown of antigorite to spinifex-textured olivine and orthopyroxene, SE Spain. *Contributions to Mineralogy and Petrology* **132**, 139–148.

Trommsdorff, V., Hermann, J., Müntener, O., Pfiffner, M. & Risold, A. C. (2000). Geodynamic cycles of subcontinental lithosphere in the Central Alps and the Arami enigma. *Journal of Geodynamics* **30**, 77–92.

Tumiati, S., Thoni, M., Nimis, P., Martin, S. & Mair, V. (2003). Mantle–crust interactions during Variscan subduction in the Eastern Alps (Nonsberg–Ulten Zone): geochronology and new petrological constraints. *Earth and Planetary Science Letters* **210**, 509–526.

Tumiati, S., Fumagalli, P., Tiraboschi, C. & Poli, S. (2012). An experimental study on COH-bearing peridotite up to 3·2 GPa and implications for crust–mantle recycling. *Journal of Petrology* **54**, 453–479, doi:10.1093/petrology/egs074.

Ulmer, P. & Trommsdorff, V. (1995). Serpentine stability to mantle depths and subduction related magmatism. *Science* **268**, 858–861.

Ulmer, P. & Trommsdorff, V. (1999). Phase relations of hydrous mantle subducting to 300 km. In: Fei, Y., Bertka, C. M. & Mysen, B. O. (eds) *Mantle Petrology: Field Observations and High Pressure Experimentation. Geochemical Society, Special Publications* **6**, 259–281.

Van Keken, P. E. (2003). The structure and dynamics of the mantle wedge. *Earth and Planetary Science Letters* **215**, 323–338.

Vils, F., Tonarini, S., Kalt, A. & Seitz, H. M. (2009). Boron, lithium and strontium isotopes as tracers of seawater–serpentinite interaction at Mid-Atlantic ridge, ODP Leg 209. *Earth and Planetary Science Letters* **286**, 414–425.

Vils, F., Müntener, O., Kalt, A. & Ludwig, T. (2011). Implications of the serpentine phase transition on the behaviour of beryllium and lithium–boron of subducted ultramafic rocks. *Geochimica et Cosmochimica Acta* **75**, 1249–1271.

Zhang, R. Y., Liou, J. G., Yang, J. S. & Yui, T. F. (2000). Petrochemical constraints for dual origin of garnet peridotites from the Dabie–Sulu UHP terrane, eastern–central China. *Journal of Metamorphic Geology* **18**, 149–166.

Zheng, Y. F. (2012). Metamorphic chemical geodynamics in continental subduction zones. *Chemical Geology* **328**, 5–48.

Ziberna, L., Klemme, S. & Nimis, P. (2013). Garnet and spinel in fertile and depleted mantle: insights from thermodynamic modelling. *Contributions to Mineralogy and Petrology* **166**, 411–421.